Near-field acoustic holography with sound pressure and particle velocity measurements

Fernandez Grande, Efren

Publication date:
2012

Document Version
Publisher's PDF, also known as Version of record

Technical University of Denmark

Efren Fernandez Grande

Near-field acoustic holography with sound pressure and particle velocity measurements

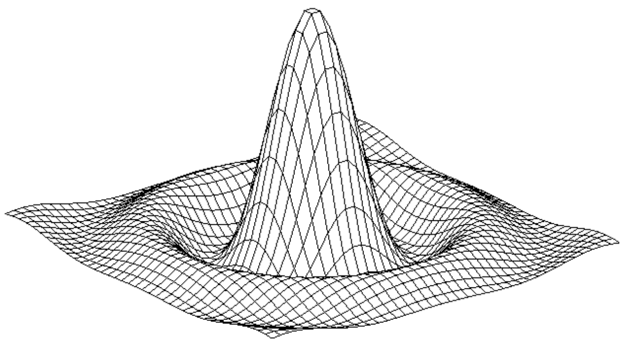

PhD thesis, June 2012

Acoustic Technology
Department of Electrical Engineering

Near-field acoustic holography with sound pressure and particle velocity measurements

PhD thesis by
Efren Fernandez Grande

Technical University of Denmark
2012

This thesis is submitted to the Technical University of Denmark (DTU) as partial fulfillment of the requirements for the degree of Doctor of Philosophy (Ph.D.) in Electronics and Communication. The work presented in this thesis was completed between January 15, 2009 and February 23, 2012 at Acoustic Technology, Department of Electrical Engineering, DTU, under the supervision of Associate Professor Finn Jacobsen. The project was funded by DTU Elektro.

Title
Near-field Acoustic Holography with Sound Pressure and Particle Velocity Measurements
Author
Efren Fernandez Grande
Supervisor
Finn Jacobsen

Department of Electrical Engineering
Technical University of Denmark
DK-2800 KONGENS LYNGBY, Denmark

ISBN 978-87-92465-82-5

Printed in Denmark by Rosendahls - Schultz Grafisk a/s

Cover illustration: *Radiation Kernel* by Efren Fernandez Grande

A mis padres, a David,

καὶ στην Ιωάννα

Abstract

Near-field acoustic holography (NAH) is a powerful sound source identification technique that makes it possible to reconstruct and extract all the information of the sound field radiated by a source in a very efficient manner, readily providing a complete representation of the acoustic field under examination. This is crucial in many areas of acoustics where such a thorough insight into the sound radiated by a source can be essential. This study examines novel acoustic array technology in near-field acoustic holography and sound source identification. The study focuses on three aspects, namely the use of particle velocity measurements and combined pressure-velocity measurements in NAH, the relation between the near-field and the far-field radiation from sound sources via the supersonic acoustic intensity, and finally, the reconstruction of sound fields using rigid spherical microphone arrays.

Measurement of the particle velocity has notable potential in NAH, and furthermore, combined measurement of sound pressure and particle velocity opens a new range of possibilities that are examined in this study. On this basis, sound field separation methods have been studied, and a new measurement principle based on double layer measurements of the particle velocity has been proposed. Also, the relation between near-field and far-field radiation from sound sources has been examined using the concept of the supersonic intensity. The calculation of this quantity has been extended to other holographic methods, and studied under the light of different measurement principles. A direct formulation in space domain has been proposed, and the experimental validity of the quantity has been demonstrated. Additionally, the use of rigid spherical microphone arrays in near-field acoustic holography has been examined, and a method has been proposed that can reconstruct the incident sound field and compensate for the scattering introduced by the rigid sphere. It is the purpose of this dissertation to present the relevant findings, discuss the contribution of the PhD study, and frame it in the context of the existing body of knowledge.

Keywords: Near-field acoustic holography, NAH, particle velocity transducers, supersonic intensity, sound radiation, sound source identification, sound visualization, spherical microphone arrays.

Resumé

Akustisk nærfeltsholografi (kendt under forkortelsen NAH) er en effektiv metode til identifikation af lydkilder som gør det muligt at rekonstruere lydfelter i alle detaljer ud fra målinger på en overflade nær en sammensat, kompliceret støjkilde. Kortlægning af delkilder er en vigtigt del af mange akustiske undersøgelser. Dette PhD-projekt har undersøgt en række forskellige målemetoder baseret på kombinationer af forskellige akustiske tranducere (trykmikrofoner og partikelhastighedstransducere). En af konklusionerne er at der er store fordele ved at kombinere sådanne transducere; bl.a. bliver det muligt at skelne mellem bidrag til lydfeltet fra kilden og refleksioner fra rummet som kommer fra den modsatte side af måleoverfladen. Projektet har også undersøgt forskellige holografiske rekonstruktionsprincipper. Endvidere er der også foretaget en undersøgelse af "sfærisk holografi", en metode baseret på mikrofoner placeret på overfladen af en hård kugle; bl.a. er der udviklet en metode der gør det mulig at kompensere for spredningen af lyd som skyldes kuglen og rekonstruere det uforstyrrede såkaldte indfaldende lydfelt. Endelig er der udført en grundig teoretisk og eksperimentel undersøgelse af begrebet “supersonic intensity", en vigtig størrelse der siger noget om en lydkildes udstråling til fjernfeltet.

Resumen

La holografía acústica de campo cercano, comúnmente conocida como NAH (*near-field acoustic holography*), es una técnica de medida que utiliza arrays de micrófonos para procesar el sonido radiado por una fuente y así, obtener un modelo tridimensional completo del campo acústico. De esta forma es posible visualizar cómo una fuente irradia sonido al medio, y determinar cuáles son los mecanismos que producen dicha radiación.

El objetivo de esta tesis es investigar el potencial de las nuevas tecnologías de transducción y arrays de transductores en holografía acústica, poniendo énfasis particular en la medición de la velocidad de la partícula sonora y la combinación de velocidad y presión sonora. El estudio ha examinado los llamados "métodos de separación" que posibilitan el uso de NAH en entornos reverberantes, ya que hacen posible distinguir entre las ondas a ambos lados del array. En esta tesis se ha propuesto una nueva metodología basada en la medición en doble capa de la velocidad de la partícula. También se ha estudiado la relación entre la radiación de campo cercano y campo lejano de fuentes sonoras mediante una nueva magnitud denominada “intensidad supersónica” (*supersonic intensity*). En este ámbito, se ha propuesto el cálculo de esta magnitud mediante distintos métodos holográficos y principios de medida, así como una formulación directa en el dominio espacial. Por último, se ha investigado el uso de arrays rígidos-esféricos de micrófonos en holografía acústica, y se ha desarrollado un método mediante el cual se puede compensar la difracción introducida por la esfera, y reconstruir el campo sonoro incidente, evitando la influencia del array.

El objetivo de esta tesis doctoral es presentar los resultados obtenidos y las conclusiones pertinentes, y enmarcar la aportación de este trabajo en el contexto del estado del arte y del conocimiento actual.

Palabras clave: Holografía acústica de campo cercano, NAH, radiación sonora, velocidad de partícula, intensidad sonora, intensidad supersónica, visualización sonora, arrays acústicos, arrays de micrófonos, arrays esféricos, control de ruido.

Acknowledgments

This thesis would not have been possible without the contribution and support of several people to whom I am most sincerely grateful. I would like to express my deepest gratitude to Finn Jacobsen, supervisor of this PhD, for his priceless supervision and advice. Working with him has been a real inspiration, and probably I owe to him more than I can realize. I could not find words that suffice to express my gratitude.

I would like to thank Quentin Leclère for his contribution, input to the project and great interest, and Antonio Pereira for the useful discussions, for his generous help and for the times spent down in the lab. I would also like to thank Yong-Bin Zhang for his contribution and all the valuable input in the early stages of the PhD. Thanks to Per Christian Hansen for the codes and advice on regularization. I would also like to thank Jørgen Rasmussen and Tom A. Petersen for the help with the experiments and the computer issues. Thanks to Elisabet Tiana-Roig and Angeliki Xenaki for the work during their theses; working with you has been a great pleasure.

It is not possible to give specific mention to everybody. I owe a lot to all the colleagues and friends at Acoustic Technology, for their interest and all the valuable discussion, praise and criticism. A very special thanks goes to everyone in 'the house of acoustics', Acoustic Technology and Hearing Research, for creating such a motivating research environment, and for the very friendly and enjoyable atmosphere, which has been extremely valuable these last years. I am also very grateful to everyone at the Laboratoire de Vibrations Acoustique (LVA), INSA-Lyon, for being so welcoming, helpful and hospitable, and for the useful feedback and contribution to the project.

The personal support received throughout the duration of my studies has been very important. I could not be more grateful to my parents and brother for their endless and unconditional support these twenty-eight years. Thanks to Ioanna for being there each day along the process, for the priceless support and for all the wonderful moments. Thanks to the good friends I have the fortune to count on, here in Denmark, in Spain, and elsewhere. You do mean a lot.

Structure of the thesis

This PhD dissertation follows a paper-based format, as recommended by the DTU PhD guidelines. It comprises a synopsis, and a collection of papers produced during the PhD study.

Chapter 1 (Introduction), defines the motivation of the project, and provides a general introduction to near-field acoustic holography and particle velocity measurements. Chapter 2 (Background), provides the general background relevant to the study, discussing the different methodologies available, the history and recent developments of near-field acoustic holography, as well as some considerations on the measurement of the particle velocity. Chapter 3 (Contributions), consists of a literature review where the contributions of the PhD study are described and put in context with the existing knowledge, and the relevant findings are discussed. Chapter 4 (Summary and concluding remarks) concludes the work. It summarizes the contribution of the PhD study, suggests some areas of future work, and provides a summary of the main conclusions.

Six papers and three manuscripts are included in the thesis (Papers A - I). They are divided in four parts: Part I (papers A to C) is concerned with sound field separation methods using pressure and velocity measurements. Part II (papers D to F) deals with the supersonic acoustic intensity and the relation between near-field and far-field radiation from sound sources. Part III (Paper G) considers the holographic reconstruction of sound fields using spherical rigid microphone arrays. The last part, "Additional papers" (Papers H and I) includes papers that have been produced during the PhD study, and are relevant, but not essential to the dissertation.

List of publications

The papers included in this dissertation consist of three published journal papers, three papers published in conference proceedings, and three manuscripts.

List of publications in the work

Paper A “Sound field separation with a double layer velocity transducer array,” J. Acoust. Soc. Am., vol. **130** (1), pp. 5-8, 2011.

Paper B “Sound field separation with sound pressure and particle velocity measurements.” Manuscript.

Paper C “A note on the coherence of sound field separation methods and near-field acoustic holography.” Manuscript.

Paper D “Supersonic acoustic intensity with statistically optimized near-field acoustic holography,” in Proceedings of Inter-Noise 2011, Osaka, Japan, 2011.

Paper E “Direct formulation of the supersonic acoustic intensity in space domain,” J. Acoust. Soc. Am., vol. **131** (1), pp. 186-193, 2012.

Paper F “A note on the finite aperture error of the supersonic intensity.” Manuscript.

Paper G “Near field acoustic holography with microphones on a rigid sphere,” J. Acoust. Soc. Am., vol. **129** (6), pp. 3461-3464, 2011.[1]

Paper H “Separation of radiated sound field components from waves scattered by a source under non-anechoic conditions,” in Proceedings of Inter-Noise 2010, Lisbon, Portugal, 2010.

Paper I “Patch near-field acoustic holography: The influence of acoustic contributions from outside the source patch,” in Proceedings of Inter-Noise 2009, Ottawa, Canada, 2009.

[1] The author of this dissertation is not the first author of this publication.

Contents

List of symbols and abbreviations

This is the meaning of the symbols and abbreviations encountered in the synopsis, unless otherwise defined in the running text.

Abbreviations	
3-D	Three-dimensional
B&K	Brüel & Kjær
BEM	Boundary element method
DFT	Discrete Fourier transform
DTU	Technical University of Denmark
ESM	Equivalent source method
FFT	Fast Fourier transform
HELS	Helmholtz equation least-squares
IBEM	Inverse boundary element method
IFRF	Inverse frequency response function
LN	Least norm
LS	Least squares
NAH	Near-field acoustic holography
SNR	Signal-to-noise ratio
SONAH	Statistically optimized near-field acoustic holography
Latin symbols	
a	Radius of a sphere
$\mathbf{A}$	Elementary wave matrix in the measurement positions
$\mathbf{A}_s$	Elementary wave matrix in the reconstruction positions
c	Speed of sound in air
$\mathscr{F}, \mathscr{F}^{-1}$	Forward and inverse Fourier transforms
G	Greens function in free-space
G_p	Propagator function of the sound pressure
G_{pu}	Propagators of the pressure-to-velocity cross-prediction
G_{up}	Propagators of the velocity-to-pressure cross-prediction

$h^{(s)}$	Radiation kernel (radiation circle in space domain)
h_n	Spherical Hankel function of the second kind of order n
$\mathbf{I}$	Active sound intensity vector
$I^{(s)}$	Normal component of the supersonic acoustic intensity
I_x, I_y	Tangential active sound intensity in the x and y directions
j	Imaginary number ($\sqrt{-1}$. Note the $e^{j\omega t}$ convention)
j_n	Spherical Bessel function of the first kind of order n
J_1	First order Bessel function of the first kind
k	Wavenumber in air
k_x, k_y, k_z	Wavenumber components in Cartesian coordinates
$\mathbf{n}$	Normal vector
p	Sound pressure
$p^{(s)}$	'Supersonic' sound pressure
p_h	Sound pressure in the hologram/measurement plane
$\mathbf{p}$	Sound pressure vector
P	Wavenumber spectrum of the sound pressure
q_l	Strength of the l^{th} equivalent source
$q(\mathbf{r_0})$	Strength of a continuous distribution of point sources
r, θ, φ	Spherical coordinates (radius, polar angle, azimuth)
$\mathbf{r}$	Position vector
$\mathbf{r}_0$	Equivalent source position
$\mathbf{r}_h$	Measurement position
$\mathbf{r}_s$	Reconstruction position
S_r	Area of the radiation circle
$u^{(s)}$	Normal component of the 'supersonic' particle velocity
u_n	Normal component of the particle velocity
u_z	Component of the particle velocity normal to the z plane
U_z	Wavenumber spectrum of the z-normal component of the particle velocity
x, y, z	Cartesian coordinates
x_h, y_h, z_h	Coordinates of the measurement/hologram plane
x_s, y_s, z_s	Coordinates of the reconstruction plane
Y_m^n	Spherical harmonic function

Greek symbols

ϵ	Regularization parameter
ϕ	Phase across the hologram plane
ρ	Density of the medium
ω	Angular frequency

Chapter 1

Introduction

1.1 Aim of the study

This PhD study examines the use of novel array technology in near-field acoustic holography and sound source identification. The primary purpose of the study is to examine the use of particle velocity measurements and the combination of sound pressure and particle velocity measurements in near-field acoustic holography.

Near-field acoustic holography, most commonly referred to as NAH, is a powerful sound source identification technique, widely used in many areas of acoustics and noise control. The technique makes it possible to extract all the information of the sound field radiated by a source in a very efficient manner, thus providing a very meaningful representation of the acoustic field under examination.

In its original formulation, and until very recently, NAH was exclusively based on sound pressure measurements, via microphone arrays or scanning procedures using microphones. However, in recent years a new type of acoustic transducer is available that makes it possible to measure the acoustic particle velocity directly. It has been shown that near-field acoustic holography can be based on particle velocity measurements using this transducer instead of conventional pressure measurements. The measurement principle seems to have considerable potential, and it is more robust to some of the inherent errors in NAH. This new transducer makes it possible to measure both the sound pressure and the particle velocity simultaneously, which opens yet a new range of interesting possibilities for application in NAH that need to be examined.

The aim of the study is to investigate near-field acoustic holography under the light of the different measurement quantities, i.e., sound pressure, particle velocity, and their combination, and to examine some of the potential advantages that the measurement principles may offer. Three aspects have been examined, the so-called sound field separation techniques on the one hand, which provide a complete solution to the Helmholtz equation, making it possible to distinguish between sound from the two sides of the array. On the other hand, the so-called supersonic acoustic intensity, which is an acoustic quantity that describes the fraction of the acoustic energy flow that is radiated effectively into the far field, has been studied too. Additionally, the possibility of using rigid-sphere microphone arrays for the holographic reconstruction of sound fields has been examined. It is the purpose of this dissertation to present and discuss the contribution of the PhD study, and frame it in the relevant context.

1.2 Near-field acoustic holography (NAH)

There are good reasons why near-field acoustic holography has become an essential sound source identification technique in modern acoustics. It provides a unique insight into how the acoustic output or the structural vibration of a source is coupled to the surrounding fluid medium, and it renders a full description of the sound field, readily providing a tremendous amount of information about the acoustic field under observation. Near-field acoustic holography can be classified as a source identification and visualization technique, which is very well the case. However, from such classification, the full potential of the technique might at first not be realized.

In an acoustical hologram, either captured in the far field or the near field of a source, the essential information of the sound waves present in the medium (i.e., their amplitude and relative phase that describe how they change across space and time), is captured via measurements over a two-dimensional 'aperture'. Making use of this information and the properties of the medium in which the waves propagate, a full three-dimensional representation of the field can be obtained. Hence the etymology of the word 'holo-graph' - from the Greek, whole-drawing - which remarks the vast amount of information contained in a hologram.

In the specific case of near-field acoustic holography, the measurement takes place in the near field of a sound source. As a result, several aspects of holography are fully exploited, in addition to obtaining a three-dimensional representation of the wave field. The near field measurement makes it possible to cover a large solid angle of the source, and by this means, capture its ‘complete’ radiation into the medium. Thus, the truncation error otherwise inherent in far-field holography is partly overcome.

Very importantly, the near field measurement makes it also possible to capture the evanescent waves radiated by the sound source, enhancing the spatial resolution of the technique, to ideally attain unlimited resolution. It should be noted that evanescent waves are waves with a wavelength shorter than the acoustic wavelength in air, and therefore do not propagate effectively but decay exponentially away from the source. By capturing this high spatial-frequency information, NAH overcomes the wavelength resolution limit (contrary to far-field acoustic holography or other sound visualization techniques, such as beamforming, where the spatial resolution is limited by the wavelength in the medium). Consequently, this makes the technique fit for studying sound sources that radiate sound at frequencies in which the wavelength in air is comparable to or larger than the radiator dimensions. This is very useful in order to study sound sources in the low frequency range, structural vibrations below coincidence, etc. It should be noted that although the measurement takes place in the near field, the far-field radiation characteristics of the source are still preserved in the near-field hologram.

In NAH, because the different acoustic quantities are related via the equations of motion, it is possible to predict all of them over the whole three-dimensional reconstruction space, namely, the sound pressure, the full particle velocity vector, hence the sound intensity vector, sound power, and when studying vibrating structural sources, their modal vibration patterns and deflection shapes via the reconstruction of the normal velocity on the boundary. It should also be noted that the technique is valid for the analysis of broadband sound sources.

Based on the foregoing considerations, it could be concluded that near-field acoustic holography makes it possible, based on near-field measurements over a two-dimensional aperture, to reconstruct the entire sound field, i.e., sound pressure, particle velocity vector and sound intensity vector, with nearly unlimited resolution, over a three-dimensional space that extends in principle from the source’s boundary out to the far field. The technique poses some challenges in its implementation in practice, e.g., the back-propagation towards the source is ill-posed due to the presence of evanescent waves, the measurement aperture is discrete and finite, the transducers are not ideal, etc. These challenges will be addressed later.

There exist multiple methods to implement near-field acoustic holography, with different names in the literature. In the next chapter, a detailed overview of the methodologies and denominations is provided.

1.2.1 Use and applications of NAH

There are countless situations in which it is essential for the acoustician to obtain a detailed understanding and a full representation of a certain observed sound field. This is essential in many cases that range, for example, from noise control problems, transportation noise, sound quality design, etc. to musical acoustics, loudspeaker systems, room acoustics, etc. In these cases and in many others, a detailed knowledge of the sound field radiated by a source is very useful, and near-field acoustic holography is a valuable tool for this purpose.

There are some attributes of NAH that make it favorable for a wide range of problems in acoustics. It is a non-contact approach, where complex acoustical mechanisms can be easily studied. No prior knowledge of the source is required, since the acoustical output of the source is measured directly, and the wave field at any other point of the source-free medium can be reconstructed, either via forward propagation towards the far field or back propagation towards the very boundary of the source. Because the air motion on the boundary of the source can be reconstructed, the vibration and deflection shapes of the source can thus be estimated, without restrictions on resolution, as explained in the previous section. The NAH technique is attractive because of its simplicity, ease of calculation, prompt results, etc.

For the above reasons, NAH has become a very popular tool in acoustics, and especially for the study of noise sources, e.g., transportation noise and vehicle interiors, industrial machinery, etc. But because of its fundamental nature, the technique can be used for a wide variety of other applications. To serve as illustration, a few references of applications in transportation and tire-road noise, musical acoustics, room acoustics and loudspeaker design are given below:

- "Sound radiation analysis of loudspeaker systems using nearfield acoustic holography (NAH) and the application visualization system (AVS)," T. Burns, Audio Eng. Soc. Conv. 93, 10 (1992).
- "Practical application of inverse boundary element method to sound field studies of tires," A. Schuhmacher, Proceedings of Internoise '99, Ft. Lauderdale (1999).
- "Interior near-field acoustical holography in flight," E. G. Williams et al., J. Acoust.

Soc. Am. 108(4), (2000).

- "Acoustic radiation from bowed violins," L. M. Wang et al., J. Acoust. Soc. Am. 110(1) (2001).
- "Visualization of acoustic radiation from a vibrating bowling ball," S. F. Wu et al.,J. Acoust. Soc. Am. 109(6) (2001).
- "Violin f-hole contribution to far-field radiation via patch near-field acoustical holography," G. Bissinger, et al. J. Acoust. Soc. Am. 121(6) (2007).
- "Measurement of the sound power incident on the walls of a reverberation room with near field acoustic holography," F. Jacobsen et al., Acta Acust. united Ac., 96(1) (2010).
- "Some characteristics of the concert harp's acoustic radiation," J.-L. Le Carrou et al., J. Acoust. Soc. Am. 127(5) (2010).

1.2.2 Relation to other techniques

In this section, some fundamental differences between NAH and other source identification and localization techniques are outlined. The aim is to note some basic differences that might be useful for illustrating where NAH stands within the different source identification, localization and inverse methods in acoustics.

Beamforming

Beamforming and near-field acoustic holography share some fundamental common background (e.g. they often share the basis functions in which the sound field is decomposed), and are somewhat complementary to each other. Beamforming is mostly a far-field sound source localization technique, based on phased array measurements. An important difference between NAH and beamforming is that beamforming is not a sound field reconstruction technique, and it just provides an approximate relative 'source strength' map, but not a quantitative reconstruction. Another fundamental difference is that in conventional beamforming, the resolution is limited to the wavelength in air. Also, beamforming can easily handle incoherent sources, but not coherent sources, such as reflections, which can give erroneous beamformed maps. In near-field acoustic holography, the coherence assumptions are different, coherent sources are easily dealt with, while incoherent sources require more elaborate processing. This is addressed further in Sect. 2.5 and Paper C.

Sound Intensity

Sound intensity is a well-known and straightforward measurement technique for sound source identification. It is an instantaneous quantity, that can nevertheless be averaged to provide the mean flow of energy and flow direction. It makes it possible to locate acoustic sources wherever a significant net energy flow is injected into the medium. However, a single measurement is not fully representative of a source, and if an intensity map is produced, the positions of the measurement are not inter-related, and it is not possible to predict other acoustic quantities apart from the emitted sound power if a closed surface scan is performed. Besides, with a conventional sound intensity measurement, it is not straightforward to identify possible circulatory flow patterns in the near-field of a source (this is addressed further in Sect. 3.3 and and Papers D, E and F).

Inverse frequency response function (Inverse FRF)

There is a "family" of methods that share a very close connection with acoustic holography. In these methods, the measured waves are decomposed into a multiple origin spherical wave expansion. In other words, the measured sound field is expressed as an approximate integral representation, consisting of a combination of point sources that model the source's radiation. If the measurements are taken in the near-field of the source, the same fundamental principles as in near-field acoustic holography are exploited. Still, these inverse-FRF methods are considered separately from NAH because there is no explicit near-field requirement.

There are several other inverse acoustic methods that will not be covered here, e.g., time reversal, inverse vibro-acoustic methods, etc. Their operating principle is clearly different from NAH. A comprehensive overview of these methods can easily be found in the literature.[1,2]

[1] "The problem of vibration field reconstruction: statement and general properties," Y.I. Bobrovnitskii, J. Sound and Vibration, 247(1): 145-163 (2001).

[2] "Time Reversal," B. E Anderson et al., Acoust. Today, 4(1): 5-16 (2008).

1.3 Measurement of the particle velocity

Finally, to conclude this introductory chapter, some general background on the measurement of the particle velocity is given.

In the mid-nineties a new type of acoustic transducer that could measure directly the acoustic particle velocity field was invented (the Microflown sensor). The transducer is inspired by hot wire anemometers: a wire is heated up by an electrical power so that when exposed to a flow, it is cooled down. Due to the temperature change in the wire, its resistance changes accordingly, producing a variable electrical current directly proportional to the incident flow. Thus, the speed of the air flow can be determined.

A conventional hot wire anemometer is not an appropriate transducer for measuring the acoustic particle velocity, because it is not a constant flow but a vibrational velocity that changes sign within every wave period, fluctuating about the static equilibrium point. The solution that led to the Microflown velocity sensor consists in using two closely placed hot wires, so that the acoustic particle velocity is proportional to the difference in the current through the wires, which results from the temperature difference between them. Thus can the particle velocity and its sign be measured. The measurement of the particle velocity is covered in greater detail in the next chapter.

The immediate application of this sensor is to serve as a sound intensity probe (p-u intensity probe), since sound pressure and particle velocity are measured simultaneously. However, there are other applications where the measurement of the particle velocity has been applied, e.g., impedance measurements, direction of arrival estimation, etc. An interesting application is to use the measurement of the particle velocity for near-field acoustic holography. This is the starting point and fundamental ground of this PhD study.

Chapter 2

Background

The purpose of this chapter is to provide a general background on near-field acoustic holography and the measurement of the particle velocity. The chapter discusses briefly the existing NAH methods, with an emphasis in the methods that have been used and are more relevant to the study. Some other relevant aspects are also discussed, namely regularization methods and coherence in NAH. In section 2.6, some fundamental considerations on the measurement of the particle velocity are discussed.

It is not the purpose of this chapter to re-write the already existing theory, thus, only some essential equations are given. For the detailed theory of the methods used in the study, the reader is referred to the following selected literature: refs. [1–8]

2.1 Origins of near-field acoustic holography

The origins of holography lie in the field of optics, and can be traced back to Dennis Gabor, who in 1948 [9] and 1949 [10] reported the discovery that an optical three-dimensional representation of an object could be obtained based on the interference between a reference illuminating beam and the resulting scattered wavefronts. In other words, when an object is illuminated with a reference light beam, and both the reference beam and the scattered light are recorded simultaneously, it is possible to retain the amplitude and phase properties of the waves, based upon which the scattered light can be reproduced in the absence of the object, providing a three-dimensional image. This was a scientific breakthrough that can be pinpointed as the origin of 'holographic vision'. Gabor's discovery was originally observed in the field of microscopy (with

Gabor's proposal of an 'electron interference microscope'), and soon extended to more general optics and imaging.

Based on these foundations, the theory of optical holography was extended to acoustics during the late sixties [11]. Initially acoustical holography was limited by the wavelength in air, and it was useful at high frequency and ultrasonic applications, but somewhat limited as a general sound source identification technique. However, the potential of the technique proved nevertheless promising.

In 1980, a new acoustical imaging method based on the foundations of holography was presented in the seminal paper by Williams, Maynard and Skudrzyk [12]. This new measurement principle was later to be known as near-field acoustic holography (NAH). The technique made use of the evanescent components present in the near field of sound sources, to achieve 'unlimited' spatial resolution. Furthermore, the imaging principle was based on the active sound radiation by the source, avoiding the need of an 'illuminating' wave field, which would restrict the resolution to the acoustic wavelength in the medium. The technique was briefly presented as well in the Physical Review Letters [13] of the American Physical Society.

In the following years, different work was presented that made use of similar principles, and which exploited the potential of the the spatial Fourier transformation, via FFT algorithms. For example, Stephanisen et al. (1982) [14] explored the forward and backward propagation of acoustic fields by means of FFT methods, in planar and cylindrical coordinates (1983) [15]. Williams et al. (1982) [16] made use of the fact that the 'Rayleigh integral' [17] has a convolutional form and can be evaluated efficiently by means of the FFT. There were other contributions which are not referred to here.

In 1985, the paper 'Near-field acoustic holography : I. Theory of generalized holography and the development of NAH' by Maynard, Williams and Lee was published in the JASA [2]. This paper covers in detail the theoretical foundations of the technique, presents the theory in different coordinate systems, planar, cylindrical and spherical, and discusses in detail its application. This paper has become the most cited reference in the field, although the technique first appeared some years earlier. The paper was followed by a second part, by Veronesi and Maynard (1987) [3], where the practical implementation of the problem, algorithms and the accuracy of the reconstruction were examined in detail.

It could be said that, by then, the foundations of near-field acoustic holography were solidly laid. From there on, and until present day, there has been a growing interest in the field, and many methods, applications, measurement principles, solution schemes, etc. have been developed. Some of these are explained in greater detail in the following.

2.2 Methods

The methods mentioned in the foregoing are based on applying a two-dimensional Fourier transform to the sound field to estimate the wavenumber spectrum, or angular spectrum, which is a representation of the sound field in the spatial-frequency domain [1]. Based on this representation, the entire sound field can be reconstructed in other planes of the medium, either back-propagating towards the source, or forward-propagating away from it.

The wavenumber spectrum of the pressure measured in a plane z_h, can be calculated as

$$P(k_x, k_y, z_h) = \iint_{-\infty}^{\infty} p(x, y, z_h) e^{j(k_x x + k_y y)} dx dy, \tag{2.1}$$

and because

$$P(k_x, k_y, z) = P(k_x, k_y, z_h) e^{-jk_z(z-z_h)}, \tag{2.2}$$

(see for example sect. 2.9 of ref. [1]) it is possible to predict the sound pressure in a different plane z_s,

$$p(x, y, z_s) = \frac{1}{4\pi^2} \iint_{-\infty}^{\infty} P(k_x, k_y, z_h) e^{-j(k_x x + k_y y + k_z(z_s - z_h))} dk_x dk_y. \tag{2.3}$$

The exponential in z can be regarded as a “propagator”,

$$G_p(k_x, k_y, z_s - z_h) = e^{-jk_z(z_s - z_h)}. \tag{2.4}$$

Using Euler’s equation of motion, $u_\chi(\mathbf{r}) = -1/(j\omega\rho)\partial p(\mathbf{r})/\partial\chi$, the three components of the particle velocity can be calculated, and consequently the full intensity vector too. The velocity normal to the reconstruction plane is,

$$u_z(x, y, z_s) = \frac{1}{4\pi^2} \iint_{-\infty}^{\infty} \frac{k_z}{\rho c k} P(k_x, k_y, z_h) e^{-j(k_x x + k_y y + k_z(z_s - z_h))} dk_x dk_y. \tag{2.5}$$

The pressure-to-velocity propagator is then

$$G_{pu}(k_x, k_y, z_s - z_h) = \frac{k_z}{\rho c k} e^{-jk_z(z_s - z_h)}. \tag{2.6}$$

There exist some practical limitations to the above described theory. Ideally, the sound field should be known over a continuous infinite aperture. In practice this is not the case, and the transformation to the wavenumber spectrum and back to the spatial domain is done via DFT's (discrete Fourier transforms), most commonly via the very efficient FFT algorithm, based on a discrete approximation of the problem. Consequently, this gives rise to the characteristic sources of error associated to the DFT (wraparound error, wavenumber leakage, etc.) [1, 18]. Besides, the evanescent waves, which are high spatial-frequency waves outside the radiation circle,[1], decay exponentially with the distance. Therefore, they are exponentially amplified in the back-propagation process. Some of the high spatial frequency components in the wavenumber spectrum do not contain any significant information about the sound field, but just background noise. These noisy components are blown up without bounds in the back-propagation. This is why the NAH source reconstruction is an ill-posed problem, and requires regularization. A straightforward solution is to filter out the high frequency components that are known a-priori to carry no information. The cut-off frequency of the filter can be determined based on the signal-to-noise ratio of the measurement and the stand-off distance from the source [1]. Alternatively, regularization techniques can be used (see Sect. 2.4).

A very complete overview of the Fourier based NAH technique is given in refs. [2] and [3]. The book Fourier Acoustics [1] is a reference text that covers in a very comprehensible manner the theory of NAH, as well as the foundations upon which it is based.

Loyau, Pascal and Gaillard (1988) [19] presented a method called broadband acoustic holography from intensity measurements (BAHIM), which has the potential of estimating the phase of the acoustic waves based on the tangential acoustic intensity. This follows from the fact that the phase gradient in the hologram plane is directly pro-

[1] The radiation circle corresponds to the limit determined by the wavenumber in air or other medium at a specific frequency $k = 2\pi f/c$ (c is the speed of sound) that indicates which plane waves are propagating and which are evanescent, depending on their spatial frequency. See chapt. 2 of ref. [1]

portional to the ratio between the active intensity and the quadratic pressure. This can be understood from the relationship [19]:

$$\mathbf{I}(\mathbf{r}) = \frac{|p(\mathbf{r})|^2}{2\rho c} \frac{-\nabla\phi(\mathbf{r})}{k}. \tag{2.7}$$

Thus, the phase of the sound pressure in the wavenumber domain can be determined as

$$\begin{aligned} \phi(k_x, k_y) = -2j\omega\rho \Bigg[\frac{k_x}{k_x^2 + k_y^2} \cdot \mathscr{F} \left\{ \frac{I_x(x,y)}{|p_h(x,y)|^2} \right\} \\ + \frac{k_x}{k_x^2 + k_y^2} \cdot \mathscr{F} \left\{ \frac{I_y(x,y)}{|p_h(x,y)|^2} \right\} \Bigg], \end{aligned} \tag{2.8}$$

from which the phase in space domain can be obtained via an inverse-Fourier transform $\phi(x, y) = \mathscr{F}^{-1}\{\phi(k_x, k_y)\}$. These relations show that it would be possible to extract the phase of a hologram (of a stationary sound field) based on a sequential scanning of the hologram's tangential intensity vector, without using reference transducers or measuring all hologram positions simultaneously. The technique poses nevertheless some measurement challenges. Equation (2.8) is singular, due to the $k_x^2 + k_y^2$ term in the denominators, that is at the origin of the radiation circle. This effect can be mitigated by smoothing the singularity, for instance by interpolating, or as in ref. [16]. Additionally, the tangential sound intensity decays slowly toward the edges of the aperture, which makes the method subject to measurement truncation error.

Hald (1989) [20] proposed a method that makes it possible to apply NAH to incoherent sound fields. The method was called spatial transformation of sound fields (STSF). It addresses a very relevant situation in general noise problems, namely that NAH in its simple stationary form cannot deal with incoherent noise sources, because it relies on the waves being mutually coherent, i.e. having a well-defined phase relationship. The method is a multi-reference procedure, where the references are used to extract a set of partial holograms, corresponding to the incoherent source mechanisms. More on this subject is covered in Sect. 2.5 and in Paper C.

One of the limitations of the original Fourier based NAH is that it is limited to separable geometries (by using planar, cylindrical or spherical coordinates). The limitation stems from the fact that the holographic reconstruction is valid only in the free-field medium where the waves propagate. Thus, if the sound field on the boundary of an arbitrary shaped source should be reconstructed, an alternative approach to Fourier-NAH is needed. This need gave rise to a new type of inverse holographic methods that are based on the numerical discretization of the Helmholtz integral equation. These methods are in essence an inverse formulation of the well-known boundary element method (BEM), thus they are commonly known as 'Inverse BEM' or 'IBEM'. Veronesi and Maynard (1989) [21] studied the numerical evaluation of the Helmholtz integral equation for relating the measured pressures in the medium to the velocity on the boundary of the source. In order to solve the inverse problem, a singular value decomposition of the transfer matrix is used, where the singular values associated with noise can be filtered out. This is equivalent to the filtering of the high spatial frequency components used in Fourier-based NAH. This was also shown by Kim and Lee (1990) [22], and by Bai (1992) [23], who examined extensively the direct BEM formulation applied to the holographic reconstruction of sound fields. Other approaches are based on an indirect BEM formulation, as those by Zhang et al. (2000) [24] and Schuhmacher et al. (2003) [25].There have been many other contributions to the Inverse BEM, e.g. refs. [26–28]. A good overview is given by Valdivia and Williams (2004) [29], and by Ih (2008) in Chap. 20 of the book in ref. [30].

Statistically optimized near-field acoustic holography, often referred to by its acronym: SONAH, is another popular holographic method that is closely related to Fourier based NAH, although this might not be apparent at first sight. The method can be categorized as an elementary wave model, because the measured sound field is expanded into a set of waves with associated coefficients that are determined in a least-squares/norm sense. Let the case of SONAH in planar coordinates be considered: The hologram, or measured field, can be decomposed into a set of plane waves, each of the waves with an amplitude and phase coefficient. Any sound field can be decomposed into such an orthogonal basis, which is essentially a Fourier expansion. However, in this case the system is not solved explicitly by means of a Fourier transform as in Eq. (2.1), but instead it is calculated implicitly, directly in the space domain. The coefficients of the waves are solved in a least squares sense, with optimal average accuracy, to fit the measured data. Based on the waves and estimated coefficients, the sound field can be calculated at any other plane via this expansion. In reality, the method operates into a single 'step', and the measured sound field in the hologram plane is projected directly into the reconstruction plane by means of a transfer matrix that accounts for the propagation of the waves from one plane to the other. This is apparent from the reconstruction equation [4],

$$\mathbf{p}(\mathbf{r}_s)^T = \mathbf{p}(\mathbf{r}_h)^T(\mathbf{A}^H\mathbf{A} + \varepsilon\mathbf{I})^{-1}\mathbf{A}^H\mathbf{A}_s, \tag{2.9}$$

where the term $(\mathbf{A}^H\mathbf{A} + \varepsilon\mathbf{I})^{-1}\mathbf{A}^H$, is the regularized pseudo-inverse of the elementary wave matrix in the measurement plane (LN solution), $\mathbf{I}$ is the identity matrix and ε the regularization parameter [31], and $\mathbf{A}_s$ is the elementary wave matrix in the reconstruction plane. Note that the transfer matrix projecting the acoustic field from $\mathbf{r}_h$ to $\mathbf{r}_s$is independent of the measured data (in the same way as the wavenumber domain propagator of the Fourier based NAH, is also independent).

The wrap-around error in SONAH can be completely overcome by using a continuous wavenumber representation (see sect. II.B. of ref. [4]), and the amplitude and phase of the elementary waves is adjusted to match the sound field inside the measurement aperture optimally. Consequently, the errors associated to the truncated finite measurement aperture are less severe than if the wavenumber spectrum was calculated directly by means of a DFT. The method is a 'patch' method, because it does not require that the measurement aperture is significantly larger than the source, but can be comparable to the dimensions of the source, or the source's region of interest. Like Fourier based NAH, the method is limited to separable geometries.

SONAH was first described by Steiner and Hald (2001) [32]. It has also been described and examined in conference proceedings [33] and technical notes [34], and described for cylindrical coordinates [35]. A very complete and detailed description of the method is found in a recent paper by Hald (2009) [4].

Another widely used method in near-field acoustic holography is the method of wave superposition or equivalent source method (ESM). This method is particularly attractive because it can handle sources with arbitrary geometry and it is computationally very light. It is simple and also its implementation is rather straightforward. The method of wave superposition was originally proposed by Koopman et al. (1989) [5]. The essential idea is that, given a certain sound source, the prescribed sound field on the boundary of the source can be 'replaced' by a superposition of the acoustic fields radiated by a distribution of point sources (the sound field radiated by the original source is expressed as a combination of the fields radiated by point sources). This can be seen as a multiple origin spherical wave expansion, and in that sense regarded as an elementary wave model. Koopmann et al. (1989) [5] show in their paper that the method is equivalent to the Helmholtz integral equation. Originally, the method was used for sound radiation and scattering problems, as an alternative to other numerical methods of greater computational complexity [36–39].

Sarkissian (2004) [40] proposed to use the method in connection to near-field acoustic holography, as a means to artificially extending the measurement aperture, or compensating for missing data. Soon after, Sarkissan (2005) [6] proposed to use the method to directly reconstruct the sound field in the surface of the source, because it is possible to obtain a holographic reconstruction of the field based on this point source expansion.

The acoustic pressure field produced by a source at a certain point in space $\mathbf{r}$ can be expressed as the contribution from the continuous distribution of point sources in $\mathbf{r}_0$, $q(\mathbf{r}_0)$, enclosed in the volume V (in the exterior problem):

$$p(\mathbf{r}) = jw\rho \int_V q(\mathbf{r}_0) G(\mathbf{r}, \mathbf{r}_0) dV, \tag{2.10}$$

where $q(\mathbf{r}_0)$ is the the strength of the point source distribution at $\mathbf{r}_0$ inside of the source volume V, and $G(\mathbf{r}, \mathbf{r}_0)$ is the Green's function in free space between the point $\mathbf{r}_0$ and the point $\mathbf{r}$ in the domain, defined as

$$G(\mathbf{r}, \mathbf{r}_0) = \frac{e^{-jk(|\mathbf{r}-\mathbf{r}_0|)}}{4\pi|\mathbf{r}-\mathbf{r}_0|}. \tag{2.11}$$

In a discrete form, the measured pressure in the hologram can be expressed in terms of the equivalent sources as

$$p(\mathbf{r}_h) = j\omega\rho \sum_{l}^{N} q_l G(\mathbf{r}_h, \mathbf{r}_{0l}), \tag{2.12}$$

from which the strength of the sources can be calculated via a regularized inversion, and the reconstructed sound pressure and the particle velocity with Euler's equation, can be estimated as

$$p(\mathbf{r}_s) = j\omega\rho \sum_{l}^{N} q_l G(\mathbf{r}_s, \mathbf{r}_{0l}) \tag{2.13}$$

$$u_n(\mathbf{r}_s) = -\sum_{l}^{N} q_l \frac{\partial G(\mathbf{r}_s, \mathbf{r}_{0l})}{\partial \mathbf{n}}. \tag{2.14}$$

The equivalent source method is also a patch method, it does not require full measurement over the entire surface of the source. Furthermore, the method can handle arbitrary geometries, and it is computationally much more efficient than the inverse-BEM. The method can be seen as a discrete implementation of the indirect formulation of the boundary element method. Valdivia and Williams (2006) [41] compared the IBEM and ESM, and showed that the accuracy of the two methods on the whole is similar. It should be noted that the point sources used for the model are singular, and it is crucial to retract them from the actual source surface where the sound field is reconstructed, to avoid the singularity. The accuracy of the method depends on how the equivalent sources are distributed: where are they placed, and how many are used. Sarkissan (2005) [6] suggests to retract the equivalent sources approximately by one lattice spacing (or grid interspacing distance), and Valdivia and Williams [41] recommend it to be between one and two lattices. These are perhaps the commonly accepted distributions as a rule of thumb. Bai et al. (2011) [42] recently studied the optimal retreat distance for the ESM-based NAH, and the results indicate that the optimal distance is of about 0.5 lattice spacing for planar sources, and of about 0.8 to 1.7 for spherical sources. These recommendations differ somewhat from the those in refs. [6, 41].

It seems that as a common practice, there should be as many equivalent sources as measurement points (there could be more, but in most cases this would not improve the results), and they should be distributed as the measurement points. Nevertheless, there does not seem to be an absolute guideline, and it is probably left to scientific judgment to decide when the above general guidelines should or not be followed. In an early stage of this project, a numerical study was conducted to examine different equivalent source distributions for the case where the sound coming from beyond the extent of the aperture ought to be accounted for (see Paper I). The study shows that distributing the equivalent sources beyond the area covered by the measurement aperture is the most accurate solution in this case (an underdetermined system with more equivalent sources than measurement positions is posed).

To the author's knowledge, the first NAH elementary wave model to be described in the literature was the so-called Helmholtz least squares method, proposed by Wang and Wu (1997) [43]. The method is often known by its acronym, HELS, and occasionally it is referred to as single origin spherical wave expansion (SOSWE) [44]. The method is based on an elementary wave expansion, where the sound field radiated by the source is approximated by a set of spherical waves (either spherical harmonics or any orthonormal series of functions that can be calculated from a Gram-Schmidt orthonormalization. In the latter case, the independent functions can be adapted to sources with arbitrary geometry [43]), minimizing the residual in a least squares sense. As in the other elementary wave models, once the coefficients of the expansion are determined, the sound field at a different location can be predicted. The method has also been applied in combination with the inverse-BEM [45]. The HELS has not been used in the present study, thus, the reader is referred to the relevant literature for further details. See for example refs. [43, 46, 47].

The last three methods that have been described in the foregoing are 'patch methods', because they do not require that the measurement aperture is significantly larger than the source. Contrarily, Fourier based NAH in its simple form requires that the sound field is known over a surface larger than the source and that the field has decayed sufficiently at the edges. If this requirement is not fulfilled, an error due to the finite measurement aperture is introduced. One approach to overcome this is to window the measured data to zero, but this is at the expense of discarding some meaningful information. An interesting solution to overcome this problem is to artificially extend the measured data outwards from the measurement aperture. Saiyou et al. (2001) [48] and Williams et al. (2003) [49, 50] suggested to use an iterative procedure that extends the pressure field outwards from the aperture and eventually converges to zero at the far end of the extrapolated area. The method uses either FFT or singular value decomposition (SVD), and makes use of a regularization filter with a regularization parameter determined by the Morozov discrepancy principle. This artificial extension has also been used in an analogous manner with the Inverse BEM [51, 52]. Other methods have also been suggested to extend the measurement aperture [53, 54].

It could be possible to extrapolate the sound field tangential to the aperture based on an extended equivalent source distribution. An extended equivalent source method formulation could be used, as in Paper I (sect. 4), measuring the field over a limited patch, and calculating the strength of the extended distribution of equivalent sources. The sound pressure can then be calculated in the measurement plane over an aperture larger than the patch, thus 'extending' the measurement data. The magnitude of the larger and smaller singular value in the inversion of the transfer matrix of the underdetermined system is an indication of how meaningful the extrapolation is, and if the underdetermination is critical [55]. This approach was investigated in an initial stage of the project, and yielded satisfactory results. However, it was not pursued further due to the fundamental question that, once an equivalent source model is developed for the problem, it can well be used for the reconstruction of the field directly rather than to be used as an input to another method, thus solving the problem twice.

This section intends to provide a modest overview of existing holographic methods, with an emphasis on the ones that have been used in the project. Good overviews of NAH that focus more on other methodologies can be found in the literature, for instance in the papers by Wu (2008) [56] and Magalhaes and Tenenbaum (2004) [57].

2.3 Time domain NAH

It should be noted that NAH has the potential of studying sound fields in time domain if the hologram data is acquired simultaneously at all measurement positions. This potential was foreseen from the early stages of the technique [2], and it has often been examined [58–60]. Because this aspect has not been studied or used in this thesis, the reader is referred to the literature for an overview [61].

2.4 Regularization

As mentioned in Sect. 2.2, the back-propagation in near-field acoustic holography is an ill-posed inverse problem due to the presence of strongly decaying evanescent waves in the measurement data. In the back-propagation, the evanescent waves are amplified exponentially because of having an imaginary valued k_z, as can be seen from the propagator operator in Eq. (2.4). Thus, noise at high spatial frequencies will be amplified without bounds leading to meaningless results.

This is a problem encountered in many disciplines (seismic exploration, astronomy, image processing, meteorology, etc.; mostly ill-conditioned problems governed by a Fredholm integral equation of the first kind), that has been studied in detail, and there exist a number of methods and solutions to it. In general, a discrete inverse problem can typically be expressed in matrix form as a $\mathbf{Ax} = \mathbf{b}$ generic system, where $\mathbf{b}$ is typically noisy data known from measurements, $\mathbf{A}$ is an ill-conditioned transfer matrix that relates the measured field with the unknown $\mathbf{x}$. Because of $\mathbf{A}$ being ill-conditioned, the solution of the system via the inversion or pseudo-inversion of $\mathbf{A}$ ought to be regularized to arrive to meaningful solutions of $\mathbf{x}$.

An intuitive manual solution in NAH is to determine a cut-off spatial frequency above which no physical information is expected, and low pass filter the solution to preserve the meaningful frequencies and discard the noisy high spatial frequencies in the reconstruction [1].

A more elaborate solution is to solve the problem using regularization methods, which automatically can provide a 'smooth' and meaningful solution to the problem where the influence of noise is minimized. This is typically done by studying the residual of the regularized solution relative to the measured data or other a-priori known information. The regularization parameter, which reflects the transition point from meaningful data to noise, can be chosen via automated criteria such as the L-curve criterion or generalized cross-validation (these were the criteria used in this study, with Tikhonov regularization [62]).

Williams (2001) [63] gives an overview of regularization methods for near-field acoustic holography. Other recommended references are the well-known paper by Hansen (1992) [31], where different methods and criteria are discussed, and his book (1998) [64] that covers the topic widely. A didactic introduction to the fundamentals of inverse problems and regularization methods was recently published also by Hansen (2010) [65]. Other well-known references are [66, 67].

2.5 Coherence

When NAH is applied to a stationary sound field that is described harmonically, in a time independent way, the sound sources under study must be mutually coherent (more on this fundamental question is discussed in Paper C). If a sound field is composed of incoherent sources that contribute to the acoustic hologram, it is necessary to separate these contributions into a set of partial holograms, to be processed independently, so that a meaningful representation of the sound field is achieved, and the reconstruction is valid. This is essentially a particular case of the well-known multiple input/output problem, that has been widely studied since the seventies [68]. There exist several methods to deal with this problem, the best-known are perhaps *conditioned spectral analysis* [68, 69] and *virtual coherence* [70].

To the author's knowledge, Hald (1989) was the first author to propose a method of solving the multiple input/output problem in near-field acoustic holography [20]. The technique not only makes it possible to separate the hologram into several coherent partial holograms, but also makes it possible to apply scan-based NAH to incoherent sound sources by means using a set of fixed references. The method makes use of a singular value decomposition as in ref. [70] to separate the partial holograms. Hallman and Bolton (1992,1994) [71, 72] proposed a method that is based on conditioned spectral analysis as in ref. [68] to separate the holograms based on multiple coherence, or Cholesky elimination. The two approaches were examined and compared by Tomlinson (1999) [73]. Nam and Kim (2001, 2004) [74, 75] proposed a method for optimally selecting a set of virtual references located at the pressure maxima of the source plane, and Kim et al. (2004) [76] proposed a similar method based on the maximization of the MUSIC power [77]. Kwon et al. (2003) [78] suggested a scan-based multi-reference NAH procedure based on measuring transfer functions and the averaged auto-spectra of the references to estimate the partial holograms. The technique guaranties stability of the estimation in the case of non-stationarity of the source during the scanning procedure. Lee and Bolton (2006) [79] examined further the influence of noise and source level variation on this method, considering the case where the cross-spectral matrix is full-rank due to noise. A similar methodology was proposed and studied by

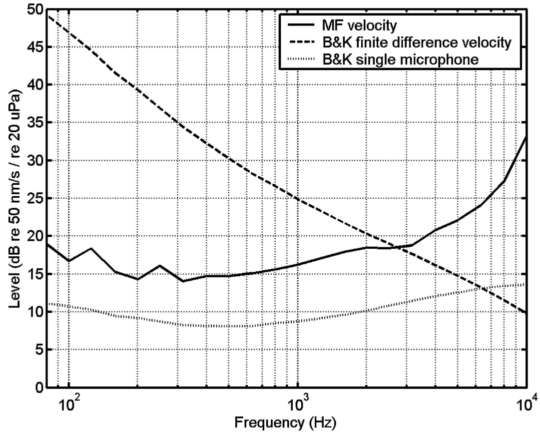

Figure 2.1: (From ref. [83]) Electrical noise of the Microflown in one-third octave bands compared with the noise in the particle velocity measured with a two-microphone B&K sound intensity probe with a 12-mm spacer, and with the noise of a single pressure microphone of type B&K 4181.

Leclère (2009) [80], who considered both the conditioned spectral analysis and the virtual source analysis approaches.

2.6 Measurement of particle velocity

This section includes an overview and some considerations about the measurement of the particle velocity. There have been attempts to measure the acoustical particle velocity vector since almost a century ago [81]. It is a well-known fact that the particle velocity vector is proportional to the gradient of the sound pressure, as apparent from Euler's equation of fluid motion. Consequently, it is in principle possible to estimate the particle velocity based on a finite difference approximation of the sound pressure. One could measure the sound pressure at two closely spaced points, and calculate the particle velocity component in the axial direction based on the time integrated difference of the measured pressures. This intuitive approach results in the fact that the noise from the two microphones is added up, and the time integration introduces an angular frequency factor that boosts the low frequency noise, as shown in Appendix A of ref. [82].

It can be shown that the signal-to-noise ratio of the pressure finite difference technique is [82]

$$SNR_u = 10\log\frac{S_{uu}(\omega)(\rho c)^2(k\Delta r)^2}{2S_{nn}(\omega)}, \tag{2.15}$$

where S_{uu} is the power spectrum of the particle velocity and S_{nn} is the uncorrelated noise. Thus, compared to the SNR of a conventional condenser microphone, the signal to noise ratio is reduced by $10\log(2/(k\Delta r)^2)$. This makes the technique critically noisy at low frequencies (it is valid only if $k\Delta r < 1$). Additionally, for estimating the particle velocity based on a finite difference approximation it would be essential that the microphones are well matched both in phase and in amplitude [82].

It seems that the finite different measurement of the particle velocity has some serious limitations, and the most severe is perhaps the low signal-to-noise ratio. This is particularly critical for NAH applications, because the evanescent components would be easily lost into the background noise. Furthermore, it would be very difficult to measure at low frequencies, where the technique is particularly useful.

Attempts have been made to measure the particle velocity using hot wire anemometers [84, 85], although not entirely successful. In the mid-nineties an acoustical particle velocity sensor that can measure directly the particle velocity became available (the Microflown). The technique uses the fundamental principle of hot wire anemometry, but using two wires in order to determine the instantaneous direction of the moving air. The technique is well described in the literature [7, 83, 86–88].

The principle of measuring directly the particle velocity is promising and has a remarkable potential. The measurement technique has however some limitations, and poses some challenges. An important aspect is the calibration of the probes: there is not a simple, accessible and straightforward way of calibrating the velocity probes. A detailed study of calibration can be found in ref. [88]. Apart from the calibration, the signal-to-noise ratio of the particle velocity transducer is definitely better than the alternative pressure finite-difference method, but it is still not as good as the one of a condenser microphone of comparable sensitivity (see Fig. 2.1 above) [89]. Also the frequency response of the transducer rolls off at high frequencies due to diffusion effects and the thermal heat capacity of the wires, although this can to some extent be compensated by electronic amplification. On the whole, it could be said that this is a 'young' technology in acoustics, and there is naturally room for technical improvement.

Chapter 3

Contributions

The purpose of this chapter is to place the contributions of the PhD study in a context. A literature review is provided where the publications by the author are included and discussed. This chapter is concerned with the existing knowledge that is closely related to the topic of this PhD study. The chapter discusses near-field acoustic holography based on velocity measurements, sound field separation methods, the far-field radiation from sources based on the supersonic acoustic intensity, and the holographic reconstruction of sound fields based on spherical microphone arrays.

3.1 Velocity based NAH

Using the particle velocity sensor (Microflown) described in the previous chapter, Jacobsen and Liu (2005) [7] proposed to use the normal component of the particle velocity as the input for the near-field acoustic holography reconstruction. They examined the measurement principle in connection with Fourier based NAH for planar geometries, and found out that NAH with velocity measurements has some advantages and interesting properties compared to NAH based on sound pressure measurements.

An immediate advantage of the technique is that the normal component of the particle velocity field decays faster than the pressure at the edges of the aperture, i.e. the normal velocity decays very rapidly beyond the extent of the source, unlike the pressure. Thus, the truncation error due to the finite aperture is reduced significantly and it is less costly to measure the complete field radiated by the source. Another advantage is that the inverse NAH problem is more robust to measurement noise when measuring velocity than when measuring sound pressure. In the ‘cross-prediction’[1] from pressure to velocity, the ‘noisy’ high spatial frequencies are amplified, whereas in the cross-prediction from velocity to pressure, they are attenuated: the particle velocity is proportional to the gradient of the sound pressure, and to obtain the sound pressure from the measured velocity, the velocity is integrated, which is a smoothing operation that attenuates the high spatial frequencies. This becomes clear when looking at it from the wavenumber spectrum, as follows.

In the case of planar velocity-based NAH, the relevant reconstruction equations are analogous to Eqs. (2.1) to (2.6) [7]:

$$U_z(k_x, k_y, z_h) = \iint_{-\infty}^{\infty} u_z(x, y, z_h) e^{j(k_x x + k_y y)} dx dy, \tag{3.1}$$

and the normal velocity can be predicted in a different plane as,

$$u_z(x, y, z_s) = \frac{1}{4\pi^2} \iint_{-\infty}^{\infty} U_z(k_x, k_y, z_h) e^{-j(k_x x + k_y y + k_z(z_s - z_h))} dk_x dk_y. \tag{3.2}$$

Making use of Euler’s equation, the pressure can also be calculated as,

$$p(x, y, z_s) = \frac{1}{4\pi^2} \iint_{-\infty}^{\infty} \frac{\rho c k}{k_z} U_z(k_x, k_y, z_h) e^{-j(k_x x + k_y y + k_z(z_s - z_h))} dk_x dk_y. \tag{3.3}$$

When measuring the normal velocity in the acoustic medium, the propagator operator in order to predict the velocity on the reconstruction plane is the same as the pressure to pressure one [Eq. (2.4)]. However, a fundamental difference exists in the cross-prediction from particle velocity to sound pressure. In this case, the velocity-to-pressure propagator has the form,

$$G_{up}(k_x, k_y, z_s - z_h) = \frac{\rho c k}{k_z} e^{-jk_z(z_s - z_h)}. \tag{3.4}$$

Comparing this expression with Eq. (2.6), it can be seen that the pressure-to-velocity transformation amplifies the high spatial frequencies due to the k_z/k ratio, because the numerator of the propagator contributes to increasing their amplitude. Contrarily, the velocity-to-pressure transformation [Eq. (3.4)] is much more robust to measurement

[1] Cross-prediction refers to predicting either the sound pressure from the measurement of the particle velocity, or the particle velocity from the sound pressure

noise, because it is subject of a k/k_z ratio that contributes to decreasing the weight of high spatial frequencies and improve the ill-conditioning of the inverse problem (as was explained in the foregoing, the high spatial frequencies are responsible for the ill-conditioning). It should be noted that the velocity-to-pressure transformation has a singularity at $k_z = 0$. This is a well-known phenomenon that can be solved, for example as in ref. [16].

There are practical challenges associated with particle velocity measurements. On the one hand the calibration of the velocity probes is not straightforward. A similar approach as in ref. [88] can be used to calibrate an array of particle velocity transducers, namely, expose the probes to an 'a priori' known sound field, where the pressure-velocity ratio is known. On the other hand, the dynamic range of the velocity probes is poorer than the one of high-quality condenser microphones [83]. This could result in the fact that some of the evanescent components could more easily be lost in background noise. In spite of the possible experimental shortcomings, the principle of using velocity measurements in NAH has some very advantageous properties.

Leclère and Lauglanget (2008) [90] proposed to measure the normal component of the particle velocity using a light membrane and a laser vibrometer. The mass of the membrane affects the acoustic field at high frequencies, which can to some extent be compensated via a mass correction term. Based on this alternative measurement principle, velocity-based NAH can also be applied [91].

Soon after the paper by Jacobsen and Liu (2005) was published, the measurement principle was applied to other holographic methods. Jacobsen and Jaud (2007) [8] examined the application of velocity measurements to statistically optimized near-field acoustic holography (SONAH). Similar advantages as in ref. [7] were found. Nevertheless, the better conditioning of the velocity based method with respect to noise is more relevant in this case, because the truncation error in SONAH is not as critical as in Fourier based NAH. The study also examined the possibility of combining sound pressure and velocity measurements for the reconstruction, which makes it possible to distinguish between sound coming from the two sides of the array. This is further explained in the next section.

Zhang et al. (2009) [92] proposed a velocity based patch-NAH method, using a continuation of the acoustic field beyond the measurement aperture as in ref. [49].

Zhang et al. (2009) [93] also examined the use of particle measurements as the input for the ESM-based NAH, with similar findings. In this case, the reconstruction of the sound field based on combined pressure-velocity measurements was also considered.

Particle velocity measurements have also been used in combination with the inverse boundary element method. Valdivia et al. (2008) [52] examined an IBEM method based on Cauchy data, that is, based on the measurement of the pressure and its gradient. However, the measurement of the gradient was approximated from the sound pressure measured in two conformal apertures. Langrenne et al. (2009) [94] examined the combined measurement of sound pressure and particle velocity for the Inverse-BEM. The method was based on an earlier paper (2007) that proposes a BEM method using double layer pressure measurements, with the purpose of applying NAH in an enclosed environment [95]. Recently, Langrenne and Garcia (2011) [96] have proposed a method based on the sound pressure and gradient of the sound pressure to solve the Helmholtz integral equation over the domain, both directly, and also using a Steklov-Poincaré formulation. To date, the method has only been demonstrated via simulated examples. There exist other source identification methods that also make use of sound pressure and particle velocity measurements, e.g. ref. [97].

3.2 Sound field separation methods

Since the beginnings of near-field acoustic holography, it became clear that its application in reverberant environments had limitations, and this was outlined as an area of future development [2]. The limitation results from the fact that the method assumes that a source is radiating into a free field, and the sound measured in the hologram is assumed to be coming only from that side of the array. Therefore, sound waves coming from the opposite side are attributed to the 'source' side. There exist methods, often referred to as sound field separation methods, that make it possible to distinguish between sound from the two sides of the array. They rely on estimating the propagation direction of the acoustic waves, in order to distinguish between waves traveling from one or the other side. They offer a complete solution to the Helmholtz equation in the sense that both outgoing and incoming waves are considered.

A very common basis for the separation methods, and the first one that was examined, is to measure the sound pressure on two closely spaced conformal surfaces. Based on the phase shift due to the propagation between the two surfaces, the direction of the waves can be estimated. Already in ref. [2], it was suggested that a technique using measurements over two closely spaced parallel planes could be used in combination with NAH, as done by Weinreich and Arnold (1980) [98]. These ‘p-p’ separation techniques were widely used for reflection and scattering problems, as the methods proposed by Tamura (1990,1995) [99, 100] based on the spatial Fourier transformation of the sound field in planar coordinates, or Cheng et al. (1995) [101] in cylindrical coordinates. The principle of measuring in two parallel planes in order to distinguish between sound traveling from the two sides was also applied to sound radiation problems and near-field acoustic holography. Villot et al. (1992) [102], Hallman and Bolton (1994) [103] and Hallman et al. (1994) [104] applied it to sources in interior spaces, such as rooms or vehicles. Williams (1997) [105] also formulated the Fourier based NAH method for outgoing and incoming waves. Hald (2006) [106] proposed and examined the possibility of applying this double layer pressure measurements to statistically optimized near-field acoustic holography. This methodology is also described in ref. [4], where the extension to more measurement planes over a volume is also discussed. Langrenne et al. (2007) [95] proposed an inverse-BEM technique to recover the free-field radiation by a source radiating in an enclosed or bounded environment. The method compensates for the back-scattering of the source, so that the actual radiated free-field is recovered. Valdivia et al. (2008) [52] studied the possibility of using the inverse-BEM with patch measurements. If the patch is in an interior space, and there is significant radiation from the back side of the array, the estimation is much more accurate if measuring the pressure and pressure gradient (Cauchy data) in two conformal patches, so that the back-side radiation is taken into account. Bi et al. (2008) [107] proposed a separation method based on the equivalent source method that also made use of sound pressure measurements in two conformal surfaces.

When Jacobsen and Jaud (2007) [8] examined SONAH with particle velocity measurements, they proposed the possibility of using the combined measurement of sound pressure and particle velocity as a means to distinguish between sound coming from the two sides of the array. The study demonstrated that the approach is feasible, although it only improves the reconstruction when the magnitude of the disturbing sound from the back is significant. Jacobsen et al. (2008) [89] also compared the performance of the p-p and the p-u separation methods, concluding that their overall accuracy is similar. The two previous studies (refs. [8] and [89]), pointed out the so called ’p-u mismatch’ error, which is an error that stems from the fact that the separation method relies critically on the pressure- and velocity-based estimates of the sound field being identical. To minimize this error, a proper calibration of the p-u probes is essential. Nevertheless, regardless of the calibration, this error is inherent to the technique and cannot be completely overcome in practice.

Zhang et al. (2009) [108] proposed a modification to the SONAH 'p-u' method suggested in [8]. The latter method implicitly requires that the outgoing and incoming waves that model the sound field are scaled in planes symmetrical to the measurement surface (the so-called virtual source planes are equidistant to the measurement plane). This is a fair assumption if the sources are placed symmetrically with respect to the measurement plane. However, if the sources at the two sides of the array are not symmetrical, it can be more accurate to express the problem in terms of two independent transfer matrices that model separately the outgoing and the incoming waves, as pointed out by Zhang el al. [108]. Thus, the waves can be scaled in different source planes depending on the specific location of the sources.

The separation principle based on pressure and velocity measurements has also been applied to the equivalent source method. Bi and Chen (2008) [109] examined such an ESM based separation method, where the particle velocity was measured using a pressure finite difference, which admittedly yielded an error greater than expected. Zhang (2009) [93], also suggested a pressure-velocity based separation method using the ESM. In the formulation, a symmetric matrix for the outgoing and incoming sound waves was used.

Langrenne et al. (2009) [94] proposed a separation technique based on the Inverse-BEM, analogous the one in ref. [95], using combined sound pressure and pressure gradient data. In this case, the particle velocity was measured directly with a particle velocity sensor rather than based on two microphone layers. The aim of the method is to recover the free-field radiation from the source. For this purpose, the incident field on the source is calculated, and applying the rigid reflection boundary condition (assuming that the source is rigid) it is possible to compensate for the back-scattered field from the source.

Paper A (Fernandez-Grande and Jacobsen (2011) [110]) proposes a new measurement principle based on the double layer measurement of the particle velocity. The aim of the methodology is to overcome some of the errors associated with the p-p and the p-u separation methods. Namely, because the method is only based on velocity measurements, it circumvents the 'p-u mismatch' error, and it only makes use of 'velocity-to-pressure' cross-predictions, rather than the more inaccurate 'pressure-to-velocity' ones. The method seems particularly favorable for recovering the normal velocity field. Consequently, Paper A proposes and examines the method for separating the particle velocity field only [110]. The method is based on a SONAH formulation, and was compared with a p-u method and with the direct reconstruction of the field.

Paper B (Fernandez-Grande et al., manuscript) proposes a technique based also on the measurement of the particle velocity in a double layer configuration, applied to the equivalent source method. This paper complements Paper A [110], by extending the measurement principle to the equivalent source method and by conducting a broader study, considering both the separation of the sound pressure and the particle velocity. The study analyzes the case of a source radiating in an enclosed space, which is perhaps the most common example where sound field separation techniques can be useful (when there are coherent sound waves incoming onto the source). The study shows that this separation principle retains some of the useful velocity-based NAH properties, combined with the ability to distinguish sound from the two sides of the array. The technique is useful in the case that there is a significant disturbance of the measured field.

Paper C (Fernandez-Grande and Jacobsen., manuscript) examines a fundamental question that can be of importance for separation methods. The study examines the influence that the duration of the time window used for the spectral analysis, or conversely the spectral resolution, might have in the coherence assumption, and in the spectral estimates that are used as the input for the sound field separation (in a stationary sound field). The analysis is also valid for the general case of NAH, although it is a somewhat trivial matter in this case. In sound field separation methods, this source of error is considerably more relevant, because the influence of late coherent sound, if overlooked, can bias the reconstruction.

In Paper H (Fernandez-Grande and Jacobsen (2010) [111]) the possibility of recovering the free-field radiation of a planar rigid sound source by compensating for the backscattered field is studied. The problem is formulated based on the SONAH method, and focuses on the separation of the pressure field. The study proved that the method is valid, and can recover in some cases a more accurate free-field radiation of the acoustic source. However, the method relies critically on an accurate modeling of the incoming waves onto the source, and a well defined boundary condition in order to model the source's scattering. This makes the accuracy of the method somewhat uncertain, and whereas it can improve the reconstruction, it might as well yield erratic results, worse than 'conventional' separation methods. This reduces considerably the method's applicability. Therefore, unless the back-scattering from the source is critical and can be modeled very accurately, the technique is not very useful. The paper focuses on the recovery of the sound pressure field, and although similar results were found for the velocity field, this is not discussed. The paper is included in the "Additional papers" section of the dissertation (Paper H).

3.3 Far-field radiation. Supersonic intensity

This study is also concerned with the identification of the far-field radiation from sources based on near-field data, and the so-called supersonic acoustic intensity. This quantity represents and quantifies the flow of acoustic energy that is effectively radiated into the far field. It makes it possible to estimate and identify, based on near-field measurements, what is the contribution from different regions of a source to its total net power output. Therefore, it provides valuable information about the source's far-field radiation characteristics, and in that sense, it is complementary to the NAH reconstruction.

The essential idea behind the calculation of the supersonic acoustic intensity is to filter out the evanescent waves that are present in the near field of a source (thus getting rid of the characteristic circulatory energy, sometimes known as the 'acoustical short-circuit'). A holographic reconstruction of the sound field is performed which involves solely the propagating waves, which are in turn the waves that relate to the far-field output of the source. The reconstructed sound field can be calculated based on the propagating waves as

$$p^{(s)}(x, y, z_s) = \frac{1}{4\pi^2} \iint_{Sr} P(k_x, k_y, z_h) e^{-j(k_x x + k_y y + k_z (z_s - z_h))} dk_x dk_y, \tag{3.5}$$

where the integration is not over the whole wavenumber domain, but only over S_r, the area of the radiation circle, $k_x^2 + k_y^2 \leq k^2$. This can alternatively be calculated directly in space domain by means of a two-dimensional convolution with the filter mask $h^{(s)}$, as shown in Paper E [112],

$$h^{(s)}(x,y) = \frac{k}{2\pi\sqrt{x^2+y^2}} J_1(k\sqrt{x^2+y^2}). \tag{3.6}$$

The same type of reconstruction based on the propagating waves inside the radiation circle, as in Eq. (3.5), can be done for the particle velocity, and the supersonic intensity can be calculated as [113]

$$I^{(s)}(x,y,z) = \frac{1}{2}\mathrm{Re}\{p^{(s)}(x,y,z)u^{(s)}(x,y,z)^*\}. \tag{3.7}$$

Because this quantity has an 'active intensity' form, i.e., the source's output is described in terms of the flow of acoustic energy per unit area, studying the potential of combined pressure-velocity measurements for its calculation seems clearly relevant.

In the following, some antecedents of the technique are briefly discussed. It is common knowledge that the study of the far-field radiation from sound sources based on near-field data is far from being a new problem in acoustics. The fundamental principles of the far-field radiation from plates and wave bearing structures have been extensively studied since long ago [114–116], providing theoretical descriptions of how a vibrating source couples energy into the acoustic medium [117, 118]. With the advent of sound intensity measurements, some of these theories were revisited under a different light. In this case, it was the detailed study of flows of acoustic energy in the near field of sources, and the energy patterns resulting from the interaction of sound waves, that corroborated some of those phenomena [119, 120]. Here, the problem was looked at from the perspective of the fluid motion of the medium rather than from the structural motion of the source. The far field radiation of sources was studied later on with a methodology based on the orthogonal decomposition of the prescribed vibration velocity of a source using singular value decomposition. The so-called velocity modes are thus obtained, and the modes that contribute to the far field output of the source can be determined using the estimated total power output as a criterion, which is calculated via the far-field radiation operator. This is closely related to the problem we address here. The approach is described in detail in refs. [121–129].

More recently, with the advent of NAH and the spatial processing of sound fields, it has become possible to study the relation between the near-field and far-field characteristics of a source based on the wavenumber filtering of the sound field. Williams (1995) [130] proposed the concept of supersonic acoustic intensity for cylindrical geometries, providing a theoretical formulation as well as numerical and experimental results. Williams (1998) [113] later extended the description of the problem to planar geometries. He showed that with the supersonic acoustic intensity, the power is conserved, thus it does rigorously describe quantitatively the far field output of the source. The conservation of power is a key point of the technique's validity. The paper included numerical results and examples, although not experimental. Williams also described the concept of the supersonic acoustic intensity in ref. [1], sect. 2.15.

Paper D (Fernandez-Grande and Jacobsen (2011) [131]) extends the existing formulation of the supersonic intensity based on the Fourier transformation of the sound field to statistically optimized near-field acoustic holography (SONAH)[2]. With this approach, no explicit transformation of the sound field into the wavenumber domain is performed. The study revealed that the calculation is somewhat more accurate when it is based on SONAH than when based on explicit Fourier transformations. This is not surprising considering that SONAH is a patch method, and the finite aperture error is not very critical. If the supersonic intensity was calculated with Fourier based patch-NAH, the accuracy would be similar to SONAH. The study examined as well the possibility of using particle velocity measurements , or combined pressure-velocity measurements for the calculation of the supersonic acoustic intensity. It was discovered that the velocity-based estimation of the supersonic intensity is the most accurate, more than pressure-based and pressure-velocity based estimations. This can be explained as a consequence of the truncation error due to the finite measurement aperture. The truncation error is critical in the estimation of the supersonic intensity because of the infinitely long filter mask resulting from the sharp cut-off in the wavenumber domain. This is further examined in Paper F, which studies and illustrates the truncation error.

Paper E (Fernandez-Grande et al. (2012) [112]) proposes a formulation of the supersonic acoustic intensity in space domain. The method proposes to identify the far field output of the source by means of a direct convolution with a filter mask that corresponds to the space domain representation of the radiation circle. The study shows the validity of the approach, and demonstrates experimentally the relation to the well-known theory of corner and edge radiation from plates. The conservation of power

[2] A discrete wavenumber approach was used for this study

of the acoustic supersonic intensity is also demonstrated experimentally, validating the method and showing good agreement with the literature. The study also shows that the truncation error due to the finite measurement aperture is critical, particularly at low frequencies (in agreement with ref. [131] - Paper D, and Paper F).

Paper F (Fernandez-Grande and Jacobsen, manuscript) is a brief note that studies the truncation error in the calculation of the supersonic intensity in planar coordinates. It provides an analytical description of the phenomena based on the space domain formulation presented in Paper E. It provides some numerical results to illustrate the significance of this source of error. The note is complementary to Papers D and E.

Additionally, Appendix A1 considers a preliminary study of the supersonic intensity generalized to a three-dimensional space. So far, this quantity has been described in planar and cylindrical coordinates. The study shows that it is possible to calculate a three-dimensional operator that yields the supersonic intensity in three dimensions. Based on this description it should be possible to estimate the supersonic intensity vector of any given sound field in a free-field space. However, the study is at present somewhat rudimentary.

Appendix A2, examines briefly a possible relation between the supersonic intensity and the so-called irrotational intensity. The irrotational intensity results from an attempt to distinguish between far-field and near-field energy of acoustic sources based on certain vector properties of sound intensity fields. Pascal (1985) [132] sugested to decompose the active intensity vector into an irrotational (zero curl) and a rotational (nonzero curl) component (via Helmholtz decomposition) [133, 134]. Pascal related the zero curl, or irrotational component of the active intensity vector to the far-field energy, whereas the non-zero curl component seemed to be mostly associated to the circulating near-field energy. However, this view was questioned by Mann et al. (1987) [135], who pointed out that this decomposition does not seem to take into account the inter-coupling between several closely spaced point sources. In any case, from a preliminary examination of the supersonic and the irrotational intensities, it seems that they are not directly related. At first sight, it is not obvious that there should be a relation between the rotational nature of a vector and a spatially filtered version of it, although they aim at describing the same phenomena. There could be some unnoticed relationship, but the author is inclined to think the contrary. In Appendix A2, an example that might serve as justification of this view is provided.

3.4 Spherical NAH

As was discussed in Sect. 2.2, near field acoustic holography in its original form can be performed in any set of separable coordinates, either planar, cylindrical or spherical. The theory of the method in the different coordinate systems is covered in the Fourier acoustics book [1], and also in the 1985 paper by Maynard et al. [2].

This section is specifically concerned with spherical microphone arrays, which have been used in acoustics since long ago, and in recent years they are becoming increasingly popular in near-field acoustic holography. These type of arrays have some interesting properties. A basic general description is given in refs. [136–138].

Given a sound field that is sampled with a spherical microphone array, the boundary value problem can be solved in spherical coordinates (the center of the array being the origin of coordinates), and the sound field can be expanded on the basis of spherical harmonics and Bessel functions. This holographic representation allows the reconstruction of the complete sound field, i.e. pressure, velocity vector and sound intensity vector, over a three-dimensional volume about the sphere. Furthermore, spherical arrays form a discrete but nevertheless 'closed' surface, thus the assumption that a full two-dimensional space is measured holds entirely. It should be noted that if the sources are outside the array, the reconstruction inside the sphere is a forward problem, but the reconstruction outside of the sphere poses an inverse problem.

Williams et al. (2006) [139] have proposed to use spherical microphone arrays in the fashion of volumetric acoustic intensity probes, because they can provide an image of the intensity vector over a sphere, thus representing the flow of acoustic energy across a certain volume. This idea can be very useful for source localization and for studying sound fields, particularly interior sound fields and enclosed spaces, as found in vehicles or conventional rooms. The idea was first described for a "transparent" spherical microphone array, with a set of microphones arranged throughout a spherical surface and exposed to the acoustic field [139].

An interesting alternative to transparent spherical arrays are rigid-sphere microphone arrays. NAH with rigid spherical arrays was first described in several conference proceedings [140–142] and some years later in journal publications. Williams and Takshima (2010) [143] proposed an intensity vector imager based on measurements with a rigid spherical array. The paper describes an approach to determine the Fourier coefficients based on singular value decomposition, irrespective of the distribution of microphones on the sphere. In this method, the reconstructed quantity is the total sound field, i.e., the incident sound on the sphere as well as the scattered sound due to the rigid sphere itself. However, because the reconstruction takes place faraway (two times the radius) from the sphere, the influence of the scattering should not be critical.

Paper G (Jacobsen et al. (2011) [144]) proposes a method that makes use of a rigid sphere for the holographic reconstruction of a sound field. The background of the method is very similar to that in ref. [143], although it is mostly concerned with the reconstruction of the sound pressure field, rather than with the visualization of the sound intensity flow. There exists a fundamental difference between the two methods: In the method in ref. [143], as mentioned above, the reconstruction of the sound field is based on the total sound field (incident + scattered). In the method described in Paper G the boundary value problem is solved for the incident sound field onto the sphere only. That is, the total measured field is decomposed into an incident and a scattered component, and the reconstruction is based exclusively on the incident component. This means that the sound field is reconstructed as if the sphere was not disturbing the sound field. This is useful for visualizing the sound field in the proximity of the rigid sphere, in order to avoid the significant scattering that it may introduce in this region.

Although the scattered pressure can be compensated for in the spherical harmonic expansion, when using a rigid array close to a vibrating source, there could be multiple reflections occurring between the source and the array. Paper G shows that such phenomenon is not critical. The number of terms used in the spherical harmonic expansion is truncated in practice, to control the noise contained in the high order terms (discretization noise, measurement, etc.). A regularization filter could have been used, in the fashion of ref. [143] in order to control the noise terms. This matter should be subject of future research.

In general terms, rigid-sphere microphone arrays are an interesting alternative to transparent arrays. They have the advantage that the assumed rigid boundary condition is accurately satisfied. This is not the case for transparent arrays, because they are not ideally transparent to the acoustic waves, and give rise to scattering and diffraction from the microphones, preamplifiers, cabling, framing structure, etc. In the case of a rigid sphere array, these components are enclosed in it, which makes it a practical measuring instrument, and conforms a very precise reproduction of the assumed boundary condition. Besides, the reconstruction based on a rigid sphere is more stable than the one based on a transparent or open array. The reconstruction equation for the transparent sphere is [144],

$$p(r,\theta,\varphi) = \sum_{n=0}^{n=\infty}\sum_{m=-n}^{m=n} \frac{\displaystyle\int_0^{2\pi}\int_0^{\pi} p(a,\theta,\varphi)Y_n^m(\theta,\varphi)^* \sin\theta d\theta d\varphi}{j_n(ka)} \cdot j_n(kr)Y_n^m(\theta,\varphi). \tag{3.8}$$

Whereas for the rigid sphere, the reconstruction equation of the incident pressure is (see Paper G),

$$p_{inc}(r,\theta,\varphi) = \sum_{n=0}^{n=\infty}\sum_{m=-n}^{m=n} \frac{\displaystyle\int_0^{2\pi}\int_0^{\pi} p_{tot}(a,\theta,\varphi)Y_n^m(\theta,\varphi)^* \sin\theta d\theta d\varphi}{j_n(ka) - \dfrac{j_n'(ka)}{h_n'(ka)}h_n(ka)} \cdot j_n(kr)Y_n^m(\theta,\varphi). \tag{3.9}$$

Thus, it is apparent that in the transparent sphere there are singularities stemming from the zeros of the spherical Bessel function ($j_n(ka)$) in the denominator of Eq. (3.8), which yields unstable results. This is however, not the case for the rigid sphere. The denominator in Eq. (3.9) does not have zeroes, which yields a much more stable reconstruction of the incident pressure. The absence of zeroes in the denominator might not be immediately apparent from Eq. (3.9), or Eqs. (4) and (5) in Paper G. However, making use of the Wronskian relation (Eqs. (6.68) and (6.58) of ref. [1])

$$j_n(ka)h_n'(ka) - j_n'(ka)h_n(ka) = -j/(ka)^2,$$

and with some simple algebra, the previous expression can be simplified to:

$$\begin{aligned} p_{inc}(r,\theta,\varphi) = j \sum_{n=0}^{n=\infty}\sum_{m=-n}^{m=n} \int_0^{2\pi}\int_0^{\pi} p_{tot}(a,\theta,\varphi)Y_n^m(\theta,\varphi)^* \sin\theta d\theta d\varphi \\ (ka)^2 h_n'(ka) j_n(kr) Y_n^m(\theta,\varphi). \end{aligned} \tag{3.10}$$

This expression, shows clearly that the singularities resulting from the zeroes in the denominator are avoided with the rigid sphere (there is no denominator), and consequently the reconstruction based on the rigid sphere is far more stable. This is further discussed in Paper G.

3.5 Overview of the included papers

A summary of the papers included in the thesis is provided in this section. The papers are divided into three main parts. The first part (papers A to C) deals with sound field separation methods using pressure and velocity measurements. The second part (papers D to F) is concerned with the supersonic acoustic intensity and the relation between near-field and far-field radiation. The third part (Paper G) is concerned with the holographic reconstruction of sound fields using spherical rigid microphone arrays. Additionally there is a fourth part including two papers, Papers H and I, which have been produced during the PhD study, and are relevant, although they are not essential to this dissertation.

It is recommended that Papers A - G are read before proceeding to the next chapter that summarizes and concludes the dissertation.

3.5.1 PART I: Papers A- C

Paper A examines a separation technique based on measurement of the particle velocity in two closely spaced parallel planes, using statistically optimized near-field acoustic holography. The purpose of the technique is to recover the particle velocity radiated by a source in the presence of sound from the opposite side of the array.

In Paper B, a separation method based on the measurement of the particle velocity in two layers and a method based on the measurement of the pressure and the velocity in a single layer are proposed. The two methods are based on an equivalent source formulation. They are examined for the case where a sound source is radiating into an enclosed space, via numerical and experimental studies.

Paper C studies the influence that the duration of the analysis window, or the spectral resolution, may have in the spectral estimation used for NAH and sound field separation techniques. This is particularly relevant for sound field separation methods in reverberant environments, or in cases where late reflections might occur. The paper comprises a fundamental analytical study, and presents several numerical and experimental examples.

3.5.2 PART II: Papers D-F

Paper D proposes a method to calculate the supersonic acoustic intensity based on statistically optimized near-field acoustic holography (SONAH). The theory, numerical results and an experimental study are presented. The possibility of using particle velocity measurements instead of conventional pressure measurements is examined, and the method is compared with the alternative existing methodology.

Paper E proposes and examines a direct formulation in space domain of the supersonic acoustic intensity. The supersonic intensity is calculated directly by means of a two-dimensional convolution between the acoustic field and the space domain representation of the radiation circle. This paper presents the theory, a numerical example, and an experimental study that serves as validation.

Paper F is complementary to Papers D and E. It is a brief note on the truncation error in the calculation of the supersonic acoustic intensity. An analytical description is given based on the direct space domain formulation of this quantity, and a numerical study is included.

3.5.3 PART III: Paper G

Paper G presents a technique, spherical near-field acoustic holography, that makes it possible to reconstruct the incident sound field about a sphere on which the sound pressure is measured with an array of microphones.

Note that the author of this dissertation is not the first author of the paper. He is only responsible for the theoretical formulation and derivation, and a modest contribution to the preliminary numerical results and coding.

3.5.4 Additional papers: Papers H-I

Paper H proposes and examines a technique for recovering the free field radiation from a planar source, which is based on compensating for the back-scattered waves at the source's boundary. It uses statistically optimized near-field acoustic holography. A numerical and an experimental study are presented.

Paper I examines numerically the influence that acoustic radiation from beyond the measurement aperture might have in patch holographic methods. The paper consists only of numerical simulations that serve to examine different distributions of equivalent sources and how accurately they model the sound field. Also, the reconstruction based on measurements of sound pressure and the normal component of the particle velocity is examined.

Chapter 4
Summary and concluding remarks

4.1 Summary of the contribution

This study has contributed to the existing body of knowledge in fundamentally three areas: the use of separation methods in near-field acoustic holography, the study of the far-field radiation from sources based on their near-field data, and the holographic reconstruction of sound fields using rigid-spherical arrays.

A novel sound field separation principle has been proposed, based on the double layer measurement of the particle velocity, and it has been formulated based on two different holographic wave models, SONAH and ESM. Also, two methods based on the single layer measurement of the sound pressure and the particle velocity have been proposed, although these are similar to previously existing ones. The separation methods have been studied in a reverberant environment. A fundamental study has been conducted that examines the influence that the time window or the spectral resolution used might have on stationary near-field acoustic holography and sound field separation methods, in particular when applied in reverberant environments. A separation method was proposed that attempts to recover the free-field radiation of a source, by compensating for the source's back-scattering. However, the method is not particularly satisfactory, because its applicability is limited.

This work is also concerned with the supersonic acoustic intensity, as a tool to identify the far-field radiation characteristics of sound sources based on prescribed near-field data. The possibility of using sound pressure, particle velocity, and combined pressure-velocity measurements for the calculation of this quantity has been examined. The estimation of the supersonic intensity has been extended to statistically optimized near-field acoustic holography. Also, an alternative formulation has been developed, where the supersonic intensity is calculated in space domain via a two dimensional direct-convolution with the spatial representation of the radiation circle. This formulation makes it possible to design finite spatial filter-masks for the calculation and visualization of this quantity in practice, and a modified Lanczos filter was proposed for this purpose. It has been demonstrated experimentally that the supersonic intensity is a valid tool for the localization and quantification of the far-field radiation of sound sources. The truncation error to which the calculation of the supersonic intensity is subject has also been examined. Additionally, a formulation of the supersonic acoustic intensity for three-dimensional spaces has been proposed, and a possible connection between the supersonic intensity and the ‘irrotational’ component of the sound intensity vector has been considered.

The work has also contributed to developing a holographic technique based on measurements with a rigid-sphere microphone array that compensates for the scattering introduced by the rigid array itself, and can successfully reconstruct the ’incident’ sound field about the array.

4.2 Suggestions for future work

Some suggestions for future research, and topics that have not been investigated in this project, are listed in the following:

A study of the use of three-dimensional velocity probes for near-field acoustic holography: The work presented here is mostly concerned with the normal component of the particle velocity vector. However, it is possible to measure the three-dimensional velocity vector with a 3-D velocity probe, and apply it to NAH. As explained in Sect. 2.2, the broadband acoustic holography from intensity measurements method (BAHIM) relies on the measurement of the tangential component of the sound intensity to extract the phase information of the hologram. The application of 3-D intensity probes in connection with this method could be practical and perhaps advantageous.

Sound field separation methods: It has been shown that although separation methods are theoretically sound, there are a number of experimental limitations that make the techniques not very recommendable unless there is a significant disturbance from incoming waves onto the source. It could be useful to gain further insight into these sources of error, and study alternative 'complete' solutions that could be more robust and accurate in the case that there is only significant sound from the one side.

Supersonic acoustic intensity: Further inspection in the fundamental aspects of the supersonic acoustic intensity is needed and could be revealing. For instance, its relation to the properties of the sound intensity vector, active and reactive intensity, rotational and irrotational components of the active intensity, etc.

It has been verified that the supersonic acoustic intensity is a useful quantity in practice. However, so far, its application is rather limited to separable geometries. It would be very convenient to formulate this quantity for the general case of sources of arbitrary geometry. In this thesis, a preliminary description of the supersonic intensity in a three-dimensional free-field space is provided, and it could serve as a starting point for an integral formulation as the Helmholtz integral equation. This is however ongoing work.

Besides the fundamental aspects, and with the experimental validity of the supersonic intensity demonstrated, this quantity might also serve to clarify some existing questions concerned with the effective radiation from acoustic sources. It could serve as a tool to investigate new phenomena, or to validate already existing theories. To serve as an illustrative example, this quantity could be used to study the sound transmission through walls due to resonant and forced bending wave excitation, for instance, which is still an open question in the field of building acoustics.

Spherical NAH: This area seems to deserve further research. This technique is at present mostly limited to the reconstruction over spherical surfaces. This is a shortcoming if the reconstruction of the sound field over a surface that is not spherical is sought. A formulation that can adapt the spherical expansion to arbitrary geometries could be useful, e.g.: combining BEM or ESM with the spherical harmonics expansion (this is ongoing work). A combination of spherical arrays and a scan based procedure could be a solution to adapt the spherical surface to approximately planar sources. As mentioned in sect. 3.4, the regularization of the spherical NAH algorithm in Paper F was based on the truncation of the spherical harmonic expansion; a more sophisticated regularization scheme can be useful. Also, as already suggested in ref. [143], it could be useful to apply incoherent NAH techniques to the spherical array, in order to study complex sources of noise.

4.3 Conclusions

This study has served to examine the application of new acoustic transducers, pressure-velocity probes and spherical microphone arrays to near-field acoustic holography and sound source identification. Three parts constitute the core of the thesis. The main parts of the work presented here are concerned with sound field separation methods and the supersonic acoustic intensity. Another part, secondary though, is near-field acoustic holography with rigid-sphere microphone arrays.

One part of the study has examined the use of sound field separation techniques in near-field acoustic holography, which make it possible to apply NAH in non-anechoic and reverberant environments, when a 'source-less' free field cannot be guaranteed. Separation methods offer a complete solution to the wave equation, because both outgoing and incoming components are considered.

The study has shown, in addition to previous studies, that it is possible to separate outgoing and incoming sound waves based on the combined measurement of the sound pressure and the particle velocity. The so-called 'p-u mismatch', the fact that the pressure- and velocity-based estimates are not identical, is critical. For this reason the accurate calibration of the velocity and pressure sensors is crucial.

It has been demonstrated that it is possible to separate the outgoing and incoming waves in a sound field by measuring the particle velocity in two closely spaced layers ('u-u' measurement). This approach overcomes some of the limitations related to the 'p-u' based techniques. The technique circumvents the pressure-to-velocity transformations that are otherwise present in 'p-u' or 'p-p' separation methods, and is more robust to measurement noise.

Although separation methods constitute theoretically a complete solution to the wave equation, they are useful in practice when both the outgoing and the incoming sound are of comparable magnitude. Otherwise, the conventional direct reconstruction is more accurate and much more robust. The direct reconstruction based on velocity measurements is particularly favorable in many cases, because it is less affected by extraneous sound, and the incoming sound waves vanish close to a rigid source.

Another part of this work has studied the relation between the sound field in the near field and the far field of acoustic sources, based on the supersonic acoustic intensity. Previously, this quantity had mostly been examined numerically. It has been demonstrated in this study that the quantity is useful and valid in practice, as an experimental measure to identify an quantify the radiation of sources into the far field.

The supersonic intensity can be calculated directly in space domain, and this formulation agrees with the well-known physical processes and the priorly established theories of sound radiation. The space domain formulation makes it possible to use window-designed finite filter masks, that are useful for the practical visualization and identification of the regions of a source that contribute to the far-field radiation.

The truncation error in the calculation of the supersonic intensity can be critical, because of the infinitely long filter mask resulting from the sharp wavenumber cut-off. For this reason, its calculation is notably more accurate when it is based on particle velocity measurements than when it is based on measurement of the sound pressure or on the combined measurement of pressure and velocity. Analogously, the calculation of the supersonic intensity based on ‘patch’ methods is more accurate than when based on conventional FFT processing, for the same reason.

No evidence relating the supersonic acoustic intensity with the irrotational component of the sound intensity vector has been found.

Finally, it has been shown that it is possible to obtain a holographic reconstruction of the sound field based on measurements with a rigid-sphere microphone array. Furthermore, it is possible to compensate for the scattering introduced by the sphere and reconstruct only the incident sound field, as if the rigid sphere was not present. It has been shown that the multiple reflections that might occur between the source and the rigid sphere in the near-field are not significant.

All in all, and in very general terms, the study has served to gain a better understanding of the potential of sound pressure and velocity measurements applied to near-field holography and to provide tools to apply NAH in non-anechoic environments. It has also contributed to a better understanding of how an acoustic source couples energy into the far-field, via the supersonic acoustic intensity, and finally to use rigid-sphere microphone arrays for the holographic reconstruction of sound fields.

Bibliography

[1] E. G. Williams, *Fourier Acoustics - Sound Radiation and Nearfield Acoustic Holography*. Academic Press, 1999.

[2] J. D. Maynard, E. G. Williams, and Y. Lee, “Nearfield acoustic holography I: Theory of generalized holography and the development of NAH,” *J. Acoust. Soc. Am*, vol. 78, no. 4, pp. 1395–1413, 1985.

[3] W. A. Veronesi and J. D. Maynard, “Nearfield acoustic holography (NAH) II. Holographic reconstruction algorithms and computer implementation,” *J. Acoust. Soc. Am.*, vol. 81, no. 5, pp. 1307–1322, 1987.

[4] J. Hald, “Basic theory and properties of statistically optimized near-field acoustical holography,” *J. Acoust. Soc. Am*, vol. 125, no. 4, pp. 2105–2120, 2009.

[5] G. H. Koopmann, L. Song, and J. B. Fahnline, “A method for computing acoustic fields based on the principle of wave superposition,” *J. Acoust. Soc. Am*, vol. 86, no. 6, pp. 2433–2438, 1989.

[6] A. Sarkissian, “Method of superposition applied to patch near-field acoustic holography,” *J. Acoust. Soc. Am*, vol. 118, no. 2, pp. 671–678, 2005.

[7] F. Jacobsen and Y. Liu, “Near field acoustic holography with particle velocity transducers,” *J. Acoust. Soc. Am.*, vol. 118, no. 5, pp. 3139–3144, 2005.

[8] F. Jacobsen and V. Jaud, “Statistically optimized near field acoustic holography using an array of pressure-velocity probes,” *J. Acoust. Soc. Am.*, vol. 121, no. 3, pp. 1550–1558, 2007.

[9] D. Gabor, “A new microscopic principle,” *Nature*, vol. 161, pp. 777–778, 1948.

[10] D. Gabor, “Microscopy by reconstructed wave-fronts,” *Proceedings of the Royal Society of London. Series A, Mathematical and Physical Sciences*, vol. 197, no. 1051, pp. pp. 454–487, 1949.

[11] T. S. Graham, “Long-wavelength acoustic holography,” *J. Acoust. Soc. Am*, vol. 46, no. 1A, p. 116, 1969.

[12] E. G. Williams, J. D. Maynard, and E. Skudrzyk, "Sound source reconstructions using a microphone array," *J. Acoust. Soc. Am*, vol. 68, no. 1, pp. 340–344, 1980.

[13] E. G. Williams and J. D. Maynard, "Holographic Imaging without the Wavelength Resolution Limit," *Phys. Rev. Lett.*, vol. 45, pp. 554–557, Aug. 1980.

[14] P. R. Stepanishen and K. C. Benjamin, "Forward and backward projection of acoustic fields using FFT methods," *J. Acoust. Soc. Am*, vol. 71, no. 4, pp. 803–812, 1982.

[15] P. Stepanishen and H. W. Chen, "The acoustic nearfield of cylindrical vibrators via the use of FFT methods," *J. Acoust. Soc. Am*, vol. 73, no. S1, pp. S22–S22, 1983.

[16] E. G. Williams and J. D. Maynard, "Numerical evaluation of the Rayleigh integral for planar radiators using the FFT," *J. Acoust. Soc. Am*, vol. 72, no. 6, pp. 2020–2030, 1982.

[17] L. Rayleigh, "XXXVII. On the passage of waves through apertures in plane screens, and allied problems," *Philosophical Magazine Series 5*, vol. 43, pp. 259–272, Apr. 1897.

[18] D. Sundararajan, *The Discrete Fourier Transform: Theory, Algorithms and Applications*. World Scientific, 2001.

[19] T. Loyau, J.-C. Pascal, and P. Gaillard, "Broadband acoustic holography reconstruction from acoustic intensity measurements. I: Principle of the method," *J. Acoust. Soc. Am*, vol. 84, no. 5, pp. 1744–1750, 1988.

[20] J. Hald, "STSF - A unique technique for scan-based near-field acoustic holography without restrictions on coherence." Brüel & Kjær Technical Review 1989-1, 1989.

[21] W. A. Veronesi and J. D. Maynard, "Digital holographic reconstruction of sources with arbitrarily shaped geometries," *J. Acoust. Soc. Am*, vol. 85, no. 2, pp. 588–598, 1989.

[22] G.-T. Kim and B.-H. Lee, "3-D Sound reconstruction and field reprodiction using the Helmholtz integral equation," *J. Sound Vib.*, vol. 136, no. 2, pp. 245–261, 1990.

[23] R. Bai, "Application of BEM (boundary element method)-based acoustic holography to radiation analysis of sound sources with arbitrarily shaped geometries," *J. Acoust. Soc. Am*, vol. 92, no. 1, pp. 533–549, 1992.

[24] Z. Zhang, N. Vlahopoulos, S. T. Raveendra, T. Allen, and K. Y. Zhang, "A computational acoustic field reconstruction process based on an indirect boundary element formulation," *J. Acoust. Soc. Am*, vol. 108, no. 5, pp. 2167–2178, 2000.

[25] A. Schuhmacher, J. Hald, K. B. Rasmussen, and P. C. Hansen, "Sound source reconstruction using inverse boundary element calculations," *J. Acoust. Soc. Am*, vol. 113, no. 1, pp. 114–127, 2003.

[26] B.-K. Kim and J.-G. Ih, "On the reconstruction of the vibro-acoustic field over the surface enclosing an interior space using the boundary element method," *J. Acoust. Soc. Am*, vol. 100, no. 5, pp. 3003–3016, 1996.

[27] A. Tekatlian, P. Filippi, and D. Habault, "Determination of vibration characteristics of noise sources solving an inverse radiation problem," *Acta Acust. united Ac.*, vol. 82, no. 1, pp. 91–101, 1996.

[28] T. DeLillo, V. Isakov, N. Valdivia, and L. Wang, "The detection of surface vibrations from interior acoustical pressure," *Inverse Problems*, vol. 19, no. 3, p. 507, 2003.

[29] N. Valdivia and E. G. Williams, "Implicit methods of solution to integral formulations in boundary element method based near field acoustic holography," *J. Acoust. Soc. Am*, vol. 116, no. 3, pp. 1559–1572, 2004.

[30] S. Marburg and B. Nolte, *Computational Acoustics of Noise Propagation in Fluids: Finite and Boundary Alement Methods*. Springer, 2008.

[31] P. C. Hansen, "Analysis of discrete ill-posed problems by means of the L-curve," *society for Industrial Applied Mathematics*, vol. 34, no. 4, pp. 561–580, 1992.

[32] R. Steiner and J. Hald, "Near-field Acoustical Holography Without the Errors and Limitations Caused by the Use of Spatial DFT," *International Journal of Acoustics and Vibration*, vol. 6, no. 2, 2001.

[33] J. Hald, "Patch Near-field Acoustic Holgraphy using a new statistically optimal method," in *Proceedings of Internoise*, 2003.

[34] J. Hald, "Sonah," *B & K Technical review - 2005 (1)*, pp. 40–50, 2005.

[35] Y. T. Cho and J. S. Bolton, "Source visualization by using statistically optimized near-field acoustical holography in cylindrical coordinates," *J. Acoust. Soc. Am*, vol. 118, no. 4, pp. 2355–2364, 2005.

[36] L. Song, G. H. Koopmann, and J. B. Fahnline, "Numerical errors associated with the method of superposition for computing acoustic fields," *J. Acoust. Soc. Am*, vol. 89, no. 6, pp. 2625–2633, 1991.

[37] R. Jeans and I. C. Mathews, "The wave superposition method as a robust technique for computing acoustic fields," *J. Acoust. Soc. Am*, vol. 92, no. 2, pp. 1156–1166, 1992.

[38] R. D. Miller, J. E. Thomas Moyer, H. Huang, and H. Uberall, "A comparison between the boundary element method and the wave superposition approach for the analysis of the scattered fields from rigid bodies and elastic shells," *J. Acoust. Soc. Am*, vol. 89, no. 5, pp. 2185–2196, 1991.

[39] A. Sarkissian, "Method of superposition applied to scattering from a target in shallow water," *J. Acoust. Soc. Am*, vol. 95, no. 5, pp. 2340–2345, 1994.

[40] A. Sarkissian, "Extension of measurement surface in near-field acoustic holography," *J. Acoust. Soc. Am*, vol. 115, no. 4, pp. 1593–1596, 2004.

[41] N. P. Valdivia and E. G. Williams, "Study of the comparison of the methods of equivalent sources and boundary element methods for near-field acoustic holography," *J. Acoust. Soc. Am*, vol. 120, no. 6, p. 3694, 2006.

[42] M. R. Bai, C.-C. Chen, and J.-H. Lin, "On optimal retreat distance for the equivalent source method-based nearfield acoustical holography," *J. Acoust. Soc. Am*, vol. 129, no. 3, pp. 1407–1416, 2011.

[43] Z. Wang and S. F. Wu, "Helmholtz equation least-squares method for reconstructing the acoustic pressure field," *J. Acoust. Soc. Am.*, vol. 102, pp. 2020–2032, 1997.

[44] J. Gomes, J. Hald, P. Juhl, and F. Jacobsen, "On the applicability of the spherical wave expansion with a single origin for near-field acoustical holography," *J. Acoust. Soc. Am*, vol. 125, no. 3, pp. 1529–1537, 2009.

[45] S. F. Wu, "Hybrid near-field acoustic holography," *J. Acoust. Soc. Am*, vol. 115, no. 1, pp. 207–217, 2004.

[46] S. F. Wu and J. Yu, "Reconstructing interior acoustic pressure fields via Helmholtz equation least-squares method," *J. Acoust. Soc. Am.*, vol. 104, pp. 2054–2060, 1998.

[47] N. Rayess and S. F. Wu, "Experimental validations of the HELS method for reconstructing acoustic radiation from a complex vibrating structure," *J. Acoust. Soc. Am*, vol. 107, no. 6, pp. 2955–2964, 2000.

[48] K. Saijyou and S. Yoshikawa, "Reduction methods of the reconstruction error for large-scale implementation of near-field acoustical holography," *J. Acoust. Soc. Am*, vol. 110, no. 4, p. 2007, 2001.

[49] E. G. Williams, "Continuation of acoustic near-fields," *J. Acoust. Soc. Am*, vol. 113, no. 3, pp. 1273–1281, 2003.

[50] E. G. Williams, B. H. Houston, and P. C. Herdic, "Fast Fourier transform and singular value decomposition formulations for patch nearfield acoustical holography," *J. Acoust. Soc. Am*, vol. 114, no. 3, pp. 1322–1333, 2003.

[51] K. Saijyou and H. Uchida, "Data extrapolation method for boundary element method-based near-field acoustical holography," *J. Acoust. Soc. Am*, vol. 115, no. 2, pp. 785–796, 2004.

[52] N. P. Valdivia, E. G. Williams, and P. C. Herdic, "Approximations of inverse boundary element methods with partial measurements of the pressure field," *J. Acoust. Soc. Am*, vol. 123, no. 1, pp. 109–120, 2008.

[53] R. Scholte, I. Lopez, N. Bert Roozen, and H. Nijmeijer, "Truncated aperture extrapolation for Fourier-based near-field acoustic holography by means of border-padding.," *J. Acoust. Soc. Am*, vol. 125, pp. 3844–54, June 2009.

[54] W.-Q. Jia, J. Chen, J.-Q. Li, and C. Yang, "Data Extrapolation Method Based on Patch Near-Field Acoustic Holography," *Acta Acust. united Ac.*, vol. 95, pp. 142–150, Jan. 2009.

[55] Q. Leclère, "Acoustic imaging using under-determined inverse approaches: Frequency limitations and optimal regularization," *J. Sound Vib.*, vol. 321, no. 3âĂŞ5, pp. 605–619, 2009.

[56] S. F. Wu, "Methods for reconstructing acoustic quantities based on acoustic pressure measurements," *J. Acoust. Soc. Am*, vol. 124, no. 5, pp. 2680–2697, 2008.

[57] M. B. S. Magalhaes and R. A. Tenenbaum, "Sound Sources Reconstruction Techniques: A Review of Their Evolution and New Trends," *Acta Acust. united Ac.*, vol. 90, no. 2, pp. 199–220, 2004.

[58] O. de La Rochefoucauld, M. Melon, and A. Garcia, "Time domain holography: Forward projection of simulated and measured sound pressure fields," *J. Acoust. Soc. Am*, vol. 116, no. 1, pp. 142–153, 2004.

[59] J.-F. Blais and A. Ross, "Forward projection of transient sound pressure fields radiated by impacted plates using numerical Laplace transform," *J. Acoust. Soc. Am*, vol. 125, no. 5, pp. 3120–3128, 2009.

[60] J.-H. Thomas, V. Grulier, S. Paillasseur, J.-C. Pascal, and J.-C. L. Roux, "Real-time near-field acoustic holography for continuously visualizing nonstationary acoustic fields," *J. Acoust. Soc. Am*, vol. 128, no. 6, pp. 3554–3567, 2010.

[61] J. Hald, "Time Domain Acoustical Holography and Its Applications," *Sound and Vibration*, vol. February, pp. 16–25, 2001.

[62] G. H. Golub, P. C. Hansen, and D. P. O'Leary, "Tikhonov Regularization and Total Least Squares," *SIAM Journal on Matrix Analysis and Applications*, vol. 21, no. 1, p. 185, 1999.

[63] E. G. Williams, "Regularization methods for near-field acoustical holography," *J. Acoust. Soc. Am*, vol. 110, no. 4, pp. 1976–1988, 2001.

[64] P. C. Hansen, *Rank-Deficient and Discrete Ill-Posed Problems: Numerical Aspects of Linear Inversion*. SIAM monographs on mathematical modeling and computation, SIAM, 1998.

[65] P. C. Hansen, *Discrete Inverse Problems: Insight and Algorithms*. Fundamentals of algorithms, Society for Industrial and Applied Mathematics, 2010.

[66] A. N. Tikhonov and V. I. A. Arsenin, *Solutions of ill-posed problems*. Scripta series in mathematics, Winston, 1977.

[67] A. Kirsch, *An Introduction to the Mathematical Theory of Inverse Problems*. Applied mathematical sciences, Springer-Verlag, New York, 1996.

[68] J. Bendat, "Solutions for the multiple input/output problem," *J. Sound Vib.*, vol. 44, no. 3, pp. 311–325, 1975.

[69] C. J. Dodds and J. D. Robson, "Partial coherence in multivariate random processes," *J. Sound Vib.*, vol. 42, no. 2, pp. 243–249, 1975.

[70] S. Price and R. Bernhard, "Virtual coherence: a digital signal processing technique for incoherent source identification," in *Proceedings of IMAC 4*, (Schenectady, NY, USA), pp. 1256–1262, 1986.

[71] D. L. Hallman and J. S. Bolton, "Multi-reference nearfield acoustic holography," in *Proceedings of Inter-Noise 92*, (Toronto, Canada), pp. 1165–1170, 1992.

[72] D. L. Hallman and J. S. Bolton, "A comparison of multi-reference nearfield acoustical holography procedures," in *Proceedings of Noise-Con 94*, (Fort Lauderdale, Florida), pp. 929–934, 1994.

[73] M. A. Tomlinson, "Partial source discrimination in near field acoustic holography," *Appl. Acoust.*, vol. 57, pp. 243–261, 1999.

[74] K. U. Nam and Y. H. Kim, "Visualization of multiple incoherent sources by the backward prediction of near-field acoustic holography," *J. Acoust. Soc. Am.*, vol. 109, no. 5, pp. 1808–1816, 2001.

[75] K. U. Nam and Y. H. Kim, "A partial field decomposition algorithm and its examples for near-field acoustic holography," *J. Acoust. Soc. Am.*, vol. 116, no. 1, pp. 172–185, 2004.

[76] Y.-J. Kim, J. S. Bolton, and H.-S. Kwon, "Partial sound field decomposition in multireference near-field acoustical holography by using optimally located virtual references," *J. Acoust. Soc. Am.*, vol. 115, no. 4, pp. 1641–1652, 2004.

[77] R. O. Schmidt, “Multiple Emitter Location and Signal Parameter,” *IEEE transactions on antennas and propagation*, vol. 34, no. 3, pp. 276–280, 1986.

[78] H. S. Kwon, Y. J. Kim, and J. S. Bolton, “Compensation for source nonstationarity in multireference , scan-based near-field acoustical holography,” *J. Acoust. Soc. Am.*, vol. 113, no. 1, pp. 360–368, 2003.

[79] M. Lee and J. S. Bolton, “Scan-based near-field acoustical holography and partial field decomposition in the presence of noise and source level variation,” *J. Acoust. Soc. Am.*, vol. 119, no. 1, pp. 382–393, 2006.

[80] Q. Leclère, “Multi-channel spectral analysis of multi-pass acquisition measurements,” *Mechanical Systems and Signal Processing*, vol. 23, pp. 1415–1422, 2009.

[81] I. Wolff and F. Massa, “Use of pressure gradient microphones for acoustical measurements,” *J. Acoust. Soc. Am*, vol. 4, no. 3, pp. 217–234, 1933.

[82] F. Jacobsen, “A note on the finite difference estimation of acoustic particle velocity,” *J. Sound Vib.*, vol. 256, no. 5, pp. 849–859, 2002.

[83] F. Jacobsen and H.-E. de Bree, “The Microflown particle velocity sensor,” in *Handbook of Signal Processing in Acoustics* (D. Havelock, S. Kuwano, and M. Vorländer, eds.), pp. 1281–1289, New York, NY,: Springer Verlag, 2008.

[84] R. L. Pratt, S. J. Elliott, and J. M. Bowsher, “Measurement of acoustic impedance of brass instruments,” *Acustica*, vol. 38, no. 4, pp. 236–246, 1977.

[85] H. H. Bruun, “Interpretation of hot-wire probe signals in subsonic airflows,” *Journal of Physics E: Scientific Instruments*, vol. 12, no. 12, p. 1116, 1979.

[86] R. Raangs, W. F. Druyvesteyn, and H.-E. de Bree, “A low cost sound intensity probe,” in *Audio Engineering Society Convention 110. May 12-15 2001*, (Amsterdam, The Netherlands), 2001.

[87] H.-E. de Bree, “The microflown: an acoustic particle velocity sensor,” *Acoustics Australia*, vol. 31, no. 3, pp. 91–94, 2003.

[88] F. Jacobsen and V. Jaud, “A note on the calibration of pressure-velocity sound intensity probes,” *J. Acoust. Soc. Am.*, vol. 120, no. 2, pp. 830–837, 2006.

[89] F. Jacobsen, X. Chen, and V. Jaud, “A comparison of statistically optimized near field acoustic holography using single layer pressure-velocity measurements and using double layer pressure measurements (L),” *J. Acoust. Soc. Am.*, vol. 123, no. 4, pp. 1842–1845, 2008.

[90] Q. Leclère and B. Laulagnet, “Particle velocity field measurement using an ultralight membrane,” *Applied Acoustics*, vol. 69, no. 4, pp. 302–310, 2008.

[91] Q. Leclere and B. Laulagnet, “Nearfield acoustic holography using a laser vibrometer and a light membrane,” *J. Acoust. Soc. Am*, vol. 126, no. 3, pp. 1245–1249, 2009.

[92] Y.-B. Zhang, F. Jacobsen, C.-X. Bi, and X.-Z. Chen, “Patch near field acoustic holography based on particle velocity measurements,” *J. Acoust. Soc. Am.*, vol. 126, no. 2, pp. 721–727, 2009.

[93] Y.-B. Zhang, F. Jacobsen, C.-X. Bi, and X.-Z. Chen, “Near field acoustic holography based on the equivalent source method and pressure-velocity transducers,” *J. Acoust. Soc. Am.*, vol. 126, no. 3, pp. 1257–1263, 2009.

[94] C. Langrenne, M. Melon, and A. Garcia, “Measurement of confined acoustic sources using near-field acoustic holography,” *J. Acoust. Soc. Am.*, vol. 126, no. 3, pp. 1250–1256, 2009.

[95] C. Langrenne, M. Melon, and A. Garcia, “Boundary element method for the acoustic characterization of a machine in bounded noisy environment,” *J. Acoust. Soc. Am*, vol. 121, no. 5, pp. 2750–2757, 2007.

[96] C. Langrenne and A. Garcia, “Data completion method for the characterization of sound sources,” *J. Acoust. Soc. Am*, vol. 130, no. 4, pp. 2016–2023, 2011.

[97] M. Aucejo, N. Totaro, and J.-L. Guyader, “Identification of source velocities on 3d structures in non-anechoic environments: Theoretical background and experimental validation of the inverse patch transfer functions method,” *J. Sound Vib.*, vol. 329, no. 18, pp. 3691 – 3708, 2010.

[98] G. Weinreich and E. B. Arnold, “Method for measuring acoustic radiation fields,” *J. Acoust. Soc. Am*, vol. 68, no. 2, pp. 404–411, 1980.

[99] M. Tamura, “Spatial Fourier transform method of measuring reflection coefficients at oblique incidence. I: Theory and numerical examples,” *J. Acoust. Soc. Am.*, vol. 88, no. 5, pp. 2259–2264, 1990.

[100] M. Tamura, J. F. Allard, and D. Lafarge, “Spatial Fourier-transform method for measuring reflection coefficients at oblique incidence. II. Experimental results,” *J. Acoust. Soc. Am*, vol. 97, no. 4, pp. 2255–2262, 1995.

[101] M.-T. Cheng, J. A. M. III, and A. Pate, “Wave-number domain separation of the incident and scattered sound field in cartesian and cylindrical coordinates,” *J. Acoust. Soc. Am*, vol. 97, no. 4, pp. 2293–2303, 1995.

[102] M. Villot, G. Chavériat, and J. Roland, “Phonoscopy: an acoustical holography technique for plane structures radiating in enclosed spaces,” *J. Acoust. Soc. Am.*, vol. 91, no. 1, pp. 187–195, 1992.

[103] D. L. Hallman and J. S. Bolton, “Nearfield acoustical holography for interior spaces,” in *Proceedings of Inter-Noise 94*, (Yokohama, Japan), pp. 1879–1882, 1994.

[104] D. L. Hallman, J. S. Bolton, S. M. Dumbacher, and M. J. Lally, “Acoustic Source Location in Vehicle Cabins and Free-field with Nearfield Acoustical Holography via Acoustic Arrays .,” in *Proceedings of the 19th International Seminar on Modal Analysis*, vol. II, (Leuven, Belgium), pp. 841–851, 1994.

[105] E. Williams, “The nearfield acoustical holography (NAH) experimental method applied to vibration and radiation in light and heavy fluids,” *Computers & Structures*, vol. 65, no. 3, pp. 323–335, 1997.

[106] J. Hald, “Patch holography in cabin environments using a two-layer hand held array with an extended SONAH algorithm,” in *Proceedings of Euronoise*, (Tampere, Finland), 2006.

[107] C.-X. Bi, X.-Z. Chen, and J. Chen, “Sound field separation technique based on equivalent source method and its application in near field acoustic holography,” *J. Acoust. Soc. Am.*, vol. 123, no. 3, pp. 1472–1478, 2008.

[108] Y.-B. Zhang, X.-Z. Chen, and F. Jacobsen, “A sound field separation technique based on measurements with pressure-velocity probes (L),” *J. Acoust. Soc. Am*, vol. 125, no. 6, pp. 3518–3521, 2009.

[109] C.-X. Bi and X.-Z. Chen, “Sound Field Separation Technique Based on Equivalent Source Method Using Pressure-Velocity Measurements and Its Application in Nearfield Acoustic Holography,” in *Proceedings of Internoise*, (Shangai, China), 2008.

[110] E. Fernandez-Grande and F. Jacobsen, “Sound field separation with a double layer velocity transducer array (L),” *J. Acoust. Soc. Am.*, vol. 130, no. 1, pp. 5–8, 2011.

[111] E. Fernandez-Grande and F. Jacobsen, “Separation of radiated sound field components from waves scattered by a source under non-anechoic conditions,” in *Proceedings of Inter-Noise 2010, Lisbon, Portugal*, 2010.

[112] E. Fernandez-Grande, F. Jacobsen, and Q. Leclere, “Direct formulation of the supersonic acoustic intensity in space domain,” *J. Acoust. Soc. Am*, vol. 131, no. 1, pp. 186–193, 2012.

[113] E. G. Williams, “Supersonic acoustic intensity on planar sources,” *J. Acoust. Soc. Am.*, vol. 104, no. 5, pp. 2845–2850, 1998.

[114] C. W. Horton and J. G. S. Innis, “The Computation of Far-Field Radiation Patterns from Measurements Made near the Source,” *J. Acoust. Soc. Am*, vol. 33, no. 7, pp. 877–880, 1961.

[115] G. Maidanik, “Response of ribbed panels to reverberant acoustic fields,” *J. Acoust. Soc. Am.*, vol. 34, no. 6, pp. 809 – 826, 1962.

[116] H. G. Ferris, “Farfield Radiation Pattern of a Noise Source from Nearfield Measurements,” *J. Acoust. Soc. Am*, vol. 36, no. 8, pp. 1597–1598, 1964.

[117] L. Cremer, M. Heckl, and E. E. Ungar, *Structure-Borne Sound*. Berlin Heidelberg New York: Springer-Verlag, 1973.

[118] F. Fahy, *Sound and Structural Vibration*. London: Academic Press, 1987.

[119] F. Fahy, *Sound Intensity*. London: Taylor & Francis, 2nd ed. ed., 1995.

[120] “Cetim - 2nd international congress on acoustic intensity,” (Senlis, France), pp. 97–104, September 1985.

[121] V. Borgiotti, “The power radiated by a vibrating body in an acoustic fluid and its determination from boundary measurements,” *J. Acoust. Soc. Am.*, vol. 88, no. 4, pp. 1884–1893, 1990.

[122] D. M. Photiadis, “The relationship of singular value dcomposition to wavevector filtering in sound radiation problems,” *J. Acoust. Soc. Am.*, vol. 88, no. 2, pp. 1152–1159, 1990.

[123] A. Sarkissian, “Acoustic radiation from finite structures,” *J. Acoust. Soc. Am.*, vol. 90, no. 1, pp. 574–578, 1991.

[124] V. Borgiotti and E. M. Rosen, “The determination of the far field of an acoustic radiator from sparse measurement samples in the near field,” *J. Acoust. Soc. Am.*, vol. 92, no. 2, pp. 807–818, 1992.

[125] G. V. Borgiotti and E. Jones, “The Determination of the Acoustic Far Field of a Radiating Body in an Acoustic Fluid From Boundary Measurements,” *J. Acoust. Soc. Am.*, vol. 93, no. 5, pp. 2788–2797, 1993.

[126] S. J. Elliott and M. E. Johnson, “Radiation modes and the active control of sound power,” *J. Acoust. Soc. Am.*, vol. 94, no. 4, pp. 2194–2204, 1993.

[127] M. N. Currey and K. A. Cunefare, “The radiation modes of baffled finite plates,” *J. Acoust. Soc. Am.*, vol. 98, no. 3, pp. 1570–1580, 1995.

[128] R. A. Tenenbaum and M. B. S. Magalhaes, “A new technique to identify arbitrarily shaped noise sources,” *Shock and Vibration*, vol. 13, pp. 219–232, 2006.

[129] M. B. Magalhaes and R. Tenenbaum, "Supersonic Acoustic Intensity for Arbitrarily Shaped Sources," *Acta Acust. united Ac.*, vol. 92, pp. 189–201, 2006.

[130] E. G. Williams, "Supersonic acoustic intensity," *J. Acoust. Soc. Am.*, vol. 97, no. 1, pp. 121–127, 1995.

[131] E. Fernandez-Grande and F. Jacobsen, "Supersonic acoustic intensity with statistically optimized near-field acoustic holography," in *Proceedings of Inter-Noise 2011, Osaka, Japan*, 2011.

[132] J.-C. Pascal, "Structure and patterns of acoustic intensity fields," in *CETIM - 2nd international congress on acoustic intensity*, (Senlis, France), pp. 97–104, 1985.

[133] J.-C. Pascal and J.-F. Li, "Irrotational intensity and boundary values," in *ICA - 17th international congress on acoustics*, (Rome, Italy), paper NÂř 5A.09.01, 2001.

[134] M. Thivant, P. B. Andersson, and J.-L. Guyader, "The intensity potential approach," *J. Acoust. Soc. Am.*, vol. 112, p. 2246, Nov. 2002.

[135] I. J. A. Mann, J. Tichy, and A. J. Romano, "Instantaneous and time-averaged energy transfer in acoustic fields," *J. Acoust. Soc. Am*, vol. 82, no. 1, pp. 17–30, 1987.

[136] B. Rafaely, "Plane-wave decomposition of the sound field on a sphere by spherical convolution," *J. Acoust. Soc. Am*, vol. 116, no. 4, pp. 2149–2157, 2004.

[137] B. Rafaely, "Analysis and design of spherical microphone arrays," *Speech and Audio Processing, IEEE Transactions on*, vol. 13, no. 1, pp. 135–143, 2005.

[138] M. Park and B. Rafaely, "Sound-field analysis by plane-wave decomposition using spherical microphone array," *J. Acoust. Soc. Am*, vol. 118, no. 5, pp. 3094–3103, 2005.

[139] E. Williams, N. Valdivia, and P. C. Herdic, "Volumetric acoustic vector intensity imager," *J. Acoust. Soc. Am.*, vol. 120, no. 4, pp. 1887–1897, 2006.

[140] F. Jacobsen, J. Hald, Fernandez-Grande. E., and G. Moreno, "Spherical near field acoustic holography with microphones on a rigid sphere," in *Acoustics '08 Paris. Vol 123*, p. 3385, 2008.

[141] E. Williams and K. Takashima, "Vector intensity reconstructions in a volume surrounding a rigid spherical measurement array," in *Acoustics '08 Paris. Vol 123*, p. 3309, 2008.

[142] K. Takashima, H. Nakagawa, and E. G. Williams, "Vector intensity measurement with a rigid spherical microphone array in a vehicle cabin," in *Acoustics '08 Paris. Vol 123*, p. 3312, 2008.

[143] E. Williams and K. Takashima, “Vector intensity reconstructions in a volume surrounding a rigid spherical microphone array,” *J. Acoust. Soc. Am.*, vol. 127, no. 2, pp. 773–783, 2010.

[144] F. Jacobsen, G. Moreno-Pescador, E. Fernandez-Grande, and J. Hald, “Near field acoustic holography with microphones on a rigid sphere,” *J. Acoust. Soc. Am.*, vol. 129, no. 6, pp. 3461–3464, 2011.

[145] M. Abramowitz and I. A. Stegun, *Handbook of Mathematical Functions*. Washington DC: Natinal Buerau of Standards, 1964.

Papers A-I

Part I

Paper A

Sound field separation with a double layer velocity transducer array (L)

Efren Fernandez-Grande[a)] and Finn Jacobsen
Acoustic Technology, Department of Electrical Engineering, DTU Technical University of Denmark, Building 352, Oersteds Plads, DK-2800 Kongens Lyngby, Denmark

(Received 16 September 2010; revised 13 May 2011; accepted 14 May 2011)

In near-field acoustic holography sound field separation techniques make it possible to distinguish between sound coming from the two sides of the array. This is useful in cases where the sources are not confined to only one side of the array, e.g., in the presence of additional sources or reflections from the other side. This paper examines a separation technique based on measurement of the particle velocity in two closely spaced parallel planes. The purpose of the technique is to recover the particle velocity radiated by a source in the presence of disturbing sound from the opposite side of the array. The technique has been examined and compared with direct velocity based reconstruction, as well as with a technique based on the measurement of the sound pressure and particle velocity. The double layer velocity method circumvents some of the drawbacks of the pressure-velocity based reconstruction, and it can successfully recover the normal velocity radiated by the source, even in the presence of strong disturbing sound. © *2011 Acoustical Society of America.*
[DOI: 10.1121/1.3598431]

PACS number(s): 43.60.Sx, 43.60.Pt, 43.20.Rz [EJS] Pages: 5–8

I. INTRODUCTION

Near-field acoustic holography (NAH) is a source identification technique that makes it possible to reconstruct the acoustic field radiated by a source based on measurements in its near-field.[1,2] One of the ultimate purposes of NAH is to determine the particle velocity on the surface of the source, since it provides very useful information about its vibration.

Conventional NAH requires that the sources are confined to only one side of the array, because it is not possible to distinguish between sound coming from the two sides. However, in cases where this requirement cannot be fulfilled, and there is sound from the other side due to, e.g., other sources or reflections, sound field separation techniques can be used to determine the contribution from each side and hence estimate the radiation from the source of interest. Some of the existing separation methods rely on measuring the sound pressure in two closely spaced parallel planes,[3–5] or on a combined measurement of the sound pressure and particle velocity in a single plane.[6,7] However, not so much attention has been put specifically on the separation of the particle velocity in the existing literature.

Previous studies indicate that it is more accurate to reconstruct the particle velocity field based on measurements of the pressure and particle velocity than based on measurements of the sound pressure in two parallel planes.[8] However, sound field separation based on pressure-velocity measurements relies critically on the pressure and velocity based estimates to be identical.[6,8] In this paper, the possibility of separating the sound field based on the measurement of the particle velocity in two parallel planes is examined. This technique would circumvent the problems associated with the pressure-velocity estimates mismatch. Additionally, a technique based on measurement of the pressure and the particle velocity in one single plane is proposed and examined.

The methods presented in this paper are based on the statistically optimized near-field holography (SONAH) wave model.[9]

II. THEORY

Given a stationary sound field in which a primary source is radiating in the presence of sound from the opposite side of the measurement plane, the total normal velocity can be expressed as the sum of the contributions coming from the two sides of the array,

$$u_z(\mathbf{r}_h) = u_o(\mathbf{r}_h) + u_i(\mathbf{r}_h), \tag{1}$$

where $u_z(\mathbf{r}_h)$ is the normal velocity in the hologram plane, $u_o(\mathbf{r}_h)$ the outgoing normal velocity from the primary source, and $u_i(\mathbf{r}_h)$ the incoming normal velocity from the opposite side. The normal component of the particle velocity in the hologram plane can be expressed as a weighted sum of elementary plane waves coming from both sides of the array,

$$u_z(\mathbf{r}_h) = \sum_n c_n^{(o)} \phi_n(\mathbf{r}_h) + \sum_n c_n^{(i)} \psi_n,(\mathbf{r}_h), \tag{2}$$

where $c^{(o)}$ and $c^{(i)}$ are the weights of the outgoing and incoming plane wave functions in which the sound field is decomposed: $\phi_n(\mathbf{r}) = e^{-j\left[k_{x,n}x+k_{y,n}y+k_{z,n}(z-z^+)\right]}$ and $\psi_n(\mathbf{r}) = e^{-j\left[k_{x,n}x+k_{y,n}y-k_{z,n}(z-z^-)\right]}$, where z^+ and z^- are the virtual source planes.[9] Similarly the pressure in the hologram plane can be expressed based on Eq. (2) and Euler's equation of motion, as

[a)]Author to whom correspondence should be addressed. Electronic mail: efg@elektro.dtu.dk

$$p(\mathbf{r}_h) = \sum_n (-j\omega\rho) \int c_n^{(o)} \phi_n(\mathbf{r}_h) + \sum_n (-j\omega\rho) \int c_n^{(i)} \psi_n(\mathbf{r}_h) dz. \quad (3)$$

A. Double layer velocity separation

If the particle velocity is measured in two parallel planes, it can be expressed as in Eq. (2) in each plane. In matrix form,

$$\mathbf{u}_{h1} = \mathbf{A}_{h1}\mathbf{c}_o + \mathbf{B}_{h1}\mathbf{c}_i, \quad (4a)$$

$$\mathbf{u}_{h2} = \mathbf{A}_{h2}\mathbf{c}_o + \mathbf{B}_{h2}\mathbf{c}_i. \quad (4b)$$

The subscripts $h1$ and $h2$ refer to the two hologram planes. Each row of $\mathbf{A}$ and $\mathbf{B}$ contains respectively the outgoing and the incoming elementary functions at each position, and $\mathbf{c}_o$ and $\mathbf{c}_i$ are the weights of the outgoing and incoming waves. The system of equations can be assembled into the simple general form

$$\mathbf{u}_h = \mathbf{M}_h \mathbf{c}, \quad (5)$$

where $\mathbf{u}_h$ is a column vector with the measured normal velocity in the two hologram planes, and $\mathbf{c}$ is a vector with the outgoing and incoming coefficients, $\mathbf{c}_o$ and $\mathbf{c}_i$. The coefficient vector $\mathbf{c}$ can be obtained from the regularized inversion of Eq. (5).[12] Thus the outgoing field from the primary source in the reconstruction plane can be calculated as

$$\mathbf{u}_s = \mathbf{A}_s \mathbf{c}_o, \quad (6)$$

where $\mathbf{A}_s$ is the matrix containing the outgoing elementary waves $\phi(\mathbf{r}_s)$ at the reconstruction positions, and weighted by the vector $\mathbf{c}_o$, which is included in $\mathbf{c}$.

B. Single layer velocity separation

The method described here is inspired by Ref. 10, but modified for separating the particle velocity instead of the sound pressure. The total pressure and particle velocity in a single hologram plane can be decomposed into a set of elementary plane waves as in Eqs. (2) and (3). The system of equations in matrix form is

$$\mathbf{u}_h = \mathbf{A}_{h1}\mathbf{c}_o + \mathbf{B}_{h1}\mathbf{c}_i, \quad (7a)$$
$$\mathbf{p}_h = \mathbf{A}_{h1}^{up}\mathbf{c}_o + \mathbf{B}_{h1}^{up}\mathbf{c}_i, \quad (7b)$$

where the matrices $\mathbf{A}_{h1}^{up}$ and $\mathbf{B}_{h1}^{up}$ contain the outgoing and incoming elementary wave functions integrated with respect to the normal direction z as in Eq. (3). This system of equations can be assembled into

$$\mathbf{b}_h = \mathbf{M}_h^{up}\mathbf{c}, \quad (8)$$

where $\mathbf{b}_h$ is a column vector with the measured pressure and normal velocity, and $\mathbf{c}$ is a vector with the outgoing and incoming coefficients. The inversion of this equation yields the coefficient vector $\mathbf{c}$, based on which the particle velocity in the reconstruction plane can be estimated with Eq. (6). Note that the matrix inversions should be regularized. In this study, Tikhonov regularization was used and the regularization parameter was chosen using generalized cross validation.[12]

III. NUMERICAL STUDY

A numerical study to examine the methods described in the previous section has been conducted. The primary source was a 30×30 cm^2 simply supported baffled aluminum plate, 3 mm thick, and centered at the origin of coordinates. The plate was driven in the center by a point force of amplitude 0.1 N. Its radiation was calculated with a numerical approximation to Rayleigh's integral using a grid of 20×20 points. The plate was radiating in the presence of a disturbing monopole source placed at (0, -0.2, 0.5) m, with a frequency independent volume acceleration $j\omega Q \approx 0.2j$ m^3/s^2. The field scattered by the rigid primary source (plate and baffle) was modeled assuming perfect reflection by means of a virtual monopole at (0, -0.2, -0.5) m. Random noise was added to the simulated measurements with a signal-to-noise ratio of 30 dB.

The two hologram planes for the double layer technique were $z_{h1} = 5$ cm and $z_{h2} = 7$ cm, and for the single layer techniques it was as well $z_{h1} = 5$ cm. The reconstruction plane was $z_s = 4$ cm. The measurement grid consisted of 11×11 points with a uniform interspacing of 3 cm. The virtual source plane used to scale the plane waves from the primary source side was $z^+ = 0.5$ cm. For the waves coming from the "back" of the array, they were $z_1^- = 6.5$ cm for the pressure-velocity method, and $z_2^- = 8.5$ cm for the double layer method. The reconstruction error is defined in dB as $20\log_{10} \|u(\mathbf{r}_s) - u(\mathbf{r}_s)_{\text{true}}\| / \|u(\mathbf{r}_s)_{\text{true}}\|$.

Figure 1 shows the reconstruction error for the methods as a function of frequency, and Fig. 2 shows the overall reconstruction error as a function of the measurement distance.

The lower error at 800 Hz is due to the higher signal-to-noise ratio at this frequency. The results indicate that the error increases as we move further away from the source. This is not surprising, considering the fact that the disturbing normal velocity vanishes close to the source due to the rigid boundary. Thus, as the measurement distance compared to the wavelength increases, the disturbance of the true normal velocity becomes larger. Contrarily, the disturbance becomes smaller as the measurement distance compared to the wavelength decreases. Therefore, when the measurement is done close to the source, the most accurate reconstruction is found with simple one layer velocity measurements, while if the measurement distance is larger, separation techniques are more accurate. On the other hand the reconstruction based on pressure-velocity measurements is less accurate at low frequencies or close to the source, due to the fact that the sound pressure field is severely disturbed by the reflection from the source.

IV. EXPERIMENTAL RESULTS

The primary source used in this experimental study was an aluminum plate mounted on a rigid wooden box and

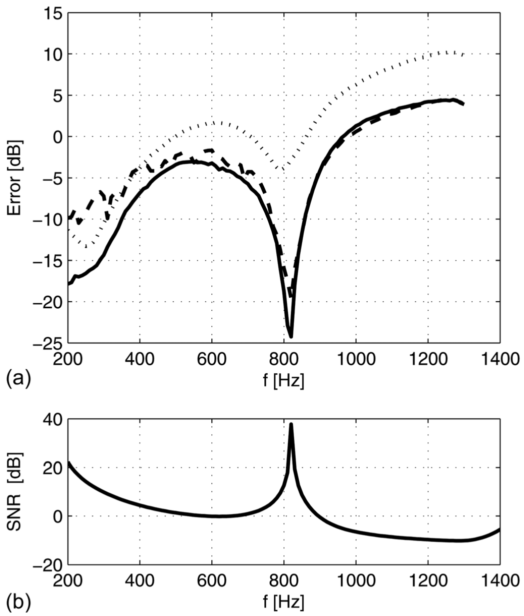

FIG. 1. (a) Reconstruction error of the particle velocity with $z_{h1} = 5$ cm, $z_{h2} = 7$ cm: double layer method (solid line); single layer velocity (dotted line); pressure-velocity method (dashed line). (b) Signal-to-noise ratio between the primary source velocity and the disturbing velocity in z_{h1}.

driven acoustically by a loudspeaker inside the box. The dimensions of the plate were 45×45 cm^2 and 3 mm thick. The plate was in the $z = 0$ plane, centered at the origin of coordinates. A loudspeaker driven coherently was used as a disturbing source. It was placed opposite to the primary source, at (0, −0.1, 0.6) m. The pressure and the normal component of the particle velocity were measured in a grid of 9×9 points with 5 cm interspacing at the hologram planes $z_{h1} = 3$ cm and $z_{h2} = 6$ cm for the double layer velocity method, and $z_{h1} = 3$ cm for the single layer techniques. The undisturbed velocity was measured in the reconstruction plane, which was as well $z_s = 3$ cm, and regarded as the true field radiated by the primary source. The virtual planes were $z^+ = 0.5$ cm for the outgoing waves from the primary source, and for the incoming waves, $z_1^- = 4.25$ cm for the pressure velocity method, and $z_2^- = 8.5$ cm for the double layer velocity method. A microflown 1/2 in. intensity probe was used to measure the particle velocity and the pressure in anechoic conditions and a manual scanning frame served to measure sequentially all the grid points.

Figure 3 shows the reconstructed particle velocity across the diagonal of the aperture with the different techniques. At 400 Hz, the measurement distance is less than 5% of the wavelength, resulting in a small disturbance of the velocity field. Therefore, the best results are found with the reconstruction based on the measurement of the particle velocity (single and double layer). The pressure-velocity based reconstruction is not accurate, due to the fact that close to the source the disturbance of the sound pressure field is very large. The overall reconstruction error is about −14 dB for

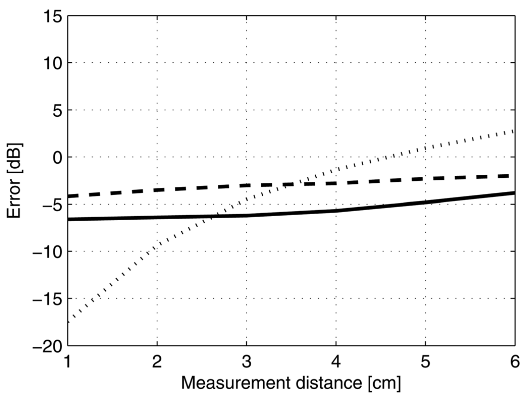

FIG. 2. Reconstruction error of the particle velocity as a function of the measurement distance: double layer velocity method (solid line); single layer velocity (dotted line); and pressure-velocity method (dashed line). $f = 500$ Hz.

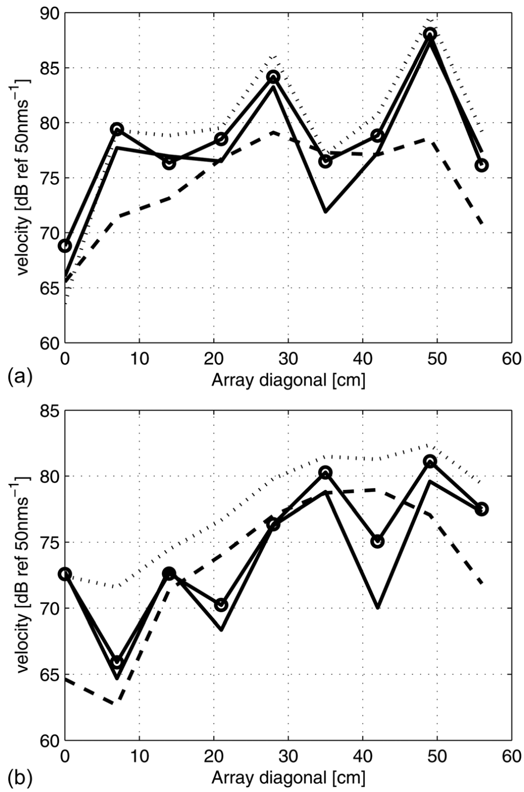

FIG. 3. Reconstructed particle velocity level along the diagonal of the array. $z_{h1} = 3$ cm, $z_{h2} = 6$ cm: true measured velocity (solid line with circles); double layer velocity method (solid line); single layer velocity (dotted line); pressure-velocity method (dashed line). (a) $f = 400$ Hz. (b) $f = 800$ Hz.

the single layer particle velocity, −12 dB for the double layer particle velocity, and −3 dB for the pressure-velocity method. At 800 Hz [Fig. 3(b)], the measurement distance compared to the wavelength is larger than in the previous case, and the reconstruction based on the double layer measurement of the particle velocity is consequently more accurate than the reconstruction based on the single layer measurement of the particle velocity. The pressure-velocity method is still less accurate than the double layer method and it tends to oversmooth the solution. The reconstruction error is about −18 dB based on the double layer velocity technique, −7.5 dB based on the pressure-velocity method and −6 dB based on the single velocity method.

The study also revealed that if the measurement distance is larger than about 12% of the wavelength (not shown), the separation techniques are significantly more accurate than the direct reconstruction based on the single layer measurement of the particle velocity. In this case, the pressure-velocity method is as accurate as the double layer velocity method.

V. DISCUSSION

It is a well known fact that the normal component of the particle velocity of extraneous noise vanishes on the boundary of a rigid source. This makes it possible to obtain a holographic reconstruction of the sound field radiated by the source based on velocity measurements, without requiring sound field separation techniques. This holds at low frequencies and or close to the source, when the measurement distance relative to the wavelength is sufficiently small (less than about 8%). However, if this is not the case, the disturbing particle velocity will influence the measurement and consequently deteriorate the reconstruction. In such case it is advantageous to use sound field separation techniques.

Previous studies have shown that it is more accurate to reconstruct the particle velocity field based on combined measurements of the pressure and the particle velocity than based on double layer measurements of the sound pressure.[8] However, the separation based on pressure and velocity measurements relies on the assumption that the reconstruction of the sound field based on either quantity is identical. This is however not true in practice, and there is an important error associated with it. Alternatively, the sound field separation based on the measurement of the particle velocity in two parallel planes circumvents the drawbacks of the pressure-velocity separation. First, the method does not rely on the estimates from the pressure and velocity being identical. Second, the prediction of the particle velocity is based on velocity measurements, which is significantly more accurate than predictions of the velocity based on pressure measurements.[11] Additionally, the double layer velocity method benefits from the fact that at low frequencies and or close to a rigid source, the velocity disturbance is small, unlike the pressure. This explains the better results obtained with the double layer velocity method. However, the method is costly, because it requires twice the number of measurement positions, and it has the disadvantage that the secondary measurement plane is further away from the primary source, which is challenging due to the larger backpropagation distance.

VI. CONCLUSIONS

A method for estimating the particle velocity radiated by a source in the presence of extraneous noise from the opposite side of the array has been examined and validated. The method relies on the measurement of the normal velocity in two parallel planes. Additionally, a method based on the measurement of the pressure and normal velocity in a single layer has been studied. Both methods can successfully estimate the particle velocity field radiated by the source, the double layer velocity method being somewhat more robust. The study reveals that if the source under study is rigid, it is possible to base the reconstruction on single layer measurements of the normal velocity close to the source, because the normal component of the disturbing particle velocity vanishes on the boundary. However, at higher frequencies, when the measurement distance cannot be sufficiently small, it is advantageous to use sound field separation techniques.

[1] J. D. Maynard, E. G. Williams, and Y. Lee, "Nearfield Acoustic Holography I: Theory of generalized holography and the development of NAH," J. Acoust. Soc. Am. **78**, 1395–1413 (1985).

[2] E. G. Williams, *Fourier Acoustics. Sound Radiation and Nearfield Acoustical Holography* (Academic, San Diego, 1999), Chap. 3.

[3] G. V. Frisk, A. V. Oppenheim, and D. R. Martinez, "A technique for measuring the plane-wave reflection coefficient of the ocean bottom," J. Acoust. Soc. Am. **68**, 602–612 (1980).

[4] M. Tamura, "Spatial Fourier transform method of measuring reflection coefficients at oblique incidence. I: Theory and numerical examples," J. Acoust. Soc. Am. **88**, 2259–2264 (1990).

[5] J. Hald, "Patch holography in cabin environments using a two-layer hand held array with an extended SONAH algorithm," in *Proceedings of Euronoise 2006*, Tampere, Finland (Acoustical Society of Finland, Helsinki, 2006).

[6] F. Jacobsen and V. Jaud, "Statistically optimized near field acoustic holography using an array of pressure-velocity probes," J. Acoust. Soc. Am. **121**, 1550–1558 (2007).

[7] Y.-B. Zhang, F. Jacobsen, C.-X. Bi, and X.-Z. Chen, "Near field acoustic holography based on the equivalent source method and pressure-velocity transducers," J. Acoust. Soc. Am. **126**, 1257–1263 (2009).

[8] F. Jacobsen, X. Chen, and V. Jaud, "A comparison of statistically optimized near field acoustic holography using single layer pressure-velocity measurements and using double layer pressure measurements (L)," J. Acoust. Soc. Am. **123**, 1842–1845 (2008).

[9] J. Hald, "Basic theory and properties of statistically optimized near-field acoustical holog raphy," J. Acoust. Soc. Am **125**, 2105–2120 (2009).

[10] Y.-B. Zhang, X.-Z. Chen, and F. Jacobsen, "A sound field separation technique based on measurements with pressure-velocity probes (L)," J. Acoust. Soc. Am. **125**, 3518–3521 (2009).

[11] F. Jacobsen and Y. Liu, "Near field acoustic holography with particle velocity transducers," J. Acoust. Soc. Am. **118**, 3139–3144 (2005).

[12] P. C. Hansen, *Rank-Deficient and Discrete Ill-Posed Problems. Numerical Aspects of Linear Inversion* (SIAM, Philadelphia, 1998), Chaps. 5–7.

Paper B

Sound field separation with sound pressure and particle velocity measurements

Efren Fernandez-Grande[a] and Finn Jacobsen
Acoustic Technology, Department of Electrical Engineering, DTU Technical University of Denmark, Building 352, Oersteds Plads, DK-2800 Kongens Lyngby, Denmark

Quentin Leclère
Laboratoire Vibrations Acoustique, INSA Lyon, F-69621 Villeurbanne Cedex, France

(Dated: June 22, 2012)

In conventional near-field acoustic holography (NAH) it is not possible to distinguish between sound from the two sides of the array, thus, it is a requirement that all the sources are confined to only one side and radiate into a free field. When this requirement cannot be fulfilled, sound field separation techniques make it possible to distinguish between outgoing and incoming waves from the two sides, and thus NAH can be applied. In this paper, a separation method based on the measurement of the particle velocity in two layers and another method based on the measurement of the pressure and the velocity in a single layer are proposed. The two methods use an equivalent source formulation with separate transfer matrices for the outgoing and incoming waves, so that the sound from the two sides of the array can be modeled independently. A weighting scheme is proposed to account for the distance between the equivalent sources and measurement surfaces and for the difference in magnitude between pressure and velocity. Experimental and numerical studies have been conducted to examine the methods. The experiment consists of a sound source radiating into an enclosed space where multiple reflections occur.

PACS numbers: 43.60.Sx, 43.60.Pt, 43.20.Rz

I. INTRODUCTION

Near-field Acoustic Holography (NAH)[1,2] is a well established sound source identification technique that makes use of near-field measurements in order to reconstruct and visualize the complete sound field radiated by a sound source, i.e., sound pressure, particle velocity and sound intensity, over a three-dimensional space near the source. In conventional NAH, it is not possible to distinguish between sound coming from the two sides of the array. Therefore, a free-field half-space is required where all the sound sources are confined to only one side.

If there are mutually incoherent sources on the two sides of the array, it is possible to separate their contribution based on their statistical properties,[3–6] or if only one source is of interest and its phase reference is available, the 'disturbing' sound can be simply averaged out. However, if the sound from the two sides of the array is due to coherent sources, it is not possible to make use of their statistical properties for the separation. In this case, sound field separation methods, which make use of directional information to estimate the propagation direction of the waves, can be very useful.

The first separation methods, some of which were proposed more than two decades ago,[7–11] rely on measurements of the sound pressure in two closely spaced parallel planes. In recent years several separation methods based on the combined measurement of the sound pressure and the particle velocity have appeared.[12–15] More recently, a method was presented that made use of particle velocity measurements in two closely spaced parallel planes.[16]

Two new methods are proposed in this paper, one that relies on measurement of the particle velocity in two layers (u-u), and another that relies on measurement of the sound pressure and particle velocity in a single layer (p-u). The present study differs from previous ones (ref. 16) in that it examines the u-u measurement principle in a general sense, considering the separation of both the sound pressure and the particle velocity fields, and is based on the equivalent source method,[17,18] thus it can be applied to arbitrarily shaped sources. Furthermore, the proposed methods (u-u and p-u) use independent transfer matrices for the outgoing and incoming waves, and an optional weighting to compensate for the distance between the equivalent sources and the measurement surface. The proposed p-u method is based on a weighted least squares inversion that compensates for the difference in magnitude between pressure and velocity.

One of the main potentials of separation techniques is the possibility of using NAH in non-anechoic environments such as conventional rooms or other enclosed spaces, where a source may be radiating in the presence of multiple reflections. The performance of double layer pressure techniques in such enclosed spaces has been addressed previously.[19–21] On the contrary, the recent separation methods based on pressure and velocity measurements have mostly been examined with a single disturbing source[12–14,16] or a single reflection,[15] but not for the case where multiple reflections from different directions occur. In fact, the measurement of the normal component of the particle velocity can be favorable in this case, because the influence of reflected waves

[a] Electronic address: efg@elektro.dtu.dk

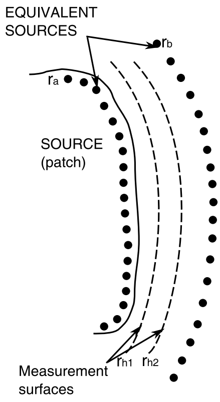

FIG. 1. Diagram of the double layer equivalent source method (for a patch of the source).

arriving from the edges of the measurement aperture is naturally suppressed. The separation methods proposed in this study are examined for the case where a sound source is radiating into an enclosed space in the presence of multiple reflections.

II. THEORY

A. Double layer particle velocity

Given a sound field consisting of outgoing and incoming waves, the normal component of the particle velocity in two layers, $\mathbf{r}_{h1}$ and $\mathbf{r}_{h2}$, can be expressed as the result of the superposition of the sound field produced by a distribution of point sources at the two sides of the measurement aperture (see Fig.1). These so-called equivalent sources are distributed over the surfaces $\mathbf{r}_a$ and $\mathbf{r}_b$, thus,

$$u_n(\mathbf{r}_{h1}) = -\sum_k^N q_{(1,k)} G_u(\mathbf{r}_{h1}, \mathbf{r}_{ak}) - \sum_k^M q_{(2,k)} G_u(\mathbf{r}_{h1}, \mathbf{r}_{bk}), \tag{1}$$

$$u_n(\mathbf{r}_{h2}) = -\sum_k^N q_{(1,k)} G_u(\mathbf{r}_{h2}, \mathbf{r}_{ak}) - \sum_k^M q_{(2,k)} G_u(\mathbf{r}_{h2}, \mathbf{r}_{bk}), \tag{2}$$

where q_k is the strength of each equivalent source and the function G_u is the derivative in the normal direction (to the equivalent source surface) of the Green's function in free-space,

$$G_u(\mathbf{r}, \mathbf{r}_0) = \frac{\partial}{\partial n} G(\mathbf{r}, \mathbf{r}_0), \tag{3}$$

$$G(\mathbf{r}, \mathbf{r}_0) = \frac{e^{-jk|\mathbf{r}-\mathbf{r}_0|}}{4\pi|\mathbf{r}-\mathbf{r}_0|}. \tag{4}$$

Note that the time dependence $e^{j\omega t}$ has been omitted.

Equations (1) and (2) can be expressed in matrix form as

$$\begin{bmatrix} \mathbf{u}_{h1} \\ \mathbf{u}_{h2} \end{bmatrix} = -\begin{bmatrix} \mathbf{G}^u_{a|h1} & \mathbf{G}^u_{b|h2} \\ \mathbf{G}^u_{a|h2} & \mathbf{G}^u_{b|h2} \end{bmatrix} \cdot \begin{bmatrix} \mathbf{q}_1 \\ \mathbf{q}_2 \end{bmatrix}. \tag{5}$$

From Eq. (5), the strength of the equivalent sources $\mathbf{q}_1$ and $\mathbf{q}_2$ can be estimated from the measured velocities by means of a regularized inversion[22] of the matrix. Then, the outgoing and incoming sound can be estimated via the Green's function between the equivalent sources and the reconstruction positions as,

$$\mathbf{u}_s^{(o)} = -\mathbf{G}^u_{a|s}\mathbf{q}_1, \tag{6}$$

$$\mathbf{p}_s^{(o)} = j\omega\rho \cdot \mathbf{G}_{a|s}\mathbf{q}_1, \tag{7}$$

$$\mathbf{u}_s^{(i)} = -\mathbf{G}^u_{b|s}\mathbf{q}_2, \tag{8}$$

$$\mathbf{p}_s^{(i)} = j\omega\rho \cdot \mathbf{G}_{b|s}\mathbf{q}_2. \tag{9}$$

The superscripts '(o)' and '(i)' denote the outgoing and incoming fields respectively and the subscript 's' the reconstruction positions.

Note that this method, because of being based on an equivalent source model, is not limited to separable geometries but can handle arbitrarily shaped sources.

B. Single layer pressure-velocity

Sound arriving from the two sides of the array can also be separated based on the combined measurement of sound pressure and particle velocity.[12–15] In the present study, the separation is based on the equivalent source method with independent transfer matrices for the outgoing and incoming sound.

Based on the measured sound pressure and particle velocity,

$$\begin{bmatrix} \mathbf{p}_h \\ \mathbf{u}_h \end{bmatrix} = \begin{bmatrix} j\omega\rho\mathbf{G}_{a|h} & j\omega\rho\mathbf{G}_{b|h} \\ -\mathbf{G}^u_{a|h} & -\mathbf{G}^u_{b|h} \end{bmatrix} \cdot \begin{bmatrix} \mathbf{q}_1 \\ \mathbf{q}_2 \end{bmatrix}, \tag{10}$$

from which $\mathbf{q}_1$ and $\mathbf{q}_2$ can be estimated by means of a regularized inversion, and the outgoing and incoming sound pressure and particle velocity can be reconstructed using Eqs. (6) to (9).

However, if this system was solved as a conventional least squares problem, the weight of the velocity field in the solution would be less than that of the pressure, because the former is typically of much smaller magnitude (by approximately ρc, as follows from Euler's equation of motion $\mathbf{u} = -\nabla p/(j\omega\rho)$), Thus the minimization of the residual would depend very strongly on the pressure vector. It is more appropriate to solve the system by means of a weighted least squares solution.[23] The solution for the vector $\mathbf{q}$ in this case is,

$$\mathbf{q} = (\mathbf{W}\mathbf{G}_h)^+ \mathbf{W}\mathbf{b}, \tag{11}$$

where $\mathbf{G}_h$ is the transfer matrix as in Eq. (10), $\mathbf{b}$ is the column vector with the measured pressure and velocity, and $\mathbf{W}$ is the weighting diagonal matrix. The superscript + denotes the regularized pseudo-inverse:

$$(\mathbf{WG}_h)^+ = ([\mathbf{WG_h}]^H \mathbf{WG_h} + \lambda \mathbf{I})^{-1} [\mathbf{WG_h}]^H, \quad (12)$$

where λ is the Tikhonov regularization parameter. Note that regularization is essential when the solution is back-propagated.

A straightforward and robust choice for the weighting matrix is to divide the pressures with the norm of all the pressure inputs, and the velocities with the norm of all velocity inputs. Thus the weighting matrix is diagonal with the inverse of the pressure and velocity norms, $[\mathbf{W}]_{2m\times 2m} = \mathrm{diag}([1/||\mathbf{p}||]_{1\times m}; [1/||\mathbf{u}||]_{1\times m})$.

The purpose of this weighting is to equalize the influence of the measured inputs to obtain a meaningful solution, equally based on the pressure and particle velocity measurements. This weighting reduces the condition number of the transfer matrix considerably. Thus, the obtained solution is much less sensitive to noise and is more robust.The results obtained with this methodology are similar to the results obtained by inverting the sound pressure and velocity separately, although in this case a single inversion is required.

Apart from the inversion, the method described here differs from the one in ref. 14 in that the equivalent sources of the outgoing and incoming fields, $\mathbf{G}_{a|h}$ and $\mathbf{G}_{b|h}$, can be placed asymmetrically, so that they can model the sound from the two sides independently. Thus, if the incoming sound is radiated by a source that is not placed equidistantly form the array, the equivalent sources from one side can be retracted accordingly, and the results can be improved. This property is also useful when the method is applied to sources with arbitrary geometries because the distribution of equivalent sources at the two sides can be modified according to the sources geometries.

It should be noted that if the retraction distance between equivalent sources at the two sides of the array is significantly different, an additional right-hand weighting would be applied to the transfer matrix, to guarantee that all equivalent sources have the same weight in the minimization of the regularized solution norm, regardless of the distance to the measurement surface. The system to be solved in this case would be

$$[\mathbf{Wb}] = [\mathbf{WG_h M}]\mathbf{q_M}, \quad (13)$$

where $\mathbf{M}$ is the new weighting diagonal matrix, and $\mathbf{q_M} = \mathbf{M^{-1}q}$. An appropriate weighting choice for the matrix $\mathbf{M}$ is the distance from each equivalent source to the measurement surface.[25] In this way, no excessive energy is attributed to the equivalent sources that are closer to the measurement positions. This weighting is however not necessary in the present study.

III. NUMERICAL STUDY

A numerical study has been conducted to examine the methods described in the foregoing. The source used for the experiment was a simply supported baffled steel plate of 30 x 30 cm^2, 1 mm thick, driven at the center by a point force of 0.1 N. The pressure and velocity radiated by the plate were calculated by numerically evaluating the Rayleigh integral using a discrete grid of 35 x 35 positions. The measurement grid consisted of 11 x 11 uniformly spaced positions over an area of 40 x 40 cm^2, with 4 cm inter-spacing distance. Normally distributed background noise of 30 dB signal-to-noise ratio was added to the simulated measurements.

The normalized error in dB between the 'true' free field radiation by the plate and the one reconstructed with the different techniques, was calculated as

$$E_p[dB] = 20\log_{10}\left(\frac{\|\mathbf{p}_{plate} - \mathbf{p}_s\|_2}{\|\mathbf{p}_{plate}\|_2}\right), \quad (14)$$

$$E_u[dB] = 20\log_{10}\left(\frac{\|\mathbf{u}_{plate} - \mathbf{u}_s\|_2}{\|\mathbf{u}_{plate}\|_2}\right), \quad (15)$$

where $\mathbf{p}_{plate}$ and $\mathbf{u}_{plate}$ are the free field pressure and normal velocity radiated by the plate, and $\mathbf{p}_s$ and $\mathbf{u}_s$ are the reconstructed ones with each of the methods.

A. Plate disturbed by an incident plane wave

In order to study how incoming sound influences the reconstruction, the case of a baffled vibrating plate radiating sound in the presence of an incoming plane wave is considered. The back-scattering from the source is modeled by means of a reflected plane wave traveling in the opposite z direction. The measurement planes are $z_{h1} = 7$ cm and $z_{h2} = 12$ cm for the u-u method, and $z_{h1} = 7$ cm for the p-u method. The reconstruction plane is also z_{h1}. The equivalent sources are retracted two inter-spacing distances from the reconstruction planes.

Figure 2 shows the reconstruction error at z_{h1} of the sound pressure and normal velocity as a function of frequency when there is an incoming plane wave from the direction normal to the plate (i.e., frontal incidence). The lower part of the figure shows the ratio in dB between the magnitude of the plate's free-field radiation and the incoming plus back-scattered plane waves at z_{h1}. In the entire low frequency range (below 400 Hz) the velocity based methods, 'u' and 'u-u', are consistently the most accurate due to the lesser disturbance of the velocity field at the source's boundary (due to the mutual canceling of incoming and scattered waves). On the whole, the accuracy of the methods depends mostly on the disturbance of the pressure and velocity fields, i.e., if the incoming and the back-scattered waves interfere constructively or destructively. This explains the accuracy of the 'p-u' and 'u-u' separation methods as a function of frequency (e.g., if the stand-off distance corresponds roughly to a quarter of a wavelength, the incident and backscattered pressures mutually cancel each other).

Figure 3 shows the reconstruction error as a function of the angle of incidence of the plane wave. The angle of incidence varies from $\theta = 90^o$, where the wave is propagating perpendicular to the normal direction of the plate

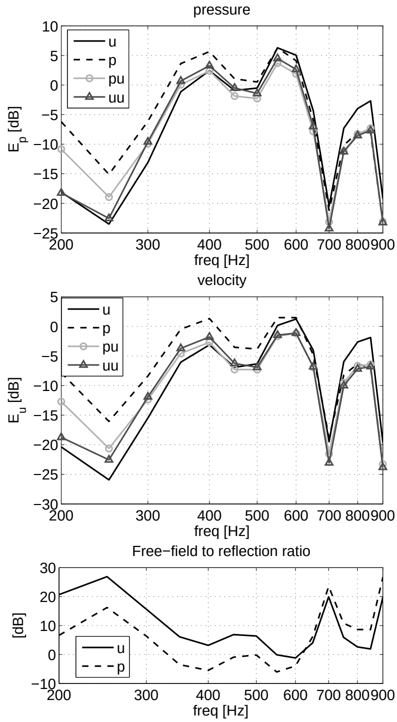

FIG. 2. Top: Reconstruction error of the field radiated by a baffled plate in the presence of an incident plane wave coming from the opposite side (frontal incidence) as a function of frequency. Bottom: Ratio between the radiated sound by the plate at z_{h1} and the incident plus backscattered plane waves.

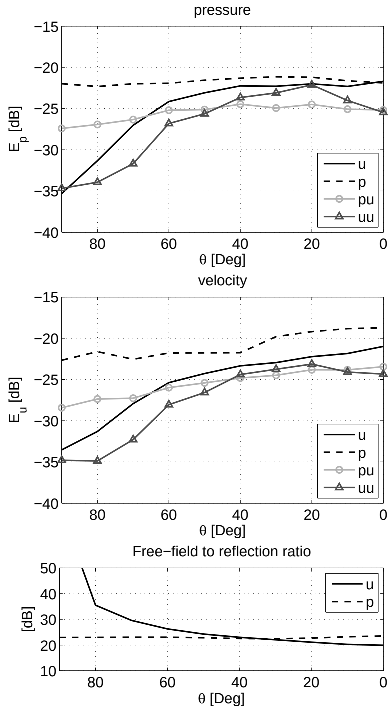

FIG. 3. Top: Reconstruction error of the field radiated by a baffled plate in the presence of an incident plane wave coming from the opposite side as a function of the incidence angle ($\theta = 0$ corresponds to frontal incidence). Bottom: Ratio between the radiated sound by the plate at z_{h1} and the incident plus backscattered plane waves (f=700 Hz).

($k_z = 0$), to $\theta = 0^o$ where it is propagating 'towards' the plate ($k_z = k$). When the incident plane wave travels tangentially to the plate ($\theta = 90^o$) the normal component of the particle velocity is undisturbed. This explains the low reconstruction error of the velocity based methods between $90^o \geq \theta \geq 60^o$.

B. Plate radiating into an enclosed space

A preliminary numerical experiment with the baffled plate radiating into a rectangular room was considered. The room is of dimensions 3 x 2.5 x 2 m^3, and the plate is baffled in the center of the 2.5 x 3 m^2 wall. In this numerical experiment, only the first reflection from each wall and the backscattering from the source were taken into account. The measurement planes were $z_{h1} = 10$ cm and $z_{h2} = 15$ cm, and the reconstruction plane was also z_{h1} (see Fig. 4). The equivalent sources were retracted two inter-spacing distances from the reconstruction planes.

Figure 5 shows the error of the reconstructions compared to the free field radiation from the plate. At low frequencies the velocity based methods are more accurate due to the lesser disturbance of the normal velocity at the boundary of the source, whereas at higher frequencies the separation methods (p-u and u-u) provide on the whole the best estimation. Above 400 Hz, the accuracy of pressure-velocity and double layer velocity is similar.

IV. EXPERIMENTAL STUDY

An experimental study to examine the methods described in this paper was conducted. The measurements took place at the LVA, INSA-Lyon, France. The setup consisted of a baffled plate radiating into a lightly damped room of dimensions 3.6 x 2.15 x 2 m^3. The plate used was a 50 x 70 cm^2, 1 mm thick steel plate, driven near its center, at (5,-10,0) cm. The sound pressure and the normal component of the particle velocity were measured with a line array of 11 particle velocity probes "Microflown p-u match", using a uniform inter-spacing of 6 cm. The field was measured sequentially at 11 x 16 positions, over a total area of 40 x 60 cm^2. The measurement planes were $z_{h1} = 10$ cm and $z_{h2} = 15$ cm, and z_{h1} served

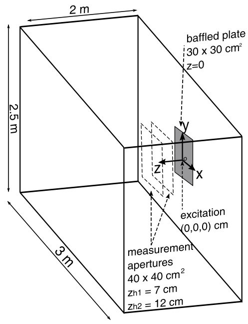

FIG. 4. Numerical set-up

also as the reconstruction plane. The equivalent sources were retracted two inter-spacing distances from the reconstruction planes. The measurement set-up is shown in Fig. 6 and a picture of the measurement is shown in Fig. 7.

A 32 channel analyzer, OROS type OR38, was used. The plate was driven with random noise, and a force transducer at the driving point was used as a phase reference. The spectral estimates were calculated with 0.33 Hz spectral resolution, corresponding to 3 s Hanning windows with 70% overlap, and 50 averages. The calibration of the probes was done by measuring at 20 cm from a monopole source in a anechoic room and calculating a correction for the probes to match the exact analytical ratio between pressure and velocity.[24]

In order to calculate the free field radiation from the plate, its vibration velocity was measured with a Polytec laser vibrometer OFV 056 over a grid of 26 x 36 positions, with 2 cm resolution. The free-field radiation was calculated using the wave superposition method, with the equivalent sources retracted 3 cm behind the plate. The results were identical to the ones obtained by evaluating numerically the Rayleigh integral.[26] The resulting sound pressure and particle velocity served as the 'true' reference fields for benchmarking.

Figure 8 illustrates the estimated sound pressure radiated from the source at 500 Hz. It shows the true sound pressure calculated from the vibration of the plate, the direct reconstruction based on the sound pressure, particle velocity, double layer velocity (u-u), and combined pressure-velocity (p-u) methods.

Figure 9 shows a comparison between the 'true' free-field radiation of the plate and the estimation as a function of frequency. The frequencies shown correspond to the main natural frequencies of the plate, where the sound radiation is maximum and yields a better signal-to-noise ratio. The overall contribution of the reflections compared to the free-field radiation from the source was estimated to be of about -10 dB. It can be seen from Fig. 9 that the reconstruction error of all the techniques is fairly high. This due to the reference 'true' field used: Because it is not possible to measure 'per se' the free-field radiation of the baffled plate with the p-u array, it

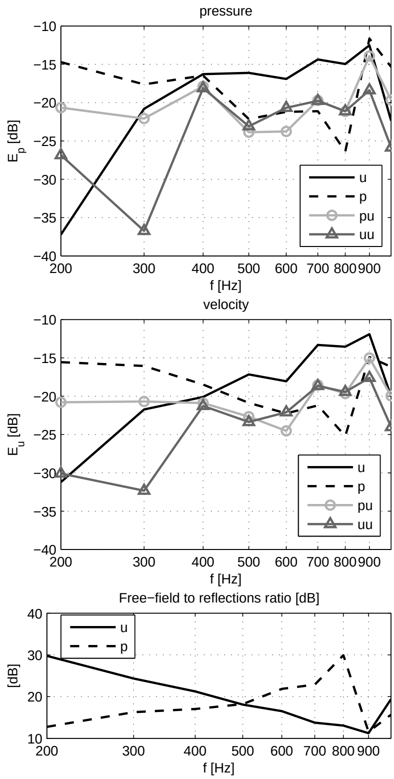

FIG. 5. Top: Error as in Eqs. (14) and (15) for a baffled plate radiating into a room. Bottom: Ratio between the pressure and velocity by the plate at z_{h1} and the reflected waves.

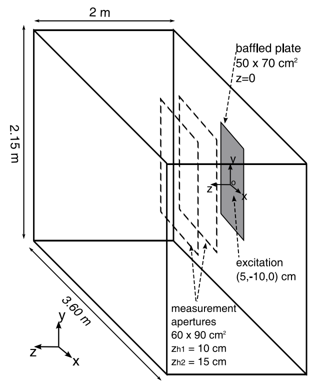

FIG. 6. Experimental set-up

FIG. 7. (Color online) Experimental measurement

is instead estimated based on the plate's vibration measured with a laser vibrometer. This introduces significant sources of error due to position bias, scattering by the array and preamplifier, calculation errors, etc., particularly at high frequencies. In spite of the high experimental error, the methods follow similar trends as in the simulated results.

At 700 Hz and above, the error increases presumably because of spatial aliasing due to the short wavelength of the evanescent waves (the flexural wavelength on the plate at 700 Hz is of about 12 cm, whereas the transducer inter-spacing is 6 cm). Although these aliased evanescent waves have decayed significantly at the measurement plane, they still can contribute to the error.

The results show that at low frequencies, the particle velocity based reconstruction and the two separation methods provide the best estimates. Particularly, at very low frequencies (below 300 Hz) the direct velocity reconstruction is very accurate, because the incoming sound vanishes at the plate's boundary. As the frequency increases, the single layer direct reconstruction deteriorates due to the increasing influence of the incoming sound, and becomes comparable to the double layer velocity and the pressure-velocity method. The accuracy of the two separation methods is similar, although on the whole, the double layer velocity technique (u-u) is closer to the free field radiation of the source. This is a result of the fact that, because of its directional characteristics, the normal component of the particle velocity is not influenced by flanking reflections from the floor, walls and ceiling. The combined pressure-velocity reconstruction suffers from the so-called 'p-u mismatch',[12] whereas the double layer velocity technique circumvents this source of error. Additionally, it has been shown in previous studies that the velocity based reconstruction is less sensitive to background noise and measurement errors, and that it is in general more accurate to predict sound pressure from velocity measurements than vice versa.[12]

Figure 10 shows the condition numbers of the matrices used by the separation methods to relate the measured field to the strength of the equivalent sources, (see Eqs. (5) and (10)), as well as of the matrices of the direct reconstructions. The condition number of the 'p-u' method is shown for the least squares and the weighted least squares solutions. It can be seen that the condition number of the weighted least squares solution is substantially lower (it is still higher than the other methods due to the intrinsic differences between the pressure and velocity propagators). The condition number is an indication of how sensitive a method is to measurement noise, and how sensitive the solution is to small changes in the input data. These results indicate that the velocity based methods, single or double layer, are significantly more robust with respect to measurement noise.

V. DISCUSSION

It should be noted that the evaluation of the methods in this paper is based on a comparison between the free-field radiation by the source and the estimation by the separation methods, which merely separate sound coming from the two sides of the array (without compensating for the back-scattered sound by the source, nor any other reflection coming from the source's side). Hence, the results evaluate how much the estimation corresponds to the free-field radiation of the source, but do not evaluate the accuracy of the separation as such. The study has shown that the over-all accuracy of the separation methods depends significantly on the magnitude of the disturbance of the measured field, pressure or particle velocity, resulting from the specific measurement situation.

Because the normal component of the particle velocity is directive, unlike the pressure, it is less affected by sound coming from the edges of the aperture. Furthermore, the normal component of incoming sound tends to vanish at the boundary of a rigid source. Therefore, when measuring close to the source, with a small stand-off distance relative to the wavelength in air ($z_h < 0.1\lambda$), the direct reconstruction of the field based on the measurement of the particle velocity provides a robust and accurate estimate of the source's radiation.[16] Nonetheless, measuring very close to the source also implies a potential risk of spatial aliasing, unless a sufficiently dense transducer array is used ($\Delta x < \lambda/2$). Consequently, the stand-off distance must be large enough so that the aliased evanescent waves have decayed at the measurement positions. When measuring at such standoff distance the separation techniques can be useful. In this respect, the double layer velocity technique combines the advantages of measuring the particle velocity (e.g., less truncation error, better conditioning to noise, decreased influence of flanking undesired sound, etc.)[27] with the ability to distinguish sound from the two sides of the array.

VI. CONCLUSIONS

Two sound field separation methods based on the equivalent source method have been proposed and examined in this paper. The methods are based on the combined measurement of pressure and velocity, and on the measurement of the particle velocity in two parallel layers. Their performance in an enclosed space has been examined numerically and experimentally, and compared with the conventional direct single layer reconstructions based on pressure and velocity.

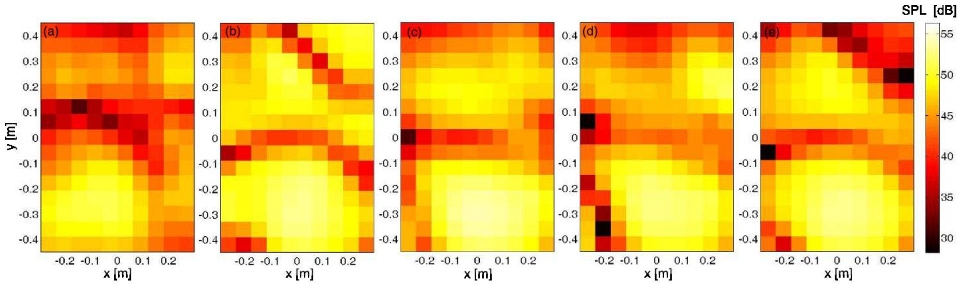

FIG. 8. (Color online) Radiation from the baffled plate at 500 Hz. Sound pressure in dB SPL. (a) free-field radiation; (b) direct reconstruction based on sound pressure measurements; (c) direct reconstruction based on normal velocity measurements; (d) reconstruction with the double layer velocity method; (e) reconstruction with the pressure-velocity method.

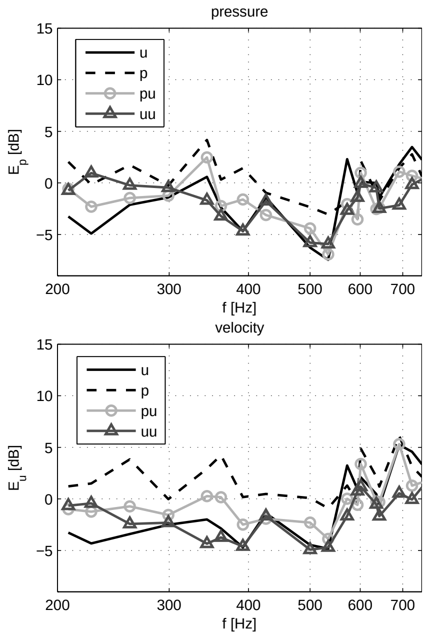

FIG. 9. Error as in Eqs. (14) and (15) for a baffled plate radiating into a lightly damped room.

The results indicate that the direct reconstruction of the field based on particle velocity measurements is robust and can provide a good estimation of the source's free-field radiation, particularly at low and mid frequencies near a rigid source, where the disturbance is minimal. At higher frequencies, where it may be difficult to measure very close to the source (due to e.g., spatial aliasing), separation techniques can be useful to avoid the influence of disturbing sound due to reflections. The accuracy of the proposed separation methods is comparable, although the u-u method is more robust to background noise and preserves the favorable properties related to measurement of the velocity field, in addition to making it possible to separate sound from the two sides of the array. Nonetheless, if the level of disturbance is not critical, the direct reconstruction based on single layer measurements is certainly more accurate and convenient than using sound-field separation techniques.

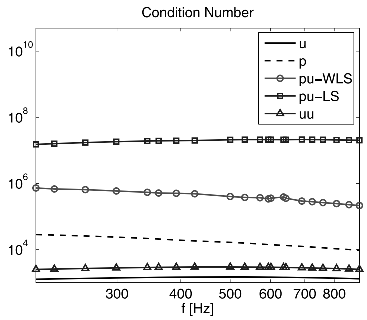

FIG. 10. Condition number (2-norm) of the matrices of the methods as used in the experimental study. The least squares is also shown for comparison with the weighted least squares method.

Acknowledgements

The authors would like to thank Antonio A. Pereira for the help with the experimental measurements and the valuable discussion.

[1] J. D. Maynard, E. G. Williams, and Y. Lee, "Nearfield Acoustic Holography I: Theory of generalized holography and the development of NAH", J. Acoust. Soc. Am **78**, 1395–1413 (1985).

[2] E. G. Williams, *Fourier Acoustics - Sound Radiation and Nearfield Acoustic Holography* (Academic Press, San Diego, 1999), Chap. 2-8.

[3] J. Bendat, "Solutions for the multiple input/output problem", J. Sound Vib. **44**, 311–325 (1975).
[4] S. Price and R. Bernhard, "Virtual coherence: a digital signal processing technique for incoherent source identification", in *Proceedings of the 4th International Modal Analysis Conference 4, vol. II* (Los Angeles, CA, USA, 1986), pp. 1256–1262.
[5] J. Hald, "STSF - A unique technique for scan-based near-field acoustic holography without restrictions on coherence", Brüel & Kjær Technical Review 1989-1 (1989). Available at www.bksv.com (date last viewed 5/18/12).
[6] M. A. Tomlinson, "Partial source discrimination in near field acoustic holography", Appl. Acoust. **57**, 243–261 (1999).
[7] M. Tamura, "Spatial Fourier transform method of measuring reflection coefficients at oblique incidence. I: Theory and numerical examples", J. Acoust. Soc. Am. **88**, 2259–2264 (1990).
[8] Z. Hu and J. S. Bolton, "The measurement of plane-wave reflection coefficients by using two-dimensional spatial transforms", J. Acoust. Soc. Am. **88**, S173 (1990).
[9] J. Hald, "Patch holography in cabin environments using a two-layer hand held array with an extended SONAH algorithm", in *Proceedings of Euronoise 2006*, Tampere, Finland (Acoust. Soc. Finland, Helsinki, 2006).
[10] C.-X. Bi, X.-Z. Chen, and J. Chen, "Sound field separation technique based on equivalent source method and its application in near field acoustic holography", J. Acoust. Soc. Am **123**, 1472–1478 (2008).
[11] N. P. Valdivia, E. G. Williams, and P. C. Herdic, "Approximations of inverse boundary element methods with partial measurements of the pressure field", J. Acoust. Soc. Am **123**, 109–120 (2008).
[12] F. Jacobsen and V. Jaud, "Statistically optimized near field acoustic holography using an array of pressure-velocity probes", J. Acoust. Soc. Am. **121**, 1550–1558 (2007).
[13] C.-X. Bi and X.-Z. Chen, "Sound field separation technique based on equivalent source method using pressure-velocity measurements and its application in nearfield acoustic holography", in *Proceedings of Inter-Noise 2008* (Shangai, China, 2008), paper IN08_0149.
[14] Y.-B. Zhang, F. Jacobsen, C.-X. Bi, and X.-Z. Chen, "Near field acoustic holography based on the equivalent source method and pressure-velocity transducers", J. Acoust. Soc. Am. **126**, 1257–1263 (2009).
[15] C. Langrenne, M. Melon, and A. Garcia, "Measurement of confined acoustic sources using near-field acoustic holography", J. Acoust. Soc. Am. **126**, 1250–1256 (2009).
[16] E. Fernandez-Grande and F. Jacobsen, "Sound field separation with a double layer velocity transducer array (L)", J. Acoust. Soc. Am. **130**, 5–8 (2011).
[17] A. Sarkissian, "Method of superposition applied to patch near-field acoustic holography", J. Acoust. Soc. Am **118**, 671–678 (2005).
[18] G. H. Koopmann, L. Song, and J. B. Fahnline, "A method for computing acoustic fields based on the principle of wave superposition", J. Acoust. Soc. Am **86**, 2433–2438 (1989).
[19] D. Hallman and J. S. Bolton, "Nearfield acoustical holography for interior spaces", in *Proceedings of Inter-Noise 94* (Yokohama, Japan, 1994), pp. 1879–1882.
[20] D. L. Hallman, J. S. Bolton, S. M. Dumbacher, and M. J. Lally, "Acoustic source location in vehicle cabins and free-field with nearfield acoustical holography via acoustic arrays", in *Proceedings of the 19th International Seminar on Modal Analysis, Vol II* (Leuven, Belgium, 1994), pp. 841–851.
[21] M. Villot, G. Chavériat, and J. Roland, "Phonoscopy: an acoustical holography technique for plane structures radiating in enclosed spaces", J. Acoust. Soc. Am. **91**, 187–195 (1992).
[22] P. C. Hansen, "Analysis of discrete ill-posed problems by means of the L-curve", SIAM Review **34**, 561–580 (1992).
[23] G. H. Golub and C. F. V. Loan, *Matrix Computations* (Johns Hopkins University Press, Baltimore, 1996), Chap. 5.
[24] F. Jacobsen and V. Jaud, "A note on the calibration of pressure-velocity sound intensity probes", J. Acoust. Soc. Am. **120**, 830–837 (2006).
[25] A. A. Pereira and Q. Leclere, "Improving the equivalent source method for noise source identification in enclosed spaces", in *18 International Congress on Sound and Vibration* (Rio de Janeiro, Brazil, 2011), paper 2016.
[26] E. G. Williams and J. D. Maynard, "Numerical evaluation of the Rayleigh integral for planar radiators using the FFT", The Journal of the Acoustical Society of America **72**, 2020–2030 (1982).
[27] F. Jacobsen and Y. Liu, "Near field acoustic holography with particle velocity transducers", J. Acoust. Soc. Am. **118**, 3139–3144 (2005).

Paper C

A NOTE ON THE COHERENCE OF SOUND FIELD SEPARATION METHODS IN NEAR-FIELD ACOUSTIC HOLOGRAPHY

Efren Fernandez-Grande, Finn Jacobsen

Acoustic Technology. Department of Electrical Engineering
Technical University of Denmark. 2800 Lyngby, Denmark. [efg@elektro.dtu.dk]

Abstract

In near-field acoustic holography (NAH) it is sometimes necessary to use sound field separation methods in order to distinguish between sound from the two sides of the array (e.g., via double-layer array measurents). This is particularly useful when studying the sound radiated by sources in enclosed spaces and reverberant environments where there is reflected sound. Nonetheless, if a delayed sound wave, coherent with the direct sound, arrives to the measurement positions after a time greater than the time window used for the spectral analysis, it will appear to be incoherent, and bias the measurement and reconstruction. This paper examines the influence of the duration of the time window in the apparent coherence of the spectral estimates used for the sound field separation methods. The paper discusses some fundamental aspects regarding coherence in NAH, and presents a fundamental analytical study, considering a continuous formulation of the problem as well as a discrete one. Several numerical and experimental examples are provided to illustrate the analysis. The study provides a fundamental basis for estimating the error introduced by the duration of the time window or spectral resolution used.
Status: Manuscript in preparation. Not yet ready for submission.

---

1. Introduction

Sound field separation methods are often used in array acoustics in order to distinguish between sound from the two sides of the array. They are particularly useful when the sound waves at both sides of the array are mutually coherent, e.g., due to reflections, because in this case the sound sources cannot be separated based on their statistical properties.[1–4] Separation methods make use of the directional information of the sound field, by measuring the pressure or the particle velocity in two parallel planes[5–7] or by combining the measurement of the sound pressure and particle velocity in a single plane[8–10] in order to estimate the propagation direction of the waves.

In stationary sound fields, 'windowed' finite time records are used to estimate the average spectral characteristics of the sound field. If a delayed sound wave, perfectly coherent with the direct sound, arrives to the measurement position after a time greater than the time window, it will appear to be incoherent. This obviously may corrupt the spectral estimation of the measured quantity and influence the accuracy of the reconstruction. However, to date, this source of error has neither been examined nor addressed in the context of sound field separation methods.

Jacobsen (1987)[11] and Jacobsen and Thibaut (2000)[12], pointed out the fact that if a source is radiating into a room and the spectral resolution of the analysis is not sufficiently fine, the apparent coherence function will be less than unity, although the source and the reflections are fully coherent. This phenomenon is closely related to the problem addressed here. The approach of the present analysis is also related to past works that studied the influence of a single initial delay between the source and the measurement position[13–16]. This paper extends these analyses to any possible delay or reflection pattern.

Concisely, the purpose of this paper is to study the influence that the duration of the analysis window, or conversely the spectral resolution, may have in the spectral estimation used for the NAH-based sound field separation techniques. It should be noted that the analysis presented is also applicable to the general stationary NAH case , albeit it is particularly relevant for sound field separation methods, because they are prone to suffer from this error because of typically involving delayed sound waves.

The paper discusses some basic aspects of coherence in NAH, and presents a fundamental analytical study. Given the theoretical background, several numerical and experimental examples are presented and the influence of the time window duration in the separation methods is examined and discussed.

2. Some fundamental considerations about coherence in NAH

In its simple form, and because of being founded on the Helmholtz equation, near-field acoustic holography relies on the measured sound field being fully coherent. In other words, it requires that there exists an established phase relationship between all the points in the hologram plane (and throughout the sound field). This requirement is met whenever the sound field is due to a single coherent source, in a strict sense, or to several mutually coherent sources, i.e., sources that are related via a defined phase shift or time delay. In practical applications it is very common to encounter sources that are not mutually coherent, hence a suitable methodology must be followed to guarantee coherence for a proper holographic processing of the sound field. In this context, two general cases can be considered: stationary NAH and non-stationary NAH, also known as time-domain, 'snap-shot', or instantaneous NAH.

In the case of time-domain NAH, the sound field at all points in the hologram is measured simultaneously, and a series of finite time records are processed separately. Thus, each of the finite time records corresponds to a hologram at a specific time. In this case, the apparent coherence of the measured signals tends to be unity, regardless of whether the sources under study are mutually coherent or not, because the approach does not rely on the sound field being stationary and the spectra from the finite time records are not averaged to estimate statistical properties of the sound field. Instead, the time records are processed sequentially to represent the time series.[17]

Contrarily, when a sound field can be regarded as stationary, it can be described via its statistical properties in a time-independent way. This is enormously convenient, and it is often the starting point of many formulations where the stationarity of the sound field is taken for granted. Stationarity provided, it is common practice to estimate the averaged spectral characteristics of the sound field based on an ensemble of finite time records. However, if the sources under study are incoherent, the interference pattern of the sound waves will not be stationary, and lacking stationarity, the acoustic signals in adjacent time segments will not be representative of the whole system, with the result that the averaged spectrum will not converge to a meaningful value. This is commonly known as the multiple input/output problem. In such case, it is still possible to, based on cross-spectral analysis, decompose the total field into separate partial contributions, each of them exhibiting coherent properties, and find a meaningful time-independent representation of the acoustic field. There are several ways to attain this, the best-known being probably conditioned spectral analysis [1,18] and virtual coherence. [2]

In the case of near-field acoustic holography this multiple input/output problem can also be solved based on an analogous contribution analysis, either on the basis of virtual coherence [2] as in ref. 3 or partial coherence [1] as in ref. 19. Several authors have examined methodologies to overcome source non-stationarity in multi-reference NAH [20,21] or the general multiple input/output problem. [22] Additionally, several methods have been presented that make use of optimally located 'virtual' references for the estimation of the partial holograms. [23–25]

The above mentioned methods make it possible to apply stationary NAH via the decomposition of the total field into partial holograms which are stationary and fully coherent. Nonetheless, whenever a sound field is characterized by estimation of its averaged spectra (via e.g., Welch's method, Barlett's method), as in stationary NAH, the duration of the finite time records or time windows used will have an influence on the estimated frequency response and coherence function. It is therefore the purpose of this paper to study the influence of the duration of the time window on coherence and the sound field separation techniques, which are prone to this error because of being subject to delayed sound.

3. Theory. Continuous formulation

The following analysis describes the case of a source radiating in the presence of extraneous coherent sound (e.g., a sound source and one or several reflections). The analysis considers the case of coherent NAH, although the case of incoherent multi-reference NAH would essentially be analogous (for each of the partial holograms).

Consider a random stationary process consisting on an acoustic source signal [x(t)] being radiated into an environment where reflections or other coherent sources exist. The quantity x(t) is available as a phase reference. The measured quantity [y(t)] includes the direct original signal and the delayed or reflected sound, and it corresponds to the measurement positions in the hologram. For simplicity, let a single measurement position be considered, then the extension to the other hologram positions is straightforward. Ideally, the cross-correlation between processes $x(t)$ and $y(t)$ is:

$$R_{xy}(\tau) = E\left[x(t)y(t+\tau)\right] = \lim_{T\to\infty} \frac{1}{T} \int_0^T x(t)y(t+\tau)dt. \tag{1}$$

However, in practice the estimation of the cross-correlation is based on a windowed finite time record T. It can be shown that the cross-correlation estimate is,[14]

$$\hat{R}_{xy}(\tau) = R_{xy}(\tau)\frac{1}{T}\int_0^T w(t,T)w(t+\tau,T)dt. \tag{2}$$

This can also be expressed as

$$\hat{R}_{xy}(\tau,T) = R_{xy}(\tau)R_{ww}(\tau,T), \tag{3}$$

where R_{ww} represents the auto-correlation of the time window function. Similarly, the auto-correlations of the processes $x(t)$ and $y(t)$ are $\hat{R}_{xx}(\tau,T) = R_{xx}(\tau)R_{ww}(\tau,T)$, and $\hat{R}_{yy}(\tau,T) = R_{yy}(\tau)R_{ww}(\tau,T)$.

Based on these auto- and cross-correlations, the auto-spectra and cross-spectrum of the signals can be estimated. Ideally, the cross spectrum between two functions x and y is $S_{xy}(\omega) = \int_{-\infty}^{\infty} R_{xy}(\tau)e^{j\omega\tau}d\tau$. In practice however, the estimation is from averaging finite records of time, as in Eq. (3), resulting in

$$\hat{S}_{xy}(\omega,T) = \int_{-T}^{T} R_{xy}(\tau)R_{ww}(\tau,T)e^{j\omega\tau}d\tau, \tag{4}$$

and analogously, $\hat{S}_{xx}(\omega,T) = \int_{-T}^{T} R_{xx}(\tau)R_{ww}(\tau,T)e^{j\omega\tau}d\tau$, and $\hat{S}_{yy}(\omega,T) = \int_{-T}^{T} R_{yy}(\tau)R_{ww}(\tau,T)e^{j\omega\tau}d\tau$. From these spectral estimates, the apparent coherence function $\hat{\gamma}_{xy}$ can be calculated as

$$\hat{\gamma}^2_{xy} = \frac{\hat{S}_{xy}\hat{S}^*_{xy}}{\hat{S}_{yy}\hat{S}_{xx}}. \tag{5}$$

Let the signal $x(t)$ be random white noise with power spectral density A,

$$R_{xx}(\tau) = A\delta(\tau). \tag{6}$$

The process $y(t)$ can be described as the convolution between the source signal and the impulse response of the system $h(t)$, which corresponds to the transfer function between the source signal and the measured quantity,

$$y(t) = x(t) * h(t) = \int x(\tau)h(t-\tau)d\tau. \tag{7}$$

On this basis, and from Eq. (1), the cross-correlation between the measurement and the reference is

$$R_{xy}(\tau) = \lim_{T\to\infty}\frac{1}{T}\int_0^T R_{xx}(\tau)h(\tau-t)dt, \tag{8}$$

Making use of Eqs. (3) and (6), the cross-correlation estimate is

$$\hat{R}_{xy}(\tau,T) = Ah(\tau)R_{ww}(\tau,T). \tag{9}$$

The auto-correlation of $y(t)$ is $R_{yy}(\tau) = \lim_{T\to\infty}(1/T)\int_0^T R_{xx}(t)R_{hh}(\tau - t)dt$, and making use of Eq. (6),

$$\hat{R}_{yy}(\tau, T) = AR_{hh}(\tau)R_{ww}(\tau, T). \tag{10}$$

Based on these auto- and cross-correlations, the cross-spectrum and auto-spectra of the processes can be estimated as,

$$\hat{S}_{xy}(\omega, T) = A\int_{-T}^{T} h(\tau)R_{ww}(\tau, T)e^{j\omega\tau}d\tau, \tag{11}$$

$$\hat{S}_{yy}(\omega, T) = A\int_{-T}^{T} R_{hh}(\tau)R_{ww}(\tau, T)e^{j\omega\tau}d\tau, \tag{12}$$

$$\hat{S}_{xx}(\omega, T) = AR_{ww}(0, T). \tag{13}$$

It follows that the coherence of the estimates is

$$\hat{\gamma}^2_{xy} = \frac{\displaystyle\int_{-T}^{T} h(\tau)R_{ww}(\tau, T)e^{j\omega\tau}d\tau \cdot \int_{-T}^{T} h(\tau)R_{ww}(\tau, T)e^{-j\omega\tau}d\tau}{\displaystyle R_{ww}(0, T)\cdot\int_{-T}^{T} R_{hh}(\tau)R_{ww}(\tau, T)e^{j\omega\tau}d\tau}. \tag{14}$$

Using Eqs. (11) and (13), the estimated frequency response is

$$\hat{H}_{xy}(\omega, T) = \frac{\hat{S}_{xy}(\omega, T)}{\hat{S}_{xx}(\omega, T)} = \frac{\displaystyle\int_{-T}^{T} h(\tau)R_{ww}(\tau, T)e^{j\omega\tau}d\tau}{R_{ww}(0, T)}. \tag{15}$$

It can be shown that the normalized bias error in the pressure measurement (or velocity), defined as the deviation between the exact pressure and the estimated one normalized by the former, $\varepsilon_p = (p - \hat{p})/p$, is:

$$\varepsilon_p = 1 - \frac{\hat{S}_{xy}}{S_{xy}}, \tag{16}$$

where it has been assumed that $S_{xx} = \hat{S}_{xx}$, which is a fair assumption because $R_{ww}(0, T) = 1$ for most of the time window functions.

The foregoing analysis serves as a continuous description of the phenomena addressed here. However, the underlying implications and physical meaning become somewhat more clear and intuitive when studying the case of single separate reflections. This is pursued in the following section, using this continuous description as a basis for it.

4. Theory. Discrete formulation

Let there be a system consisting of multiple separate reflections, thus with an impulse response which is a delta pulse train, each of the pulses with a certain time delay t_n and an amplitude coefficient H_n,

$$h(t) = \sum_{n=0}^{N} H_n \delta(t - t_n), \tag{17}$$

so that

$$y(t) = \sum_{n=0}^{N} x(t) H_n \delta(t - t_n). \tag{18}$$

Making use of the shifting property of the Dirac delta function, Eqs. (11) to (13) can be expressed as

$$\hat{S}_{xy}(\omega, T) = A \sum_{n=0}^{N} H_n R_{ww}(t_n, T) e^{j\omega t_n}, \tag{19}$$

$$\hat{S}_{yy}(\omega, T) = A \sum_{n=0}^{N} \sum_{n'=0}^{N'} H_n H_{n'} R_{ww}(t_n - t_{n'}, T) e^{j\omega(t_n - t_{n'})}, \tag{20}$$

$$\hat{S}_{xx}(\omega, T) = A R_{ww}(0, T). \tag{21}$$

Substituting Eqs. (19) to (21) into Eq. (5), and combining the summation terms of the numerator yields

$$\hat{\gamma}_{xy}^2 = \frac{\displaystyle\sum_{n=0}^{N} \sum_{n'=0}^{N'} H_n H_{n'} R_{ww}(t_n, T) R_{ww}(t_{n'}, T) e^{j\omega(t_n - t_{n'})}}{\displaystyle R_{ww}(0, T) \sum_{n=0}^{N} \sum_{n'=0}^{N'} H_n H_{n'} R_{ww}(t_n - t_{n'}, T) e^{j\omega(t_n - t_{n'})}}. \tag{22}$$

The frequency response estimate is

$$\hat{H}_{xy}(\omega, T) = \frac{\displaystyle\sum_{n=0}^{N} H_n R_{ww}(t_n, T) e^{j\omega t_n}}{R_{ww}(0, T)}. \tag{23}$$

Based on Eqs. (22) and (23) an estimate of the bias introduced when the system consists of a single or several separate reflections (or other coherent sources) can be obtained .

From Eq. (16), the normalized error is in this case

$$\varepsilon_p = 1 - \frac{\sum_{n=0}^{N} H_n R_{ww}(t_n, T) e^{j\omega t_n}}{\sum_{n=0}^{N} H_n e^{j\omega t_n}}. \tag{24}$$

In the case that there exist multiple reflections, the error results from the "late" sound interfering with the direct and "early" sound that arrives within the span of the time window.

In the case that there is a single delay path without reflections or secondary sources, i.e., just initial delay, the bias error throughout the hologram is

$$\varepsilon_p|_m = 1 - R_{ww}(t_m, T), \tag{25}$$

where $t_m = |\mathbf{r}_m - \mathbf{r}_s|/c$ is the time lapse between the source at $\mathbf{r}_s$ and the specific hologram position $\mathbf{r}_m$ (the case of multiple reflections can be estimated by expanding Eq. (24)).

Equation (24) shows that the bias will be dominated by the initial delay between the source and the measurement, as well as by the reflections of significant amplitude. In the general case of NAH, the initial delay is not very critical because of measuring in the near-field. However, if there is delayed sound, as in sound filed separation methods, the error introduced by the reflections can be of importance.

4.1. Rectangular window

For simplicity, let a rectangular window be considered in the following. Its autocorrelation is a triangular function of $2T$ time span,

$$R_{ww}(t, T) = \begin{cases} \left(1 - \frac{|t|}{T}\right) & \text{if } |t| \leq T \\ 0 & \text{if } |t| > T. \end{cases} \tag{26}$$

Within the interval $|t| \leq T$, considering that t_n is positive, from Eq. (22)

$$\hat{\gamma}_{xy}^2 = \frac{\sum_{n=0}^{N} \sum_{n'=0}^{N'} H_n H_{n'} e^{j\omega(t_n - t_{n'})} \left(1 - \frac{t_n}{T}\right)\left(1 - \frac{t_{n'}}{T}\right)}{\sum_{n=0}^{N} \sum_{n'=0}^{N'} H_n H_{n'} e^{j\omega(t_n - t_{n'})} \left(1 - \frac{|t_{n'} - t_n|}{T}\right)}. \tag{27}$$

Further inspection reveals that the imaginary parts of the reciprocal terms of the summation, $[n, n']$ and $[n', n]$, cancel each other. This is expected, since the coherence function is real valued, and Eq. (14) can be expressed as

$$\hat{\gamma}_{xy}^2 = \frac{\sum_{n=0}^{N}\sum_{n'=n}^{N'} H_n H_{n'} \left(1-\frac{t_n}{T}\right)\left(1-\frac{t_{n'}}{T}\right)\cos[\omega(t_n - t_{n'})]}{\sum_{n=0}^{N}\sum_{n'=n}^{N'} H_n H_{n'} \left(1-\frac{|t_{n'}-t_n|}{T}\right)\cos[\omega(t_n - t_{n'})]}. \tag{28}$$

This expression can be decomposed into the $n = n'$ summation terms and the cross terms $n \neq n'$, where it becomes clear that given a decaying impulse response where $H_n > H_{n+1}$ and $t_n < t_{n+1}$, the expression will be dominated by the initial delay and the $(1 - t_n/T)^2$ terms of the significant reflections.

It is interesting to examine the implications regarding coherence of Eq. (28): When the length of the time window tends to infinity, $T \to \infty$,

$$\lim_{T\to\infty} \hat{\gamma}_{xy}^2 = 1. \tag{29}$$

Simlarly, when there is no delay between the source signal and the measurement $t_n = 0$,

$$\lim_{t_n\to 0} \hat{\gamma}_{xy}^2 = 1. \tag{30}$$

Furthermore, if the delay between the reference signal and the measurement data is greater than the time window, $t_n > T$ (see Eq. (26)), the coherence drops to zero,

$$if\ \ t_n > T,\ \Rightarrow\ \hat{\gamma}_{xy}^2 = 0. \tag{31}$$

This confirms that if the time window used for the analysis is not sufficiently long, part of the original signal may add up as incoherent sound.

The same analysis can be followed if some other time window rather than the rectangular one is considered, but the analytical results become cumbersome. These windows are nonetheless used in the numerical results that follow. The expressions of $R_{ww}(\tau, T)$ for the Hann and Hamming windows are given in the appendix.

5. Preliminary results

5.1. Single delay

This section considers a single delay between the source signal $x(t)$ and the measured quantity $y(t)$. This case was analyzed by Seybert and Hamilton using rectangular windows,[13] and by Trethewey and Evensen using rectangular and Hann or Hanning windows.[14] The present analysis is extended to Hamming windows and Tukey or cosine tapered windows with a taper-to-constant ratio of $\alpha = 0.5$ (the Hanning and rectangular windows are also used for comparison).[26]

Figure 1 shows the estimated frequency response and coherence, as calculated from Eqs. (14) and (15) or from Eqs. (22) and (23), divided by their true values. Note that the normalized bias error can easily be calculated as $1 - (|\hat{H}_{xy}|/|H_{xy}|)$ and the coherence bias as $1 - \sqrt{\hat{\gamma}_{xy}^2/\gamma_{xy}^2}$.

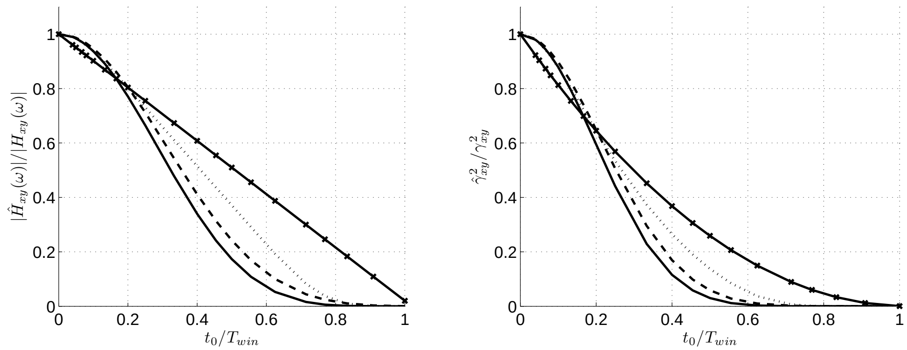

FIG. 1: Effect of a delay bias in the estimation of the frequency response and the coherence as a function of the length and type of the time window used; Rectangular window (crossed solid line); Hanning (solid line); Hamming (dashed line); Tukey with α = 0.5 (dotted line).

These results are in clear agreement with those in refs. 13 and 14. The results obtained with the Hamming window are very similar to those with the Hanning window, but they seem to converge faster towards the exact frequency response and coherence. This is presumably due to the fact that the window is not tapered completely to zero at the edges. The Tukey window is the result of a convolution between a rectangular function and a cosine window, it could be said that it is a cross over between a rectangular and a Hanning window, regulated by the α parameter. It is thus not surprising that the bias of the spectral estimates is between the rectangular and Hanning windows. On the whole, apart from the rectangular window, the general behavior of all the windows is fairly similar. It could be concluded that the time window should be about ten times longer that the initial delay for the estimates to be within the 10% bias error.

5.2. Two reflections

The previous results with a single delay can be extended to the case of multiple reflections or delays with Eq. (22). This example considers the case in which there is the direct sound, with a short delay of 10 ms, and a later reflection at 100 ms of the same magnitude. The same window functions as in the previous section are used.

The results are shown in Fig. 2. It can be seen how at T_{win} = 0.1 s, there is a “jump” in the errors due to the fact that the second delay, or late reflection is included within the analysis window. In this case, the results indicate that the time window should be about four to five times longer that the last significant reflection for the estimates to be within the 10% error.

5.3. Experimental room impulse responses

This section considers the case of a multiple reflection environment, i.e., a room, using the actual measured impulse response of a room. In addition to the experimental results, several numerically simulated impulse responses were generated, and the bias of the coherence and frequency response functions was

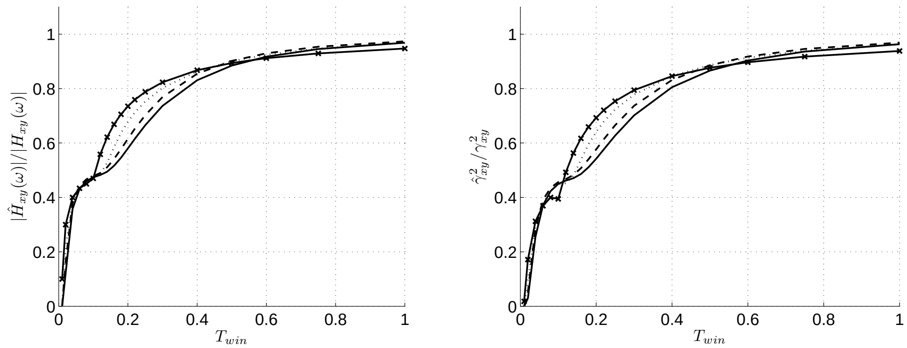

FIG. 2: Effect of two delays of 10 ms and 100 ms in the estimated frequency response and coherence as a function of the length and type of time window used; Rectangular window (crossed solid line); Hanning (solid line); Hamming (dashed line); Tukey with α = 0.5 (dotted line).

studied. The results agree with the experimental ones presented in this section. For brevity, these results are not presented here, just in the appendix the results for one room are included.

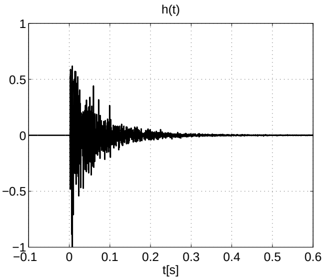

FIG. 3: Measured impulse response of a 162 m^3 lecture room with T_{60} = 0.5s.

The room used for this experimental study is a lecture room of dimensions 9 x 6 x 3 m^3 and reverberation time, based on the T_{30} estimate, of 0.5 s. The impulse response of the room is shown in Fig. 3 and the results are shown in Fig. 4.

Other rooms were also studied and yielded similar results. It seems that in the case of a room, the time window should be approximately as long as the reverberation time T_{60} for the results to be within the 10% error. This result is in agreement with ref. 12. However, this depends considerably on the specific room and at which interval of time might significant reflections occur.

6. Experimental results

This section considers the use of sound field separation techniques in a lightly damped room with multiple reflections. The room is of dimensions 3.6 x 2.15 x 2 m^3 and has a reverberation time (in the

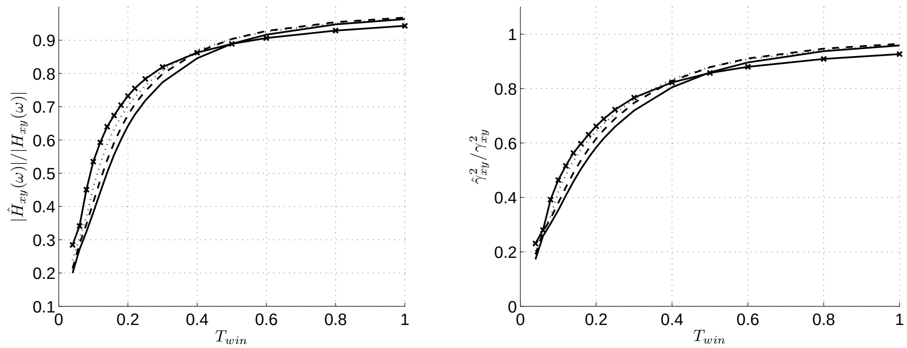

FIG. 4: Normalized spectral estimates (frequency response and coherence) as a function of the length and type of time window; Rectangular window (crossed solid line); Hanning (solid line); Hamming (dashed line); Tukey with α = 0.5 (dotted line).

frequency range of concern) of 0.8 s. In the 3.6 x 2.15 m^2 wall there is a baffled plate radiating into the room. The plate was a 50 x 70 cm^2, 1 mm thick steel plate, driven near its center, at (5,-10,0) cm. The sound field was measured with a line array of 11 particle velocity probes “Microflown p-u match”, using a uniform inter-spacing of 6 cm. The field was measured sequentially at 11 x 16 positions, over a total area of 40 x 60 cm^2 over two planes at 10 cm and 15 cm form the plate. A picture of the measurement is shown in Fig. 5. In order to calculate the ‘true’ radiation from the plate, its vibration velocity was measured with a Polytec laser vibrometer OFV 056 over a grid of 26 x 36 positions, and its radiation was calculated by evaluating numerically the Rayleigh integral.

A 32 channel analyzer, OROS type OR38, was used for the measurements. The plate was driven with random white noise, and a force transducer at the driving point was used as a phase reference. The time series were recorded to be later analyzed with Hanning windows of different lengths. The separation method is based on the measurement of the particle velocity in two parallel planes.[7] Other separation methods were also studied, and yielded similar results.

The results are shown in Fig. 6, where the reconstruction error can be seen as a function of frequency for four different window lengths, 0.5, 1, 2 and 3 s. The resulting error changes with frequency depending on the frequency response of the room. The results show that for the windows of duration 2 and 3 seconds, the accuracy is very similar, since the window length is significantly larger than the response of the system. However, as the duration of the time window decreases, which is equivalent to using a coarser spectral resolution, the error of the separation increases significantly.

The results seem to agree with the foregoing analysis, the numerical and the experimental results. Nonetheless, it should be noted that the decay time of the plate is similar to the one of the room. Therefore, the length of the time window influences both the estimation of the sound by the room as well as the one by the plate.

FIG. 5: Array measurements of a plate radiating in a lightly damped room with T_{60} = 0.8 s.

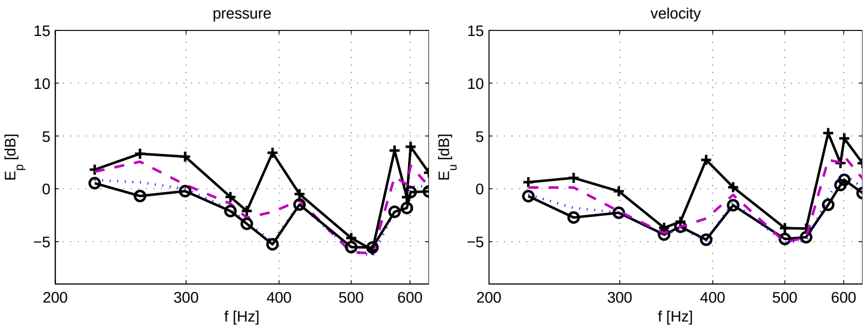

FIG. 6: Error of the u-u separation method as a function of frequency for different Hanning window lengths. Circled solid line T_{win} = 3 s; Dotted blue line T_{win} = 2 s; Dashed red line T_{win} = 1 s; Crossed solid line T_{win} = 0.5 s

7. Summary and discussion of the analysis

Equations (14) to (16), and (22) to (24) provide a basis for estimating the error introduced by the duration of a certain window function given the impulse response of the measured system. Equations (14) to (16) are valid for the general continuous case, e.g. given the measured impulse response of the system. Equations (22) to (24) are valid for the case where the source is radiating in the presence of separate distinct reflections or other coherent sources, which can be modeled as delta pulses.

The analysis indicates that if the system's impulse response is longer than the correlation length of the time window, the late reflected sound (apparently incoherent) will interfere with the coherent 'early' sound at the hologram positions, and bias the measurement. The appropriate window length depends strongly on the specific experimental situation. Some guidelines based on the examples studied here are given. It could be summarized that in order to limit the error below 10%, the time window should be about 10 times longer than the initial delay between the source signal and the measurement positions; in the case of a few separate reflections, it should be about four to five times longer than the last significant reflection. In the case of a room with multiple reflections, the time window should be approximately as long as the reverberation time T_{60}. Obviously, these requirements impose a limit on the minimum spectral resolution needed for the analysis, since the duration of the window and the spectral resolution are inversely related.

Several time window functions have been examined, i.e., Rectangular, Hanning, Hamming and Tukey with $\alpha = 0.5$. All of the windows perform rather similarly, with exception of the rectangular window, that provides only a better estimate if the window length is very short compared to the decay of the system. Otherwise, the Hann and Hamming windows seem to be the most robust.

8. Conclusions

The present study has examined the underlying coherence requirements for sound field separation methods and how they might be affected by the duration of the time window or the spectral resolution used.

The analysis considers a complex system described in terms of the impulse response between the source signal and the measurement positions. A theoretical description has been given, both considering a continuous system as well as a discrete system where single separate reflections occur. Numerical and experimental studies have been conducted, finding a fairly good agreement.

The study shows that it is essential to consider and choose an appropriate window length relative to the delays that will be processed in the sound field separation. The time window should not be in any case shorter than the latest significant delay. If this requirement is not fulfilled, the delayed sound would appear to be incoherent, biasing the spectral estimation, and ultimately deteriorating the sound field separation and reconstruction.

Acknowledgements

The authors would like to thank Cheol-Ho Jeong and Jonas Brunskog for their useful contribution and help with the measured and simulated room impulse responses.

[1] J. S. Bendat. Solutions for the multiple input/output problem. *J. Sound Vib.*, 44(3):311–325, 1975.

[2] S. M. Price and R. J. Bernhard. Virtual coherence: a digital signal processing technique for incoherent source identification. In *Proceedings of IMAC 4*, pp. 1256–1262, Schenectady, NY, USA, 1986.

[3] J. Hald. STSF - A unique technique for scan-based near-field acoustic holography without restrictions on coherence, 1989.

[4] M. A. Tomlinson. Partial source discrimination in near field acoustic holography. *Appl. Acoust.*, 57:243–261, 1999.

[5] M. Tamura. Spatial Fourier transform method of measuring reflection coefficients at oblique incidence. I: Theory and numerical examples. *J. Acoust. Soc. Am.*, 88:2259–2264, 1990.

[6] J. Hald. Patch holography in cabin environments using a two-layer hand held array with an extended SONAH algorithm. In *Proceedings of Euronoise*, Tampere, Finland, 2006.

[7] E. Fernandez-Grande and F. Jacobsen. Sound field separation with a double layer velocity transducer array. *J. Acoust. Soc. Am.*, 130(1):5–8, 2011.

[8] F. Jacobsen and V. Jaud. Statistically optimized near field acoustic holography using an array of pressure-velocity probes. *J. Acoust. Soc. Am.*, 121:1550–1558, 2007.

[9] Y.–B. Zhang, X.–Z. Chen, and F. Jacobsen. A sound field separation technique based on measurements with pressure-velocity probes (L). *J. Acoust. Soc. Am.*, 125:3518–3521, 2009.

[10] Y.–B. Zhang, F. Jacobsen, C.–X. Bi, and X.–Z. Chen. Near field acoustic holography based on the equivalent source method and pressure-velocity transducers. *J. Acoust. Soc. Am.*, 126:1257–1263, 2009.

[11] F. Jacobsen. Spatial correlation and coherence in a reverberant sound field. *J. Sound Vib.*, 118(1):175–180, 1987.

[12] F. Jacobsen and T. Roisin. The coherence of reverberant sound fields. *J. Acoust. Soc. Am.*, 108(1):204–210, 2000.

[13] A. F. Seybert and J. F. Hamilton. Time delay bias errors in estimating frequency response and coherence functions. *J. Sound Vib.*, 60(1):1–9, 1978.

[14] M. W. Trethewey and H. A. Evensen. Time-dealy bias errors in estimating frequency response and coherence functions from windowed samples of continuous and transient signals. *J. Sound Vib.*, 97(4):531–540, 1984.

[15] H. Schmidt. Resolution bias errors in spectral density, frequency response and coherence function measurements, iv: time delay bias errors. *J. Sound Vib.*, 101(3):405–412, 1985.

[16] H. A. Evensen and M. W. Trethewey. Bias errors in estimating frequency response and coherence functions from truncated transient signals. *J. Sound Vib.*, 145(1):1–16, 1991.

[17] J. Hald. Time Domain Acoustical Holography and Its Applications. *Sound and Vibration*, February:16–25, 2001.

[18] C. J. Dodds and J. D. Robson. Partial coherence in multivariate random processes. *J. Sound Vib.*, 42(2):243–249, 1975.

[19] D. L. Hallman and J. S. Bolton. Multi-reference nearfield acoustic holography. In *Proceedings of Inter-Noise 92*, pp. 1165–1170, Toronto, Canada, 1992.

[20] H. S. Kwon, Y. J. Kim, and J. S. Bolton. Compensation for source nonstationarity in multireference , scan-based near-field acoustical holography. *J. Acoust. Soc. Am.*, 113(1):360–368, 2003.

[21] M. Lee and J. S. Bolton. Scan-based near-field acoustical holography and partial field decomposition in the presence of noise and source level variation. *J. Acoust. Soc. Am.*, 119(1):382–393, 2006.

[22] Q. Leclère. Multi-channel spectral analysis of multi-pass acquisition measurements. *Mechanical Systems and Signal Processing*, 23:1415–1422, 2009.

[23] K. U. Nam and Y. H. Kim. Visualization of multiple incoherent sources by the backward prediction of near-field acoustic holography. *J. Acoust. Soc. Am.*, 109(5):1808–1816, 2001.

[24] K. U. Nam and Y. H. Kim. A partial field decomposition algorithm and its examples for near-field acoustic holography. *J. Acoust. Soc. Am.*, 116(1):172–185, 2004.

[25] Y.–J. Kim, J. S. Bolton, and H.–S. Kwon. Partial sound field decomposition in multireference near-field acoustical holography by using optimally located virtual references. *J. Acoust. Soc. Am.*, 115(4):1641–1652, 2004.

[26] F. J. Harris. On the use of windows for harmonic analysis with the discrete Fourier transform. *Proceedings of the IEEE*, 66 (1):51–83, 1978. ISSN 0018-9219.

[27] L. Cremer, H. A. Muller, and T. J. Schultz. *Principles and Applications of Room Acoustics, Vol. 1*. Applied Science Publishers, London, 1982.

AppendixA. Appendix

AppendixA.1. Other time windows

The function $R_{ww}(\tau, T)$ in Eqs. (14) or (22), should be for the Hann or Hanning window (in the interval $|\tau| \leq T$):

$$R_{ww}(t,T) = \left(1 - \frac{|t|}{T}\right)\left(\frac{2}{3} + \frac{1}{3}\cos\frac{2\pi t}{T}\right) + \frac{1}{2\pi}\sin\frac{2\pi|t|}{T} \tag{A.1}$$

or for the Hamming window

$$R_{ww}(t,T) \approx \left[\left(1 - \frac{|t|}{T}\right)\left(0.2916 + 0.1058\cos\frac{2\pi t}{T}\right) + 0.391\frac{1}{2\pi}\sin\frac{2\pi|t|}{T}\right]/0.3974. \tag{A.2}$$

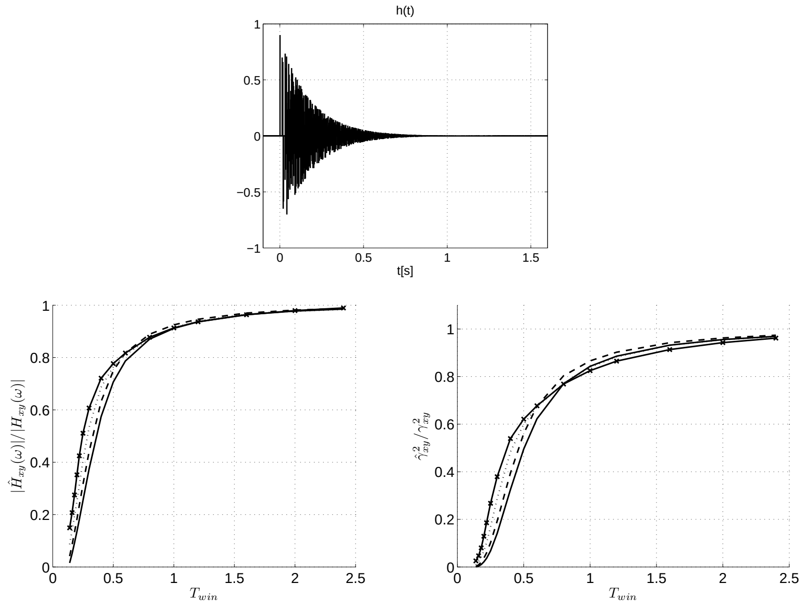

FIG. A.7: (Top) Simulated impulse response of a 144 m^3 room. (Bottom) Bias in the spectral estimation introduced by the room as a function of the length and type of time window; Rectangular window (crossed solid line); Hanning (solid line); Hamming (dashed line); Tukey with $\alpha = 0.5$ (dotted line).

AppendixA.2. Additional results: Simulated impulse response

This section presents the analysis of the bias error introduced by reflections in a room using Eq. (14), Eq. (15) and the simulated impulse response of a room. The reflection density of a room depends on its volume,[27]

$$\frac{\Delta N}{\Delta t} = \frac{4\pi c^3 t^2}{V} \tag{A.3}$$

an the reverberation time depends on the room constant, which dictates the decay rate of the room via a decaying exponential envelope. The probability of a reflection occurring can be modeled as a Poisson distribution where λ is the reflection density dN/dt.

Figure A.7 shows the simulated impulse response of a room with volume 6 x 8 x 3 m^2, a room constant of $\tau = 0.175$ (given an envelope $E = E_0 e^{-t/\tau}$), and thus a reverberation time $T_{60} = 1.2$ s. There is an initial delay of 1 ms. The figure also shows the bias of the frequency response and coherence estimates as a function of the time window duration. The results can also be shown relative to the reverberation time of the room T60 (see Fig. A.8). Several other rooms were studied, and similar results were found (not shown here).

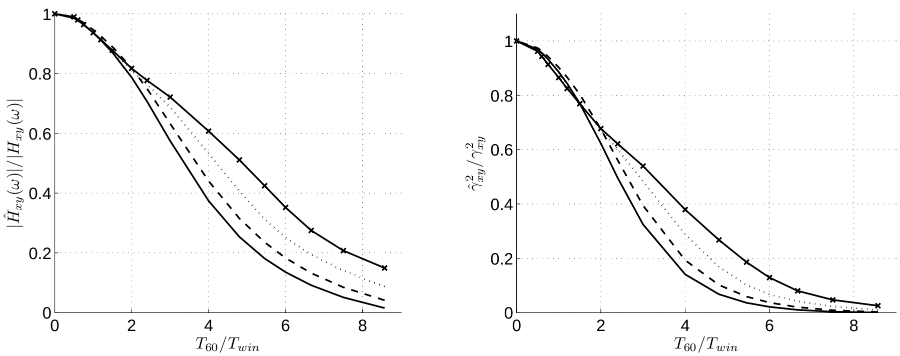

FIG. A.8: Bias as in Fig. A.7 but relative to the T_{60} of the room ($T_{60} = 1.2s$).

Part II

Paper D

大阪
inter.noise 2011
Osaka Japan September 4-7

Supersonic acoustic intensity with statistically optimized near-field acoustic holography

Efren Fernandez-Grande[1], Finn Jacobsen[2]

[1] Acoustic Technology. B. 352, Department of Electrical Engineering

DTU (Technical University of Denmark). 2800 Lyngby, Copenhagen, Denmark.

ABSTRACT

The concept of supersonic acoustic intensity was introduced some years ago for estimating the fraction of the flow of energy radiated by a source that propagates to the far field. It differs from the usual (active) intensity by excluding the near-field energy resulting from evanescent waves and circulating energy in the near-field of the source. This quantity is of concern because it makes it possible to identify the regions of a source that contribute to the far field radiation, which is often the ultimate concern in noise control. Therefore, this is a very useful analysis tool complementary to the information provided by the near-field acoustic holography technique. This study proposes a version of the supersonic acoustic intensity applied to statistically optimized near-field acoustic holography (SONAH). The theory, numerical results and an experimental study are presented. The possibility of using particle velocity measurements instead of conventional pressure measurements is examined. The study indicates that the calculation of the supersonic intensity based on measurement of the particle velocity is more accurate than the one based on sound pressure measurements. It also indicates that the method based on SONAH is somewhat more accurate than the existing methodology based on Fourier transform processing.

Keywords: Near-Field Acoustic Holography, NAH, Sound Radiation, Sound Intensity.

1. INTRODUCTION

In noise control and many areas of acoustics, the far field radiation of sources is frequently the ultimate quantity of concern, because it is typically this quantity that is perceived by a potential observer. Therefore, it is often important to identify the regions of a source that contribute to the far field output. This is precisely the aim of the method proposed in the present paper.

Wave bearing structures generally have strong near-field components, namely evanescent waves that decay exponentially and do not transport energy to the far field. An evanescent wave in isolation does not contribute to the active sound intensity because its sound pressure and particle velocity are in quadrature. Nevertheless, in the near-field of vibrating structures, the evanescent waves and propagating waves interact with each other, giving rise to regions of circulatory energy flow [1]. In other words, there is a circulation of active sound intensity flowing from one region of the source into an adjacent one.

In near-field techniques, where measurements take place in the near-field of the source or directly on its surface, this circulatory energy flow makes it difficult to immediately identify the regions that radiate efficiently into the far field and contribute to its net power output. This is for instance the case

[1] efg@elektro.dtu.dk
[2] fja@elektro.dtu.dk

in near-field acoustic holography (NAH) [2-3], which is a powerful source identification technique that characterizes completely the sound field radiated by a source, in principle with "unlimited" spatial resolution, making it possible to reconstruct the sound pressure, particle velocity vector, and sound intensity based on near-field acoustic measurements.

Williams [4-5] proposed the useful concept of "supersonic acoustic intensity" for identifying and characterizing the regions of a source that radiate into the far field. The method is based on NAH and the wavenumber space processing of the sound field. Its fundamental principle is to filter out the evanescent waves in the near-field of the source and estimate the active sound intensity based exclusively on the propagating waves. Hence only the efficient radiation of the source is taken into account. So far, the calculation of the supersonic acoustic intensity has only been formulated on the basis of Fourier based NAH.

The authors are inclined to think that the term "supersonic acoustic intensity" can be somewhat confusing, since it might lead to the misunderstanding that the energy in the sound field travels with supersonic speed. Therefore, in the present paper the alternative term "effective sound intensity" has been introduced. However, the notation established in refs. [4-5] is maintained.

Statistically optimized near-field acoustic holography [6-7], most frequently referred to as SONAH, is a holographic method that has the outstanding advantage of operating directly in the spatial domain, avoiding some of the errors associated with the discrete Fourier transformation. This makes the method very useful for the holographic reconstruction of sound fields and patch-NAH.

The aim of this paper is to extend the concept of effective sound intensity or supersonic intensity to SONAH. Because this method relies on an elementary wave decomposition, the evanescent waves can be separated from the propagating ones without Fourier transforming the sound field explicitly. The paper gives the theoretical background, and studies several examples. It also considers the reconstruction based on measurement of the particle velocity instead of sound pressure.

2. THEORY

Statistically optimized near-field acoustic holography (SONAH) is based on an elementary plane wave expansion of the acoustic field. Let the plane wave functions be

$$\psi(\mathbf{r}) = e^{-j(k_x x + k_y y + k_z (z - z^+))} , \tag{1}$$

where z^+ is the so called virtual source plane, where the elementary waves are scaled [6]. The wavenumber in the z direction, k_z, depends on k, k_x and k_y as:

$$k_z = \begin{cases} \sqrt{k^2 - (k_x^2 + k_y^2)} & \text{if } k^2 \geq k_x^2 + k_y^2 \\ -j\sqrt{(k_x^2 + k_y^2) - k^2} & \text{if } k^2 < k_x^2 + k_y^2 \ . \end{cases} \tag{2}$$

This shows that the plane waves are both propagating and evanescent. In SONAH, the pressure in the measurement plane is decomposed as:

$$\mathbf{p}(\mathbf{r}_h) = \begin{bmatrix} \psi_1(\mathbf{r_1}) & \psi_2(\mathbf{r_1}) & \cdots & \psi_n(\mathbf{r_1}) \\ \vdots & \vdots & & \vdots \\ \psi_1(\mathbf{r_m}) & \psi_2(\mathbf{r_m}) & \cdots & \psi_n(\mathbf{r_m}) \end{bmatrix} \begin{bmatrix} c_1 \\ c_2 \\ \vdots \\ c_n \end{bmatrix} = \mathbf{Bc} \ , \tag{3}$$

where $\mathbf{p}(\mathbf{r}_h)$ is a column vector with the measured pressure, $\mathbf{B}$ is a matrix containing the elementary wave functions and $\mathbf{c}$ is the coefficient vector. On the basis of this elementary wave expansion, the pressure in the reconstruction plane is expressed as

$$\mathbf{p}(\mathbf{r}_s) = \mathbf{B}_s \mathbf{c} \ , \tag{4}$$

where $\mathbf{B}_\mathrm{s}$ denotes the matrix with the elementary wave functions in the reconstruction plane z_s. From the inversion of eq. (3), the coefficients are determined. It follows that the pressure in the reconstruction plane can be estimated as:

$$\mathbf{p}(\mathbf{r}_s) = \mathbf{B}_s \mathbf{B}^+ \mathbf{p}(\mathbf{r}_h) \ , \tag{5}$$

where the superscript $^+$ denotes the regularized pseudo-inverse, i.e: $\mathbf{B}^+ = (\mathbf{B}^\mathrm{H}\mathbf{B} + \varepsilon\mathbf{I})^{-1}\ \mathbf{B}^\mathrm{H}$, with $\mathbf{I}$ the identity matrix and ε the regularization parameter.

Nevertheless, if we are only interested in the fraction of the flow of energy that propagates into the far field, the evanescent waves must be discarded in the reconstruction to get rid of the near-field circulating energy. An alternative set of elementary waves is thereby defined as

$$\psi_n^{(s)}(\mathbf{r}) = \begin{cases} e^{-j(k_{x,n}x+k_{y,n}y+k_{z,n}(z-z^+))} & \text{if } k^2 \geq k_x^2 + k_y^2 \\ 0 & \text{if } k^2 < k_x^2 + k_y^2 \ . \end{cases} \tag{6}$$

Based on these propagating wave functions, a reconstruction matrix $\mathbf{B}_s^{(s)}$ is defined. It follows that the pressure that propagates to the far field is

$$\mathbf{p}^{(s)}(\mathbf{r}_s) = \mathbf{B}_s^{(s)}\mathbf{B}^+\mathbf{p}(\mathbf{r}_h) \ . \tag{7}$$

Making use of Euler's equation of motion, the normal component of the particle velocity that propagates to the far field can be estimated as

$$\mathbf{u}_z^{(s)}(\mathbf{r}_s) = \mathbf{B}_s^{(s)}\frac{\mathbf{K}_z^{(s)}}{\rho_0 ck}\mathbf{B}^+\mathbf{p}(\mathbf{r}_h) \ , \tag{8}$$

where $\mathbf{K}_z^{(s)}$ is a diagonal matrix with the k_z corresponding to each elementary wave of $\mathbf{B}_s^{(s)}$.

The reconstruction can as well be based on the measurement of the particle velocity [8]. In this case the reconstruction equations are:

$$\mathbf{u}_z^{(s)}(\mathbf{r}_s) = \mathbf{B}_s^{(s)}\mathbf{B}^+\mathbf{u}_z(\mathbf{r}_h) \ , \tag{9}$$

$$\mathbf{p}^{(s)}(\mathbf{r}_s) = \mathbf{B}_s^{(s)}\rho_0 ck\mathbf{K}_z^{(s)-1}\mathbf{B}^+\mathbf{u}_z(\mathbf{r}_h) \ . \tag{10}$$

Once the propagating part of the pressure and particle velocity have been calculated, the effective sound intensity can be obtained as

$$\mathbf{I}^{(s)}(\mathbf{r}) = \frac{1}{2}\mathrm{Re}\{p^{(s)}(\mathbf{r})\mathbf{u}^{(s)}(\mathbf{r})^*\} \ , \tag{11}$$

with the superscript * denoting the complex conjugate.

3. NUMERICAL RESULTS

In this section, the calculation of the effective or supersonic intensity with SONAH is examined based on simulated measurements. The results are compared for benchmarking to the existing FFT based methodology [5]. Additionally, the reconstruction based on measurement of sound pressure, particle velocity and a combined measurement of pressure and velocity is examined.

The source used in the experiment was a baffled point source located at the origin of coordinates. The hologram plane was z = 10 cm, which served also as the reconstruction plane. The measurement grid consisted of 15 x 15 positions, over an aperture of 60 x 60 cm. The virtual source plane used to scale the plane waves was retracted half an inter-spacing distance behind the reconstruction plane and the wavenumber resolution used was $\Delta k_{(x,y)}$ =0.3. Noise of 35 dB signal-to-noise ratio was added to the simulated measurements.

The effective sound intensity is a quantity that cannot be measured directly, and seldom can it be known analytically. It is however possible to determine it for point sources. Thus, it can be used for assessing the accuracy of a given methodology. The reconstruction error was calculated as:

$$Error[\%] = 100 \cdot ||I^{(s)} - I_{true}^{(s)}||/||I_{true}^{(s)}||.$$

The true field of the baffled point source $I_{true}^{(s)}$ was calculated following similar derivations as in ref. [5], but without assuming z=0. Numerical integration was therefore required to evaluate the true field. An adaptive recursive Simpson's rule was used, with an error below 10^{-6}.

Figure 1 (a) shows the calculation error based on measurement of the sound pressure with the SONAH method and the FFT based one. SONAH is somewhat more accurate, especially at low frequencies, where the wavelength is comparable to or larger than the measurement aperture. However, at higher frequencies, as the measurement aperture becomes larger in comparison to the wavelength, the truncation error due to the finite aperture decreases, and the accuracy of the two methods is similar.

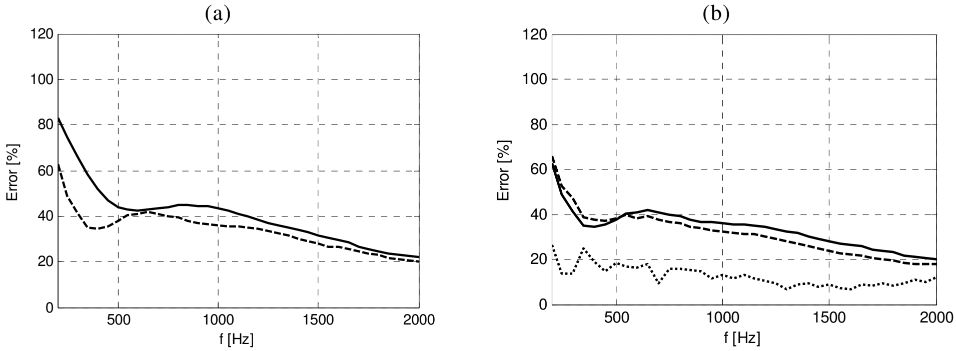

Figure 1 - (a) Calculation error of the effective intensity of a point source using the Fourier based NAH method (solid line), and the SONAH method (dashed line); (b) Calculation error of the effective intensity of a point source with SONAH based on pressure (solid line), on particle velocity (dotted line) and on combined pressure-velocity measurements (dashed line).

Figure 1 (b) shows the calculation error with SONAH based on the measurement of the velocity, the pressure and a combined measurement of sound pressure and particle velocity. The velocity based calculation is consistently better than the pressure or velocity-and-pressure based ones. This is an interesting result, which can be as well explained by the lower truncation error (this will be discussed further in the following, see section 5). At high frequencies, above 1500 Hz, the accuracy of the pressure based calculation improves and is comparable to the velocity based one. The fluctuations of the velocity based reconstruction error are a result of the singularity in the velocity-to-pressure transformation due to the k/k_z ratio in eq. (10), when k_z=0.

4. EXPERIMENTAL RESULTS

An experimental study was conducted to study the method proposed and examine further the concept and implications of the effective sound intensity. The measurements took place at the LVA, INSA-Lyon, France. The source used was a steel plate, mounted on a rigid wall of a semi-anechoic chamber. The plate was centered in the origin of coordinates and it was of dimensions (49 x 69) cm and 1 mm thick. It was driven at (7,-15) cm with random noise excitation from 100 Hz to 2500 Hz, and 3 s long Hanning windows for the analysis. The plate was measured at 10 cm distance with a line array of 11 p-u probes (see Figure 2). A grid of 11 x 16 positions was measured, over an aperture of 60 x 90 cm. The measured particle velocity was used for the calculation.

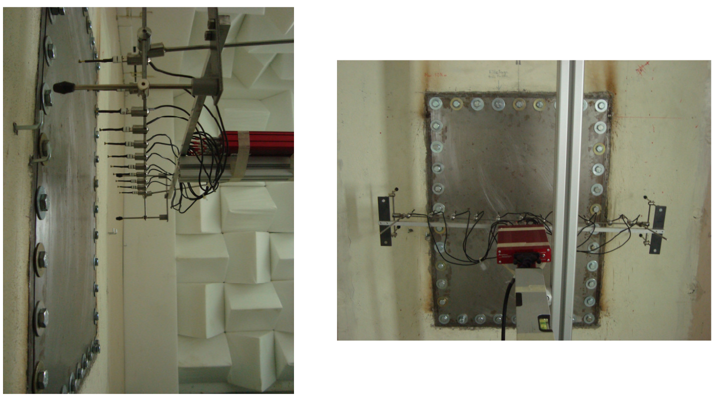

Figure 2 – Experimental set-up: Baffled plate in a semi-anechoic chamber and line array.

Figure 3 and 4 show the measured velocity, the active sound intensity and the effective intensity at 158 Hz and 1 kHz respectively. At 158 Hz (Figure 3), the plate is vibrating in a (1,4) mode-like shape. The measured velocity at 10 cm indicates that the structural wavelength is much smaller than the wavelength in air, creating a highly reactive field with a strong circulatory flow of energy. This is reflected in the active sound intensity map, which shows how there are two regions of the pate that act as ‘sinks’ of energy, with negative sound intensity, as opposed to the adjacent regions, that have a positive intensity. Note also that the effective intensity level in this case is one order of magnitude less than the active sound intensity, and its maximum level is found at the driving point.

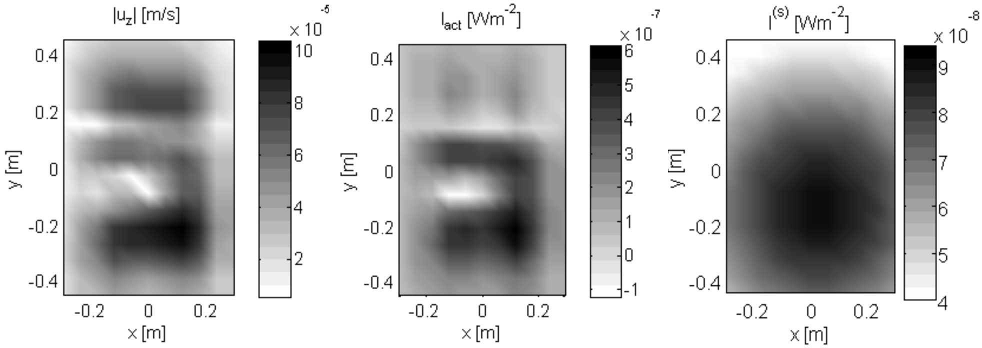

Figure 3 – Measured normal velocity (left), calculated active intensity (centre) and effective intensity (right) at frequency f=158 Hz. All quantities at 10 cm from the plate.

Figure 4 shows the same quantities at 1 kHz. Note that at this frequency, the structural wavelength is approximately 10 cm, and the evanescent waves radiated by the source have decayed significantly at the measurement plane. Therefore, the propagating waves dominate, and as a result, the active intensity and the effective intensity are nearly identical, since there is no circulatory energy in the measurement plane. This result validates the consideration that the effective intensity and the active intensity essentially differ by the circulatory flow of energy being removed or not.

Figure 5 shows the active and the effective sound intensity, as in Figures 4 and 5, but plotted through a vertical line at x= -12 cm. In this plot, the intensity levels can be understood more clearly.

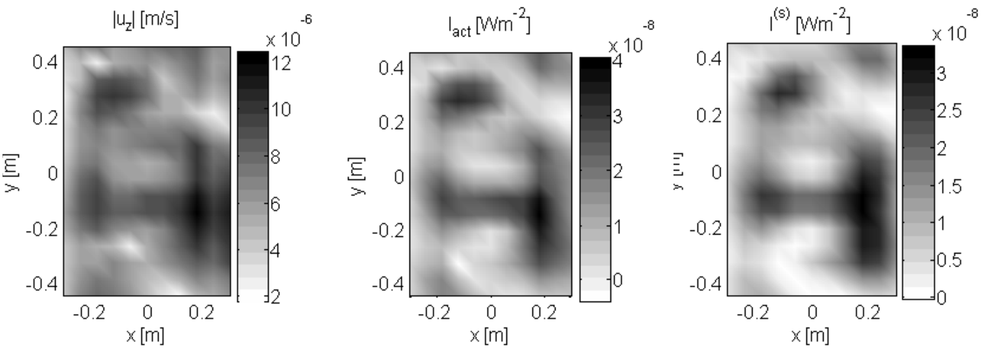

Figure 4 – Measured normal velocity (left), calculated active intensity (centre) and effective intensity (right) at frequency f=1000 Hz. All quantities at 10 cm from the plate.

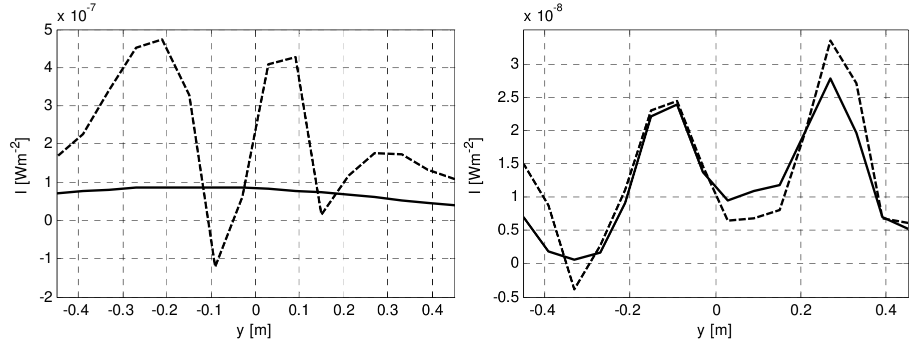

Figure 5 – Active intensity (dashed line) and effective intensity (solid line) at frequency f=160 Hz (left) and at 1000 Hz (right) through a vertical line at x=-12 cm of the measurement grid.

5. DISCUSSION

One of the strengths of statistically optimized near-field acoustic holography is that it is a patch method that overcomes some of the errors associated with the discrete Fourier transform by directly operating in the spatial domain. It is therefore not surprising that the effective sound intensity calculated with SONAH is more accurate than when it is calculated with conventional FFT based NAH. However, the results of the latter method could be improved by artificially extending the measurement aperture by means of extrapolation [9], making it suitable for patch-NAH.

The results of the investigation show that there is an important error associated with the estimation of the effective intensity, reflected in the high calculation errors of the methods as shown in section 3. This is presumably a natural consequence of the sharp separation between the effective and ineffective radiation, namely, the waves inside and outside the radiation circle (see eq. 6). This is an ideal separation of the wavenumber spectrum in which a "brick-wall" filter is implicitly used. Such a filter has an infinite impulse response in space domain that is much larger than the measurement aperture used in practice. This explains the large relative error of the numerical experiments. Note that this error is not a consequence of the sharp transition between the measured data inside the aperture and the "zeroes" outside, but a consequence of not measuring over an infinite aperture.

This last consideration explains as well why the velocity based calculation is notably more accurate than the other methods, namely because the normal component of the particle velocity decays much faster than the pressure towards the edge of the aperture. When measuring the normal velocity sufficiently close to the source, the measurement aperture could be regarded as virtually infinite, because the normal component of the particle velocity is zero outside of it. Contrarily, this is not the case with the sound pressure. This explains why the calculation based on measurement of the particle velocity is more accurate than the one based on combined measurement of pressure and velocity, a result that at first might seem surprising.

6. CONCLUSIONS

This study has examined the concept of effective sound intensity, or supersonic acoustic intensity, based on the statistically optimized near-field acoustic holography method (SONAH), as well as the possibility of basing the reconstruction on measurement of the particle velocity. The study indicates that the calculation based on particle velocity measurements is the most accurate. The SONAH based method provides a somewhat more accurate calculation than the existing methodology. Additionally, an experimental study served to validate the method and verify the relationship between the conventional active intensity and the effective sound intensity.

REFERENCES

[1] F. Fahy, "Sound Intensity" (Elsevier Science Publishers Ltd, Barking, Essex, 1989).

[2] J D Maynard, E. G Williams, and Y. Lee, "Nearfield acoustic Holography I: Theory of generalized holography and the development of NAH," J. Acoust. Soc. Am, 78(4):1395–1413 (1985).

[3] E. G. Williams, "Fourier Acoustics. Sound Radiation and Nearfield acoustic Holography" (Academic Press, San Diego, 1999).
[4] E. G. Williams, "Supersonic acoustic intensity," J. Acoust. Soc. Am., 97(1):121–127 (1994).
[5] E. G. Williams, "Supersonic acoustic intensity on planar sources," J. Acoust. Soc. Am., 104(5), 2845–2850 (1998).
[6] J. Hald, "Basic theory and properties of statistically optimized near-field acoustical holography," J. Acoust. Soc. Am, 125(4): 2105–2120 (2009).
[7] R. Steiner and J. Hald, "Near-field Acoustical Holography Without the Errors and Limitations Caused by the Use of Spatial DFT," International Journal of Acoustics and Vibration, 6(2) (2001).
[8] F. Jacobsen and V. Jaud, "Statistically optimized near field acoustic holography using an array of pressure-velocity probes," J. Acoust. Soc. Am., 121(3):1550–1558 (2007)
[9] E.G. Williams, "Continuation of acoustic near-fields," J. Acoust. Soc. Am. 113(3) , 1273–1281 (2003).

Paper E

Direct formulation of the supersonic acoustic intensity in space domain

Efren Fernandez-Grande[a] and Finn Jacobsen
Acoustic Technology, Department of Electrical Engineering, Technical University of Denmark (DTU), Building 352, Ørsteds Plads, DK-2800 Kongens Lyngby, Denmark

Quentin Leclère
Laboratoire Vibrations Acoustique, INSA Lyon, F-69621 Villeurbanne Cedex, France

(Received 19 July 2011; revised 7 October 2011; accepted 17 October 2011)

This paper proposes and examines a direct formulation in space domain of the so-called supersonic acoustic intensity. This quantity differs from the usual (active) intensity by excluding the circulating energy in the near-field of the source, providing a map of the acoustic energy that is radiated into the far field. To date, its calculation has been formulated in the wave number domain, filtering out the evanescent waves outside the radiation circle and reconstructing the acoustic field with only the propagating waves. In this study, the supersonic intensity is calculated directly in space domain by means of a two-dimensional convolution between the acoustic field and a spatial filter mask that corresponds to the space domain representation of the radiation circle. Therefore, the acoustic field that propagates effectively to the far field is calculated via direct filtering in space domain. This paper presents the theory, as well as a numerical example to illustrate some fundamental principles. An experimental study on planar radiators was conducted to verify the validity of the technique. The experimental results are presented, and serve to illustrate the usefulness of the analysis, its strengths and limitations. © *2012 Acoustical Society of America*. [DOI: 10.1121/1.3662052]

PACS number(s): 43.40.Rj, 43.60.Sx, 43.20.Rz, 43.20.Ye [EGW] Pages: 186–193

I. INTRODUCTION

The concept of efficient radiation is central in the analysis of sound radiation from plates and other wave bearing structures, because it gives an indication of the flow of acoustic energy that is radiated effectively into the far field. It indicates how much of the acoustic energy flow in the near field of a source is energy that propagates to the far field, and how much is circulating energy resulting from the interaction of propagating and evanescent waves near the source.

The far field radiation of sources is often the quantity of concern in acoustics and noise control, because this is the quantity to which a potential observer is typically exposed. Consequently, it has been studied extensively in the literature for decades, e.g., sound radiation from plates and panels,[1–3] identification of velocity patterns that radiate effectively into the far field based on singular value analysis,[4–6] etc.

The wave number processing of sound fields and the development of near-field acoustic holography (NAH),[7,8] have laid a new ground for calculating in practice the efficient and inefficient radiation from sound sources. Williams[9,10] introduced the concept of supersonic acoustic intensity for identifying and characterizing the regions of a source that radiate effectively into the far field.

The term "supersonic intensity" was chosen because of its close connection with the supersonic flexural waves in a structure.[10] However, this terminology might lead to the notion that the acoustic waves related to this quantity are supersonic, although this is not the case, their propagation speed is perfectly sonic.

So far, the calculation of the supersonic intensity has been formulated in the framework of Fourier based NAH, where the sound field is explicitly transformed into the wave number domain. The wave number components outside the radiation circle,[8] which correspond to evanescent waves, are filtered out, and the reconstruction is based only on the terms inside the radiation circle, which correspond to the waves that propagate to the far field.

The purpose of this paper is to propose and examine a formulation of the supersonic intensity directly in the space domain. The calculation is expressed as a two-dimensional convolution product between the acoustic field and a spatial operator or filter mask. The implementation of the method is straightforward and does not require transformations into the wave number domain. This approach can be convenient for estimating the efficient radiation of a source when the Fourier transformation of the sound field is not otherwise required. This is the case, for instance, when using holographic methods that are not based on FFT processing,[11–14] applied directly to measured data, etc.

The paper presents the theory and provides a numerical illustration of a one-dimensional radiator, revisiting the concept of effective and ineffective radiation. An experimental study is also included, which aims at illustrating the usefulness of the supersonic acoustic intensity in practice.

II. THEORY

A. Fourier based supersonic acoustic intensity

Consider the wave number spectra of the pressure and normal component of the particle velocity in a plane z:[8]

[a]Author to whom correspondence should be addressed. Electronic mail: efg@elektro.dtu.dk

$$P(k_x,k_y,z) = \iint_{-\infty}^{\infty} p(x,y,z)e^{j(k_x x+k_y y)}dxdy, \quad (1)$$

$$U(k_x,k_y,z) = \iint_{-\infty}^{\infty} u(x,y,z)e^{j(k_x x+k_y y)}dxdy, \quad (2)$$

where the time dependence $e^{j\omega t}$ is omitted. The sound pressure and particle velocity that are radiated into the far field are associated with the spectral energy inside the radiation circle,

$$p^{(s)}(x,y,z) = \frac{1}{4\pi^2}\iint_{Sr} P(k_x,k_y,z)e^{-j(k_x x+k_y y)}dk_x dk_y, \quad (3)$$

$$u^{(s)}(x,y,z) = \frac{1}{4\pi^2}\iint_{Sr} U(k_x,k_y,z)e^{-j(k_x x+k_y y)}dk_x dk_y, \quad (4)$$

where Sr denotes the surface corresponding to the radiation circle. The flow of acoustic energy that is radiated effectively into the far field, i.e., the supersonic intensity, is defined as

$$I^{(s)}(x,y,z) = \frac{1}{2}Re\{p^{(s)}(x,y,z)u^{(s)}(x,y,z)^*\}, \quad (5)$$

where the subscript asterisk denotes the complex conjugate.

It is apparent that the supersonic intensity is essentially a spatially low-pass filtered version of the conventional active intensity, where the evanescent waves are filtered out.

B. Direct formulation in space domain

Let the function $H(k_x,k_y)^{(s)}$ be defined as the unit circle function,

$$H(k_x,k_y)^{(s)} = \begin{cases} 1 & \text{if } (k_x^2+k_y^2) < k^2 \\ \frac{1}{2} & \text{if } (k_x^2+k_y^2) = k^2 \\ 0 & \text{if } (k_x^2+k_y^2) > k^2, \end{cases} \quad (6)$$

which represents a two-dimensional circular unit pulse, with the transition from zero to one at the boundary of the radiation circle.

The pressure and velocity that are radiated into the far field, Eqs. (3) and (4), can be expressed as

$$p^{(s)}(x,y,z) = \iint_{-\infty}^{\infty} P(k_x,k_y,z)\cdot H^{(s)}(k_x,k_y) \times e^{-j(k_x x+k_y y)}dk_x dk_y, \quad (7)$$

$$u^{(s)}(x,y,z) = \iint_{-\infty}^{\infty} U(k_x,k_y,z)\cdot H^{(s)}(k_x,k_y) \times e^{-j(k_x x+k_y y)}dk_x dk_y. \quad (8)$$

From the convolution theorem, the products in the wave number domain in Eqs. (7) and (8) are equivalent in space domain to a two-dimensional convolution between the acoustic field and $h^{(s)}(x,y)$,

$$p^{(s)}(x,y,z) = p(x,y,z) * h^{(s)}(x,y), \quad (9)$$

$$u^{(s)}(x,y,z) = u(x,y,z) * h^{(s)}(x,y). \quad (10)$$

The two-dimensional convolution is defined as

$$p^{(s)}(x,y,z) = \iint_{-\infty}^{\infty} p(x',y',z)h^{(s)}(x-x',y-y')dx'dy'. \quad (11)$$

Note that the function $h^{(s)}(x,y)$ is the space domain version of the radiation circle. Because of its relation with the radiation circle, it will be referred to as the *radiation filter mask* or *radiation kernel*. It can be calculated by inverse transformation of the function $H^{(s)}(k_x,k_y)$ from the wave number domain to the space domain,

$$h^{(s)}(x,y) = \frac{1}{4\pi^2}\iint_{-\infty}^{\infty} H^{(s)}(k_x,k_y)e^{-j(k_x x+k_y y)}dk_x dk_y. \quad (12)$$

Due to the geometry and properties of $H^{(s)}(k_x,k_y)$, it is convenient to introduce polar coordinates, so that $\rho = \sqrt{x^2+y^2}$ and $k_\rho = \sqrt{k_x^2+k_y^2}$. The function $H^{(s)}(k_\rho)$ is defined in polar coordinates as

$$H^{(s)}(k_\rho) = \begin{cases} 1 & \text{if } k_\rho < k \\ \frac{1}{2} & \text{if } k_\rho = k \\ 0 & \text{if } k_\rho > k. \end{cases} \quad (13)$$

Because $H^{(s)}(k_\rho)$ is circularly symmetric, the inverse Fourier transform of Eq. (12) can be expressed as an inverse Hankel transform,

$$h^{(s)}(\rho) = \frac{1}{2\pi}\int_0^{\infty} H_k^{(s)}(k_\rho)J_0(k_\rho\rho)k_\rho dk_\rho. \quad (14)$$

The $H_k^{(s)}(k_\rho)$ function is zero for $k_\rho > k$. Therefore, the previous integral is equivalent to

$$h^{(s)}(\rho) = \frac{1}{2\pi}\int_0^{k} J_0(k_\rho\rho)k_\rho dk_\rho. \quad (15)$$

This integral can be evaluated analytically making use of the relation $\int xJ_0(ax)dx = (x/a)J_1(ax)$,[15] and therefore, the radiation filter mask is

$$h^{(s)}(\rho) = \frac{k}{2\pi\rho}J_1(k\rho), \quad (16)$$

which back in rectangular coordinates is

$$h^{(s)}(x,y) = \frac{k}{2\pi\sqrt{x^2+y^2}}J_1(k\sqrt{x^2+y^2}). \quad (17)$$

This function is shown in Fig. 1.

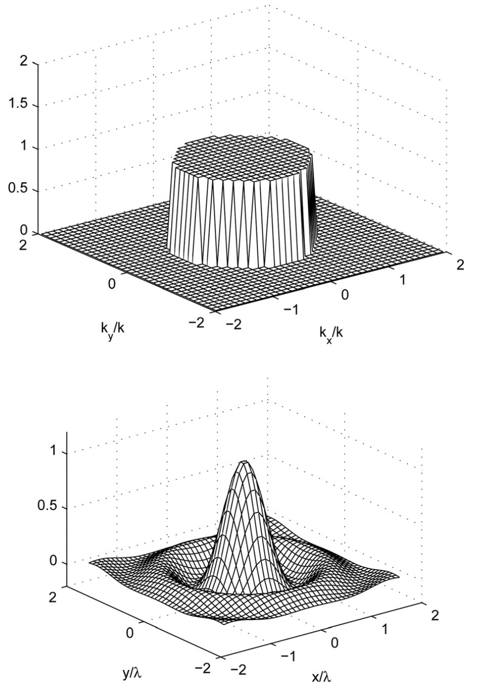

FIG. 1. (Top) Radiation filter in the wave number domain $H^{(s)}(k_x, k_y)$ and (bottom) the corresponding radiation kernel in the space domain $h^{(s)}(x, y)$. The axes are normalized. Note that the width of the mainlobe of $h^{(s)}$ is equal to the wavelength in air.

Using Eq. (17) for $h^{(s)}(x, y)$, the supersonic intensity can easily be calculated from Eqs. (5), (9), and (10)

Consider the example of a baffled monopole with volume velocity Q radiating into free field half-space. In the source plane ($z = 0$), the particle velocity component normal to the x, y plane is $u_z(x, y, 0) = Q\delta(x)\delta(y)$. From Eq. (10) and the shifting property of the Dirac delta function, it follows that the supersonic normal velocity of the baffled point source is

$$u_z^{(s)}(x, y, 0) = \frac{kQ}{2\pi\rho} J_1(k\rho). \tag{18}$$

This expression is identical to the expression derived in Ref. 10.

C. Discrete formulation

Consider a square uniform array of dimensions $N \times N$ and a radiation kernel of $L \times L$. The general left justified form of the discrete two-dimensional convolution is

$$p^{(s)}(x, y, z) = H_0 \sum_{m=0}^{N-1} \sum_{n=0}^{N-1} p(x'_m, y'_n, z) \times h^{(s)}(x - x'_m, y - y'_n), \tag{19}$$

where H_0 corresponds to the area of each grid position, $H_0 = \Delta x \Delta y$. Note that due to the circular symmetry of the filter mask, the convolution product is equivalent to a two-dimensional correlation. The output of the convolution is of dimensions $M \times M$, where $M = N + L - 1$.

The convolution sum can be formulated in vector-space as

$$\boldsymbol{p}^{(s)}_{[M^2 \times 1]} = \boldsymbol{T}_{[M^2 \times N^2]} \cdot \boldsymbol{p}_{[N^2 \times 1]}, \tag{20}$$

where $\boldsymbol{T}$ is a $M^2 \times N^2$ matrix containing the "shifting" radiation filter mask. Each column of $\boldsymbol{T}$ operates on a single point of the input matrix, and it accounts for the shifting of the spatial filter mask through that point. For details of the implementation see Refs. 16 and 17.

III. ONE-DIMENSIONAL RADIATOR

It is interesting to consider a one-dimensional finite radiator because it is a simple illustration and yet the generalization to the two-dimensional case is straightforward. The one-dimensional supersonic filter in the wave number domain is ideally a rectangular step function with a cutoff frequency determined by the wave number in air, k. The inverse Fourier transform of this filter is the radiation kernel in one dimension,

$$h_{1D}^{(s)}(x) = A_h \mathrm{sinc}(kx), \tag{21}$$

with $A_h = 2k$. It follows from this expression that the filter has an infinite impulse response in space domain, due to the ideal cut-off. This infinitely long response is not well compatible with a finite measurement aperture. Furthermore, it is a well-known fact that the ideal low-pass filtering introduces unwanted ringing artifacts via the Gibbs phenomenon. Therefore, it is convenient to define a finite filter mask that is more suited in practice to the non-ideal case. A simple and well established solution in signal processing and imaging to minimize ringing artifacts and preserve the general profile of the ideal filter is to use a Lanczos filter,[18,19]

$$h_{w,1D}^{(s)}(x) = \begin{cases} A_h \mathrm{sinc}(kx)\mathrm{sinc}(kx/a), & \text{for} -a < kx < a \\ 0 & \text{otherwise}, \end{cases} \tag{22}$$

where a determines how many sidelobes of the ideal filter are included before tapering to zero. This filter can be seen as an ideal brick-wall filter, weighted with the mainlobe of a sinc function. Typical values of a are $a = [1, 2, 3, ...]$, because integer numbers make the two sincs of Eq. (22) be zero at the edge of the filter mask, providing a smooth cut-off.

The source considered is a theoretical one-dimensional plate, 4 m long and simply supported at the boundaries. Figures 2(a) and 2(b) show the two radiation filter masks from Eqs. (21) and (22) for a wave number in air of $k = 5$ rad/m. Figures 2(c) and 2(d) show the normal velocity profile of the 1-D radiator in its $m = 5$ and $m = 9$ modes, respectively. Figures 2(e) and 2(f) show the result of the direct convolution between the two modes and the radiation filter masks. The spatial wave number of the $m = 5$ mode is $k_x = m\pi/L \approx 4$ rad/m. In this case, the main-lobe width of the supersonic operator, ∼1.25 m, is smaller than the spatial wavelength of the plate,

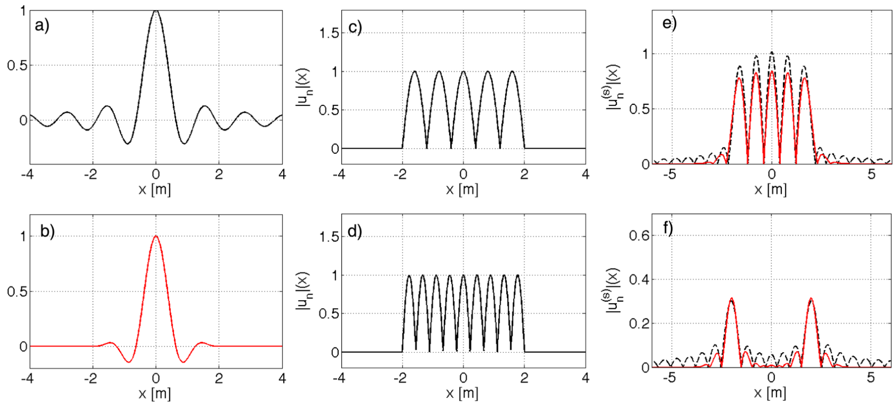

FIG. 2. (Color online) One-dimensional radiator above and below coincidence. (a) Wave number in air $k = 5$ rad/m: Ideal radiation filter mask, as in Eq. (21). (b) Finite radiation filter mask, as in Eq. (22) with $a = 3$. Normal velocity profile of the radiator (c) for an $m = 5$ mode and (d) for an $m = 9$ mode. Result of the convolution with the filter mask (e) for the $m = 5$ mode and (f) for the $m = 9$ mode, with the ideal filter (dashed line) and with the finite filter (solid line). The ordinate axes are normalized.

1.6 m, and all regions contribute efficiently to the far field radiation. For the $m = 9$ mode, the spatial wave number is $k_x \approx 7$ rad/m (spatial wavelength of 0.8 m), and the plate does not radiate efficiently because neighboring regions cancel each other under the mainlobe of the filter mask in the convolution process. There is only efficient sound radiation at the boundary of the plate due to the partial lack of cancellation. In two-dimensions, this corresponds to the well known theory of corner and edge radiation in plates for modes vibrating below the critical frequency.[1,2] The results also show that the ideal filter of Eq. (21) introduces ringing artifacts due to the infinite impulse response, whereas these artifacts are much less present in the Lanczos filter of Eq. (22). The ringing artifacts introduced are apparent in Figs. 2(e) and 2(f).

This example is reminiscent of well-known analyses[2,3] where the efficient and inefficient radiation from plates can be seen as a result of the convolution in the wave number domain between a Dirac delta and a sinc function. The Dirac delta results from the modal spatial frequency of the plate, and the sinc function from the finite extent of the plate. This results in a wave number spectrum with two sinc functions centered at $(\pm k_x)$. Above the critical frequency, the main lobes of the sinc functions fall within the radiation circle, resulting in efficient radiation. Below the critical frequency, only some sidelobes of the sinc functions fall within the radiation circle, giving rise to inefficient radiation. With the approach proposed in this paper, this phenomena can be seen directly as a convolution between the space domain representation of the radiation circle and the acoustic field, as described in the foregoing.

IV. EXPERIMENTAL STUDY

An experimental study has been conducted to examine the validity and applicability of the method proposed in this paper. To date, only simulations of the supersonic intensity on planar radiators have been published in the literature.

The source under study was a baffled steel plate of dimensions 50 cm × 70 cm, and 1 mm thick, rigidly mounted at the boundaries (see Fig. 3). The plate was driven at ($x = 5$, $y = -10$) cm. The normal vibration velocity of the plate was measured with a Polytec laser vibrometer OFV 056, over a grid of 26 × 36 positions. Based on these measurements, an equivalent source method model[11,20] was used to calculate the sound pressure and sound intensity on the surface of the plate. The equivalent sources were conformal to the measurement positions, retracted 3 cm behind the plate. To verify the calculation of the pressure, the results were compared to the ones obtained by evaluating the Rayleigh integral via FFT as in Ref. 21 The results from the two methods were nearly identical, with a deviation lower than 5%.

FIG. 3. (Color online) The laser measurements.

Note that an analogous methodology could be used if instead of measuring the normal velocity of the plate, the sound pressure was measured with a microphone array in the near-field of the source, as in near-field acoustic holography. However, in this study, laser measurements have been used for simplicity and because they provide a clear illustration.

In order to minimize ringing artifacts in the estimation of the supersonic intensity and limit the extent of the filter mask, a windowed version of the ideal filter is proposed. It follows the concept of Lanczos filtering, but it is adapted to the circularly symmetric filter mask, basing the window weights on the mainlobe of a first order Bessel function of the first kind. Therefore, a non-separable radiation kernel is used in which the infinite ideal response is weighted with the mainlobe of a Bessel function. This kernel is better suited for the discrete nature of the practical measurement. It not only minimizes the ringing artifacts, but it also reduces the size of the filter mask, making it computationally more efficient,

$$h_w^{(s)}(\rho) = \begin{cases} \dfrac{Ak}{2\pi\rho^2} J_1(k\rho) J_1(k\rho/\xi), & \text{for } k\rho < \xi \\ 0 & \text{otherwise,} \end{cases} \tag{23}$$

where A is a normalizing factor of the window. The value of the parameter ξ determines the size of the filter and the number of sidelobes included in the filter mask, and consequently the greater or lesser cut-off slope. The value of ξ could be any positive real number, but it is advantageous when it is one of the zero crossings of the first order Bessel function of the first kind $[\xi = 3.8317, 7.0156, 10.1735, 13.3237, ...]$. In such case, the ideal infinite filter and the weighting Bessel mainlobe are both zero at the edge of the filter mask, making it continuous and differentiable to second order, providing a smooth cut-off.

In this study, the third zero-crossing of the Bessel function was used, $\xi = 10.1735$. Nevertheless, using other values ($\xi = 7.0156, 13.3237, ...$) does not change the results significantly. The filter is shown in Fig. 4. Comparing it with the ideal filter in Eq. (17), shown in Fig. 1, it is worth noting that the mainlobes of the two filter masks are virtually identical, whereas the sidelobes of the finite filter are soon tapered to zero, limiting its extent and consequently minimizing the characteristic ringing of the ideal filter.

Figure 5 shows the active sound intensity and the supersonic acoustic intensity on the surface of the plate at 125 Hz, which corresponds to a (2, 2) modal shape. Note the alternating positive and negative active intensity regions, indicating a circulating flow of energy from one region of the plate into another, giving rise to a very poor far field radiation, as shown by the supersonic intensity map. It should be noted that the wavelength in air is much larger than the dimensions of the plate, and the supersonic intensity just shows a maximum near the driving point, as a source of far field radiation. It is apparent that there is an imaging constraint due to the resolution limit of the wavelength in air compared to the size of the aperture.

Figure 6 shows the active sound intensity and the supersonic intensity on the surface of the plate at 950 Hz, which

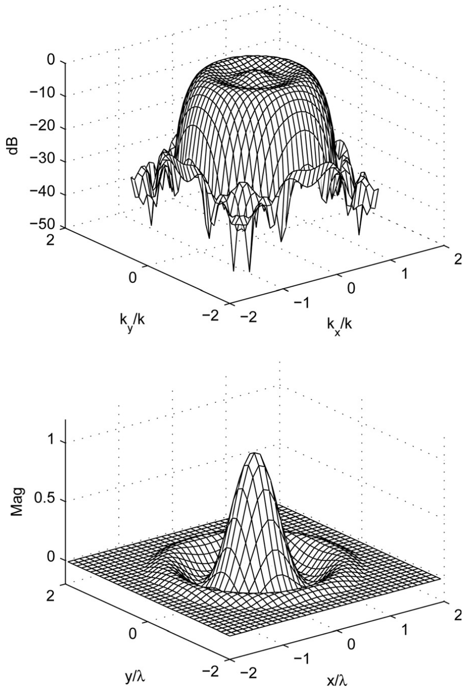

FIG. 4. (Top) Finite radiation filter in the wave number domain $H^{(s)}(k_x, k_y)$ and (bottom) the corresponding radiation kernel in the space domain $h_w^{(s)}(x, y)$ as in Eq. (23), with $\xi = 10.1735$. The overshooting at the pass band is of ± 1.2 dB and the highest sidelobe level in the frequency response is -30 dB.

corresponds to a (4, 10) modal shape. This frequency is also below coincidence, and a very reactive sound field is found. In this case, there are multiple regions with alternating positive and negative intensities, making it more difficult to identify and quantify how are they contributing to the net power output of the source. However, the supersonic intensity map indicates that the main radiation is from the corners of the plate, where there is a partial lack of cancellation at the edges. This result agrees with the well-known theory of corner and edge radiation from plates.

Figure 7 shows the active intensity and the supersonic intensity on the surface of the plate at 1135 Hz. At this frequency both corner and edge modes seem to be excited. There is a very high modal density, and the vibration pattern cannot be associated with an individual mode shape. The supersonic intensity map shows that there is in fact effective sound radiation from the corners and edges of the plate into the far field. Note that in all three cases (Figs. 5–7) the supersonic intensity level is significantly lower than the active sound intensity due to the circulation of energy occurring below coincidence.

Figure 8 shows the supersonic intensity of the plate at 950 and 1135 Hz calculated using FFT based convolution. The results are closely similar to those in Figs. 6 and 7, obtained via direct convolution with the finite filter in

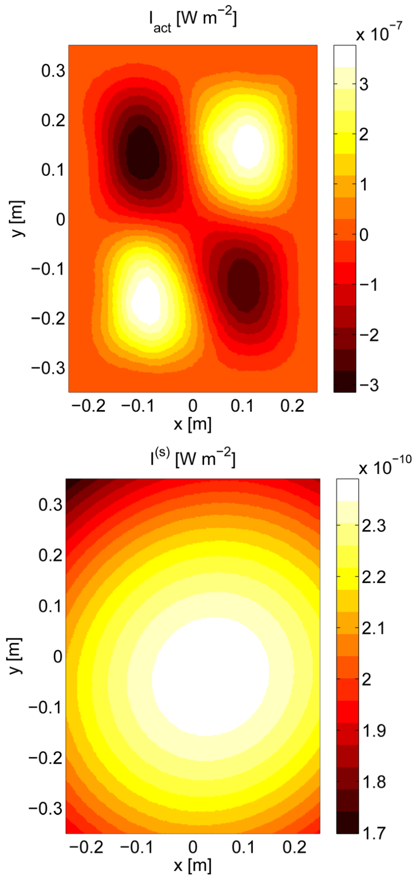

FIG. 5. (Color online) (Top) Active sound intensity on the source plane and (bottom) the supersonic sound intensity at 125 Hz. Note the negative active sound intensity.

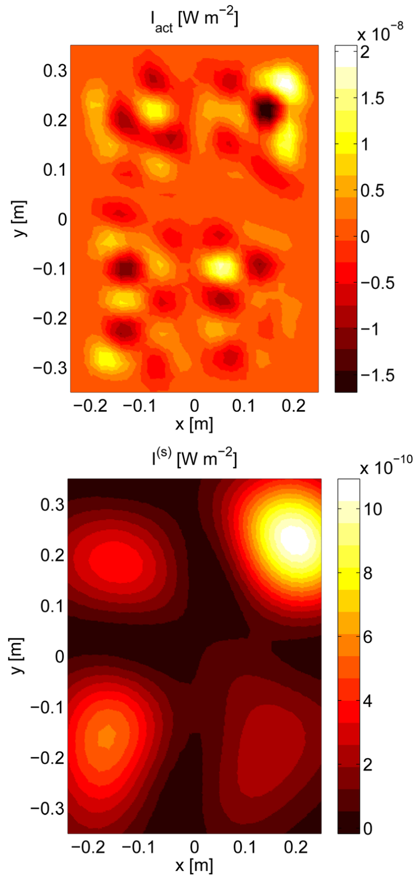

FIG. 6. (Color online) (Top) Active sound intensity on the source plane and supersonic sound intensity (bottom) at 950 Hz.

Eq. (23), indicating the underlying equivalence between the two methodologies.

It has been shown that the supersonic intensity represents the fraction of acoustic energy that contributes to the total power output from the source, in other words, that there is conservation of power.[9,10] In this experimental study, the total power radiated by the source has been calculated from the active sound intensity, as well as from the estimated supersonic intensity. At 950 Hz, the power calculated from the active intensity is 1.5×10^{-10} W and from the supersonic intensity it is 1×10^{-10} W ($\sim$1.7 dB deviation). At 1135 Hz, the power calculated from the active intensity is 2.5×10^{-9} W, and from the supersonic intensity it is 1.5×10^{-9} W ($\sim$2 dB deviation).

The sound power calculated from the supersonic intensity is somewhat underestimated due to the truncation introduced by the finite measurement aperture. The underestimation of the sound power is more pronounced in the low frequency range, where the acoustical wavelength, which determines the width of the radiation kernel, is much larger than the aperture. In the present experiment, at 127 Hz, there was an underestimation of the power of about 8 dB. However, if the size of the measurement aperture is increased to 82×102 cm^2 (this was done by zero-padding the measured normal velocity and calculating the corresponding sound pressure over a larger aperture), the underestimation at 127 Hz is reduced to 4 dB, whereas at 950 and 1135 Hz it is less than 1 dB. Eventually, the estimation always converges to the correct radiated power by sufficiently extending the measurement aperture, also at lower frequencies, due to the conservation of power.

Lastly, regarding the calculation method, the total power estimated via either direct convolution or FFT processing was practically the same, within $\pm$0.25 dB. On the whole, the experimental results confirm that the supersonic intensity is a meaningful measure of the net far field output of the source.

V. DISCUSSION

The formulation presented in this paper seems to be convenient for applications where the explicit transformation of sound fields into the *k*-space domain is not required. This is the

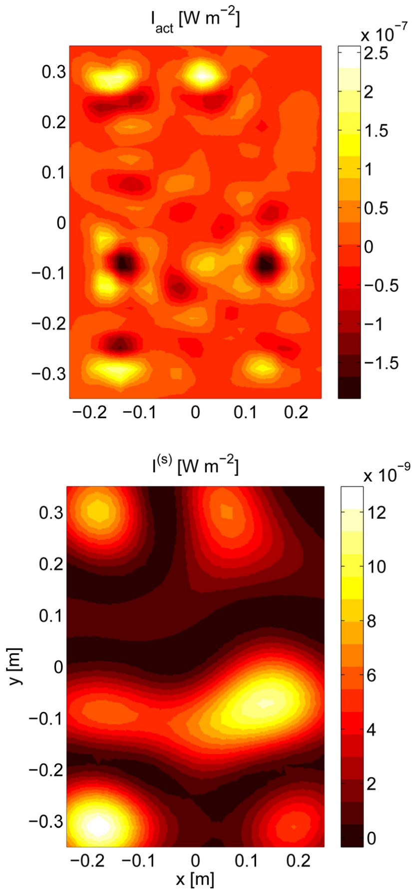

FIG. 7. (Color online) (Top) Active sound intensity on the source plane and (bottom) the supersonic intensity at 1135 Hz.

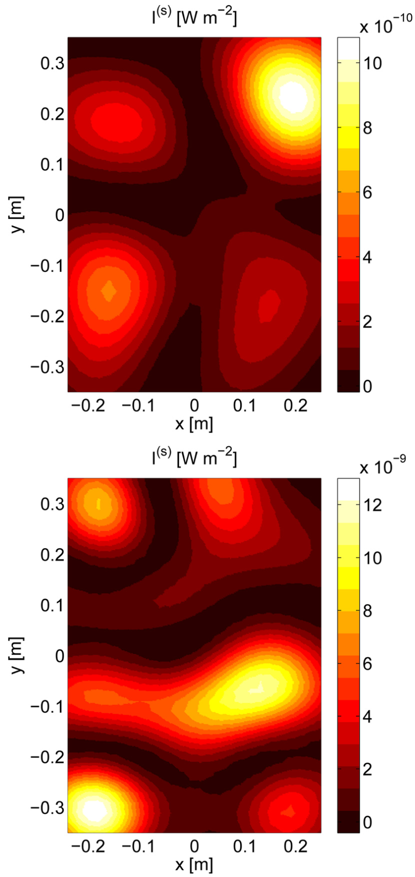

FIG. 8. (Color online) Supersonic intensity (as in Figs. 6 and 7), calculated using FFT-based filtering. (Top) 950 Hz; (bottom) 1350 Hz.

case for many of the existing holography techniques, where the direct formulation proposed here could be applied directly after the reconstruction of the acoustic field. The methodology could also be applied directly to measurements or to numerical calculations of vibrating sources, in order to provide an estimation of the effective radiation of the source into the far field.

The Fourier based convolution and the direct convolution operations are closely related to each other, yielding similar results, although there are some fundamental differences. Most notably, the Fourier based convolution assumes periodicity of the signals, and therefore proper zero padding is required (to at least the size of the measurement positions plus the filter mask), to avoid possible errors. The direct convolution does not assume periodicity, and it is a simple operation that can be more accurate on the boundaries of the data regardless of the size of the measurement and the filter mask.

Regarding the computational complexity of the two implementations, given an array of size $N \times N$, a radiation filter mask of dimensions $L \times L$, and an output array of $M \times M$, where $M = N + L - 1$, the number of operations required in a two-dimensional convolution is of order M^2N^2. The number of operations using FFT has a lower bound of order $M^2(1 + 2\log_2(M^2))$.[16,22] In some disciplines, such as image processing, the input vectors or matrices are typically very large, containing at least several millions of elements. Therefore, the FFT implementation of the filtering process can save a tremendous computation effort. However, in the case of array acoustics, where typically the input vectors are of a few hundred points or less, there is not a clear computational basis for preferring an FFT implementation, because the complexity of the operation is small in any case. Furthermore, for few points, the direct convolution can be computationally lighter.

It has been shown in the foregoing how the sharp cut-off in the wave number domain due to the ideal filter introduces ringing artifacts via the Gibbs phenomenon. Although the sharp ideal cut off is theoretically rigorous, it poses some difficulties in practice. Therefore, it is convenient to use instead a finite filter that is suited for the practical implementation. In the wave number domain this can be done by choosing an appropriate lowpass FIR filter

(Butterworth, etc.).[22] Alternatively, the space domain formulation proposed in this paper makes it possible to design the desired filter mask by means of the straightforward and well-known windowing method.[23]

It is not the purpose of this paper to make a comparison between the many available filters. Nevertheless, a non-separable circularly symmetric filter suited to the problem has been proposed. It provides a good compromise between sharp cut-off, and low ringing artifacts.

VI. CONCLUSIONS

In this paper, the concept of supersonic acoustic intensity has been examined and formulated as a direct filtering operation in space domain. The method makes it possible to identify the regions of a source that radiate into the far field and to estimate how much of the acoustic energy flow propagates to the far field, contributing to the net power output of the source.

A numerical example as well as an experimental study have served to illustrate the method and examine its advantages and limitations. The method is appealing due to its simplicity and the fact that it does not require transformations into the wave number domain. Hence, it can be useful in the general case for applications in which the Fourier transformation of sound fields is not required. Ultimately, the formulation presented in this paper contributes to an alternative, yet equivalent description of the near field and far field radiation from acoustic sources.

[1] G. Maidanik, "Response of ribbed panels to reverberant acoustic fields," J. Acoust. Soc. Am. **34**, 809–826 (1962).

[2] L. Cremer, M. Heckl, and E. E. Ungar, *Structure-Borne Sound* (Springer-Verlag, New York, 1973), Chap. 6.

[3] F. J. Fahy, *Sound and Structural Vibration,* 2nd ed. (Academic Press, London, 1987), Chap. 3.

[4] V. Borgiotti, "The power radiated by a vibrating body in an acoustic fluid and its determination from boundary measurements," J. Acoust. Soc. Am. **88**, 1884–1893 (1990).

[5] D. M. Photiadis, "The relationship of singular value decomposition to wave-vector filtering in sound radiation problems," J. Acoust. Soc. Am. **88**, 1152–1159 (1990).

[6] R. A. Magalhaes and M. B. S. Tenenbaum, "Supersonic acoustic intensity for arbitrarily shaped sources," Acta. Acust. Acust. **92**, 189–201 (2006).

[7] J. D. Maynard, E. G. Williams, and Y. Lee, "Nearfield acoustic holography I: Theory of generalized holography and the development of NAH," J. Acoust. Soc. Am, **78**, 1395–1413 (1985).

[8] E. G. Williams, *Fourier Acoustics: Sound Radiation and Nearfield Acoustic Holography* (Academic Press, San Diego, 1999), Chaps. 2–3.

[9] E. G. Williams, "Supersonic acoustic intensity," J. Acoust. Soc. Am. **97**, 121–127 (1995).

[10] E. G. Williams, "Supersonic acoustic intensity on planar sources," J. Acoust. Soc. Am. **104**, 2845–2850 (1998).

[11] A. Sarkissian, "Method of superposition applied to patch near-field acoustic holography," J. Acoust. Soc. Am. **118**, 671–678 (2005).

[12] R. Bai, "Application of BEM (boundary element method)-based acoustic holography to radiation analysis of sound sources with arbitrarily shaped geometries," J. Acoust. Soc. Am. **92**, 533–549 (1992).

[13] J. Hald, "Basic theory and properties of statistically optimized near-field acoustical holography," J. Acoust. Soc. Am. **125**, 2105–2120 (2009).

[14] E. Fernandez-Grande and F. Jacobsen, "Supersonic acoustic intensity with statistically optimized near-field acoustic holography," in *Proceedings of Inter-Noise 2011 (CD-Rom)*, Osaka, Japan (September 4–7, 2011).

[15] M. Abramowitz and I. A. Stegun, *Handbook of Mathematical Functions* (National Bureau of Standards, Washington, D.C., 1964), Chap. 9.

[16] W. K. Pratt, *Digital Image Processing*, 3rd ed. (Wiley-Interscience, New York, 2001), Chap. 7.

[17] W. K. Pratt, "Vector space formulation of two-dimensional signal processing operations," Comput. Vision Graph. **4**, 1–24 (1975).

[18] C. E. Duchon, "Lanczos filtering in one and two dimensions," J. Appl. Meteorol. **18**, 1016–1022 (1979).

[19] W. Burger and M. J. Burge, *Principles of Digital Image Processing: Core Algorithms*, 1st ed. (Springer-Verlag, London, 2009), Chap. 10.

[20] G. H. Koopmann, L. Song, and J. B. Fahnline, "A method for computing acoustic fields based on the principle of wave superposition," J. Acoust. Soc. Am. **86**, 2433–2438 (1989).

[21] E. G. Williams and J. D. Maynard, "Numerical evaluation of the Rayleigh integral for planar radiators using the FFT," J. Acoust. Soc. Am. **72**, 2020–2030 (1982).

[22] R. C. Gonzalez and R. E. Woods, *Digital Image Processing*, 3rd ed. (Prentice Hall, Upper Saddle River, NJ, 2008), Chap. 4.

[23] A. V. Oppenheim and R. W. Schafer, *Discrete-Time Signal Processing*, international edition (Prentice-Hall, Upper Saddle River, NJ, 1989), Chap. 7.

Paper F

A NOTE ON THE FINITE APERTURE ERROR OF THE SUPERSONIC ACOUSTIC INTENSITY

Efren Fernandez-Grande, Finn Jacobsen

Acoustic Technology. Department of Electrical Engineering
Technical University of Denmark. 2800 Lyngby, Denmark. [efg@elektro.dtu.dk]

Abstract

This note examines the influence of the truncation error due to the finite measurement aperture in the calculation of the supersonic acoustic intensity in planar coordinates. An analytical description based on a direct formulation in space domain of the supersonic intensity is given. A numerical study has been conducted to illustrate the analysis and study this source of error.

Note: This manuscript is a brief supplementary note to Paper D and Paper E.

1. Introduction

The supersonic acoustic intensity [1–3] is a useful quantity that makes it possible to identify the regions of a source that radiate acoustic energy effectively into the far field, and yields a quantitative representation of their contribution to the total net power output from the source. The quantity relies on discarding from the reconstruction the near-field evanescent waves, whose interaction gives rise to the circulatory paths of acoustic energy that take place in the near-field of wave-bearing structures. [4]

It follows that this quantity is based on the wavenumber processing of sound fields, and can be calculated either by filtering in the wavenumber domain, explicitly [2] or implicitly [5], or alternatively by direct filtering in the space domain. [3]

In any case, the concept of supersonic intensity implies in theory an ideal separation between the propagating and the evanescent waves. This, in the wavenumber domain corresponds to a filter with an ideal cut-off slope that can separate the spatial frequencies inside the radiation circle [6] from the ones outside of it. This ideal two-dimensional filter results in an infinite impulse response in the space domain, or an infinite filter mask. [3]

In planar coordinates, the measurement aperture used to estimate the supersonic intensity is naturally finite, and this results in truncation error. This truncation error is particularly relevant given the idealized filter and the resulting infinite extent of the filter mask. This can be a practical challenge for the estimation of the supersonic intensity experimentally. Recent studies that calculated the supersonic intensity indicated that the truncation error in the calculation of the supersonic intensity is notable. [3,5] It is the aim of this brief note to examine and illustrate this source of error, via an analytical description of the phenomena and numerical experiments.

It should be noted that the term ‘supersonic’ is used to denote the waves inside the radiation circle (due to their *trace* velocity). This are indeed the propagating waves that are radiated into the far-field (as opposed to the evanescent waves of subsonic trace velocity). However, in spite of the terminology, the speed of these waves is sonic. Thus, when referring to supersonic pressure, velocity or intensity, we are just referring to the pressure, velocity and intensity of the propagating waves.

2. Theory

Let there be a certain pressure distribution over an infinite plane $p_\infty(x, y, z_s)$. As shown in ref. 3, the sound-field components that propagate effectively into the far field can be expressed as the result from a two-dimensional convolution in space domain between the sound field and the space domain representation of the radiation circle (or the radiation filter mask) $h^{(s)}(x, y)$,[3]

$$p_\infty^{(s)}(x, y, z_s) = \iint_{-\infty}^{\infty} p_\infty(x', y', z_s) \cdot h^{(s)}(x - x', y - y')dx'dy'. \tag{1}$$

This integral represents the true, ideal, quantity that extends over the infinite plane. This can be expressed as a finite estimate of the propagating, or so-called ‘supersonic’ pressure, $\tilde{p}^{(s)}(x, y, z_s)$, plus an error due to the finite aperture truncation, ε_p,

$$p_\infty^{(s)}(x, y, z_s) = \tilde{p}^{(s)}(x, y, z_s) + \varepsilon_p(x, y, z_s). \tag{2}$$

If we consider an aperture of dimensions $(L \times L)$, the finite estimate of the pressure that propagates to the far field is

$$\tilde{p}^{(s)}(x, y, z_s) = \iint_{-L/2}^{L/2} p(x', y', z_s) \cdot h^{(s)}(x - x', y - y')dx'dy', \tag{3}$$

and the error due to truncation is

$$\begin{aligned} \varepsilon_p(x, y, z_s) = &\iint_{-\infty}^{-L/2} p(x', y', z_s) \cdot h^{(s)}(x - x', y - y')dx'dy' \\ &+ \iint_{L/2}^{\infty} p(x', y', z_s) \cdot h^{(s)}(x - x', y - y')dx'dy'. \end{aligned} \tag{4}$$

This can alternatively be described by expressing the true pressure in an infinite plane as the sum of the pressure inside and outside the aperture,

$$p_\infty(x, y, z_s) = p_i(x, y, z_s) + p_o(x, y, z_s), \tag{5}$$

where p_i is the pressure within the aperture area, and p_o is the pressure that extends beyond the aperture to infinity.

We recall here that the 'supersonic' pressure (or alternatively particle velocity) can be obtained from the convolution with the radiation filter mask as in Eq. (1) [$p_\infty^{(s)}(x, y, z_s) = p_\infty(x, y, z_s) * h^{(s)}(x, y)$]. From the distributivity property of the convolution, and from Eq. (5), the exact supersonic pressure over the infinite plane is

$$p_\infty^{(s)}(x, y, z_s) = p_i(x, y, z_s) * h^{(s)}(x, y) + p_o(x, y, z_s) * h^{(s)}(x, y), \tag{6}$$

which corresponds indeed to the finite estimate plus an error term due to the truncation:

$$\begin{aligned} \tilde{p}^{(s)}(x, y, z_s) &= p_i(x, y, z_s) * h^{(s)}(x, y), \\ \varepsilon_p(x, y, z_s) &= p_o(x, y, z_s) * h^{(s)}(x, y). \end{aligned} \tag{7}$$

Similarly, for the normal component of the particle velocity, the finite estimate and the truncation error are:

$$\begin{aligned} \tilde{u}^{(s)}(x, y, z_s) &= u_i(x, y, z_s) * h^{(s)}(x, y), \\ \varepsilon_u(x, y, z_s) &= u_o(x, y, z_s) * h^{(s)}(x, y). \end{aligned} \tag{8}$$

Finally, the exact supersonic intensity results from the product between $p_\infty^{(s)}$ the conjugate of $u_\infty^{(s)}$ (thus the product of the approximations plus the errors),

$$I_\infty^{(s)}(x, y, z_s) = \frac{1}{2} Re\{[\tilde{p}^{(s)}(x, y, z_s) + \varepsilon_p] \cdot [\tilde{u}^{(s)}(x, y, z_s) + \varepsilon_u]^*\}. \tag{9}$$

It follows that the estimated supersonic intensity is

$$\tilde{I}^{(s)}(x, y, z_s) = \frac{1}{2} Re\{\tilde{p}^{(s)}(x, y, z_s) \cdot \tilde{u}^{(s)}(x, y, z_s)^*\}, \tag{10}$$

and the truncation error is

$$\varepsilon_I = \frac{1}{2} Re\{\varepsilon_p \cdot \varepsilon_u^* + \varepsilon_p \cdot \tilde{u}^{(s)}(x, y, z_s)^* + \tilde{p}^{(s)}(x, y, z_s) \cdot \varepsilon_u^*\}. \tag{11}$$

3. Numerical results

In this section, the error introduced by the finite aperture in the calculation of the supersonic intensity is examined numerically. The error introduced in the pressure, normal velocity and intensity is shown. The estimated supersonic intensity of a sound source is calculated based on the finite aperture data, and the error is calculated based on the convolution between the truncated field and the infinite filter mask, as in Eqs. (7) to (11).

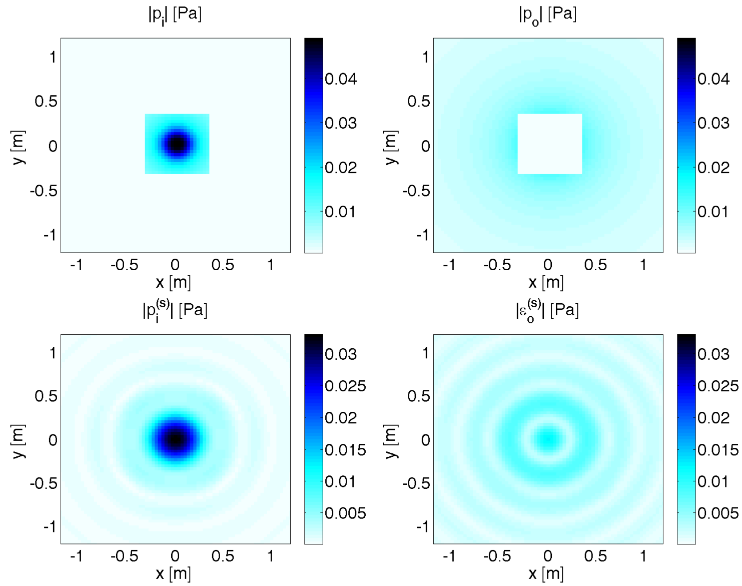

FIG. 1: Error introduced by the finite aperture in the calculation of $p(s)$. The source is a 30×30 cm baffled plate. Wavenumber in air $k = 10$ rad/m. Sound pressure inside the aperture (top-left); Truncated sound pressure outside the aperture (top-right); Estimated $\tilde{p}^{(s)}$ (bottom-left); Truncation error due to the finite aperture (bottom-right).

The normalized relative error of a quantity χ is defined as

$$\bar{\varepsilon}_{\chi}(\%) = \frac{||\varepsilon_{\chi}||_2}{||\chi||_2} \cdot 100. \tag{12}$$

The source used in this example is a simply supported baffled aluminium plate of dimensions 30×30 cm^2, and 3 mm thick. The plate is centered at the origin of coordinates, where it is driven by a point force of amplitude 0.3 N and at 546 Hz ($k = 10$ rad/m). The pressure and particle velocity radiated by the plate are calculated with the Rayleigh's integral using a grid of 35×35 points. The measurement standoff distance is $z = 5$ cm. The measurement aperture is 60×60 cm^2, thus covering an area four times larger than the plate, and the inter-spacing distance between grid points is $\delta_x = 3$ cm. For the calculation of the truncation error the sound field extending throughout a 10×10 m^2 area outside the aperture is considered. Beyond this area the influence of the truncation is neglected.

Figure 1 shows the sound pressure in the aperture, the truncated pressure, the estimated supersonic pressure and the corresponding truncation error in the calculation. All the quantities are shown over an area of 2.4×2.4 m^2. Figure 2 shows the same quantities for the normal component of the particle velocity. It is apparent that the effects of the finite aperture are much less severe in the case of the velocity. Figure 3 shows the computed supersonic intensity and the error within the aperture, across its diagonal.

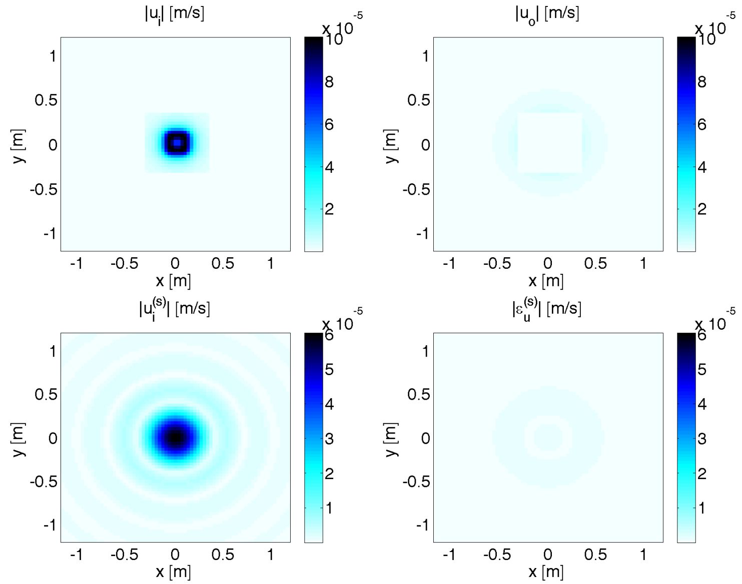

FIG. 2: Error introduced by the finite aperture in the calculation of $u(s)$. Wavenumber in air $k = 10$ rad/m. Normal velocity inside the aperture (top-left); Truncated normal velocity outside the aperture (top-right); Estimated $\tilde{u}^{(s)}$ (bottom-left); Truncation error (bottom-right).

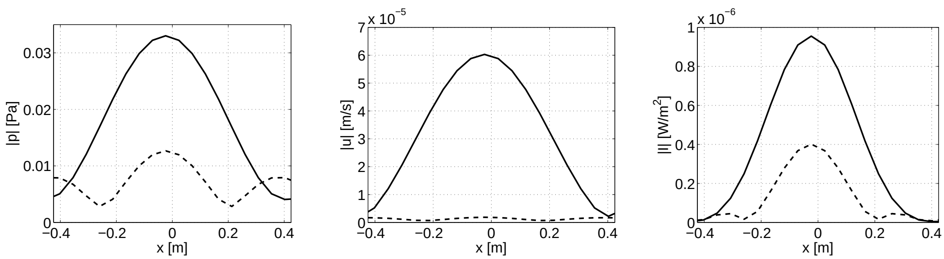

FIG. 3: Error introduced by the finite aperture in the calculation of the supersonic intensity of a 30×30 cm baffled plate. Wavenumber in air $k = 10$ rad/m. Supersonic pressure (left), supersonic normal velocity (center), and supersonic intensity (right) across the diagonal of the aperture. For each quantity, the finite estimate (solid lines) is plotted against the error (dashed lines).

The averaged error throughout the aperture is of 30 % for the supersonic pressure, where as only 4 % for the supersonic velocity. The overall error in the estimation of the supersonic intensity is of about 24 %.

A similar experiment has been conducted, but using a point source instead of a baffled plate. The results (not shown) confirm previous results and observations shown in refs. 5 and 3. The set-up of the experiment is identical to the previous case, except for the source used. For a wavenumber in air of $k = 10$ rad/m, the averaged error inside the aperture due to the effect of spatial truncation is of 35 % in the case of the pressure, while it is only of 4 % in for the particle velocity, and 27 % for the supersonic intensity. At high frequencies, as the wavelength in air becomes smaller compared to the measurement aperture, the error decreases gradually. For instance at $k = 15$, the error is approximately 32 % 4 % and 24 %, and at $k = 20$ rad/m, the error is approximately 29 % 4 % and 22 % for the supersonic pressure normal velocity and intensity, respectively.

As a simple and illustrative example, it is interesting to consider the case in which the supersonic intensity is calculated directly in the source plane of a point source. The sound pressure in this plane decays with the distance, but only vanishes completely at infinity. It follows that there is inevitably a truncation error in the estimation. Contrarily, the particle velocity is a Dirac delta function, and the normal velocity outside the aperture is completely zero. Consequently, there is no truncation error associated with the normal velocity.

It should be noted that this study analyses only the effects of truncation, therefore, it assumes that the pressure and velocity are known, and studies how the finite extent of the aperture influences the calculation of the quantities that propagate into the far field. The purpose of this study is not to investigate the accuracy of estimating the supersonic radiation with either pressure or velocity measurements (this was examined in ref. 5). However, this analysis reveals why the velocity based calculation is more accurate than the pressure or the pressure-velocity one.

4. Conclusion

The truncation error introduced by the finite measurement aperture in the calculation of the supersonic intensity has been addressed in this note. This source of error is significant, and seems to be a result of the sharp cut-off frequency in the frequency domain and the corresponding infinite filter mask in space domain. A description of the phenomenon and a numerical study have been presented. The results corroborate the importance of capturing the entire radiation by the source and of calculating the supersonic intensity over an area significantly larger than the source and the wavelength in air.

References

[1] E. G. Williams, “Supersonic acoustic intensity,”. J. Acoust. Soc. Am. **97**, 121–127 (1995).

[2] E. G. Williams, “Supersonic acoustic intensity on planar sources,” J. Acoust. Soc. Am. **104**, 2845–2850 (1998).

[3] E. Fernandez-Grande, F. Jacobsen and Q. Leclere. “Direct formulation of the supersonic acoustic intensity in space domain,” J. Acoust. Soc. Am. **131** (1), 186–193 (2012).

[4] F.J. Fahy, *Sound and Structural Vibration*, 2nd ed. (Academic Press, London, 1987).

[5] E. Fernandez-Grande, and F. Jacobsen, "Supersonic acoustic intensity with statistically optimized near-field acoustic holography," on CD: *Proceedings of Inter-Noise 2011*, Osaka, Japan, September 4-7, 2011.

[6] E. G. Williams, *Fourier Acoustics: Sound Radiation and Nearfield Acoustic Holography* (Academic Press, San Diego, 1999).

Part III

Paper G

Near field acoustic holography with microphones on a rigid sphere (L)[a]

Finn Jacobsen,[b] Guillermo Moreno-Pescador, and Efren Fernandez-Grande
Acoustic Technology, Department of Electrical Engineering, Technical University of Denmark, Building 352, DK-2800 Kongens Lyngby, Denmark

Jørgen Hald
Brüel & Kjær, Skodsborgvej 307, DK-2850 Nærum, Denmark

(Received 2 December 2010; revised 16 March 2011; accepted 20 March 2011)

Spherical near field acoustic holography (spherical NAH) is a technique that makes it possible to reconstruct the sound field inside and just outside a spherical surface on which the sound pressure is measured with an array of microphones. This is potentially very useful for source identification. The sphere can be acoustically transparent or it can be rigid. A rigid sphere is somewhat more practical than an open sphere. However, spherical NAH based on a rigid sphere is only valid if it can be assumed that the sphere has a negligible influence on the incident sound field, and this is not necessarily a good assumption when the sphere is very close to a radiating surface. This Letter examines the matter through simulations and experiments. © *2011 Acoustical Society of America.*
[DOI: 10.1121/1.3575603]

PACS number(s): 43.60.Pt, 43.60.Jn [EJS] Pages: 3461–3464

I. INTRODUCTION

Since the advent of multichannel analyzers and powerful computers, microphone arrays have been used more and more for many different purposes, e.g., noise mapping and source identification,[1] determination of room acoustic parameters,[2] and recording of sound.[3] In the past decade spherical microphone arrays have been used increasingly. The reason is that microphone arrays with this geometry have several attractive features. For example, it is obvious that a beamformer based on a spherical microphone array with a high density of the transducers will have essentially the same angular resolution in all directions.

Beamforming usually takes place relatively far from the sources under examination, and the purpose is to provide a directional resolution of the incident sound field. However, spherical microphone arrays can also be used for near field acoustic holography (NAH), that is, for reconstructing the sound field inside and just outside the sphere.[4,5] Reconstructing the sound field between the source and the sphere is an inverse problem, and here the spherical array has a significant advantage compared with conventional planar arrays that the usual problem of a finite measurement aperture is completely avoided.

Williams *et al.* have described a technique for spherical NAH with an open (acoustically transparent) sphere,[4] and, more recently, with a rigid sphere.[5] A rigid sphere is somewhat more practical than an open sphere, and the boundary conditions are well defined, whereas it seems unlikely that an arrangement with, say, 50 microphones with preamplifiers and cables placed relatively close to each other should not disturb the sound field. On the other hand, there is a potential problem in mounting the microphones on a solid sphere: In NAH the measurement array is always placed fairly near the source under test, because otherwise the evanescent waves will have died out and cannot be reconstructed near the source. Thus the waves that are backscattered from the sphere are likely to be reflected by the surface of the source, and therefore may modify the incident field; there is no way to distinguish between the original sound field and such multiple reflections. The purpose of this study is to examine the matter.

II. A BRIEF SUMMARY OF THE THEORY

As shown by Williams *et al.*, the sound pressure inside and just outside of an acoustically transparent sphere of radius a can be expressed in terms of the pressure on the surface of the sphere as follows:[4]

$$p(r,\theta,\varphi) = \sum_{n=0}^{\infty}\sum_{m=-n}^{n} A_{mn} j_n(kr) Y_n^m(\theta,\varphi), \tag{1}$$

where j_n is a spherical Bessel function, k is the wave number, r, θ, and φ are coordinates in a spherical coordinate system, Y_n^m is a "spherical harmonic,"[6] and the coefficients of the expansion are

$$A_{mn} = \frac{\int_0^{2\pi}\int_0^{\pi} p(a,\theta,\varphi) Y_n^m(\theta,\varphi)^* \sin\theta \, d\theta \, d\varphi}{j_n(ka)}. \tag{2}$$

The corresponding theory for a rigid sphere is a straightforward extension. The pressure in a region outside the sphere becomes[7]

---

[a]Portions of this work were presented in "Near field acoustic holography with microphones mounted on a rigid sphere," *Proceedings of Inter-Noise 2008*, Shanghai, China, October 2008.

[b]Author to whom correspondence should be addressed. Electronic mail: fja@elektro.dtu.dk

$$p_{\rm tot}(r,\theta,\varphi)=\sum_{n=0}^{\infty}\sum_{m=-n}^{n}B_{mn}\left(j_n(kr)-\frac{j_n'(ka)}{h_n'(ka)}h_n(kr)\right)\times Y_n^m(\theta,\varphi), \tag{3}$$

where h_n is a spherical Hankel function of the second kind because of the sign convention used in this Letter, $e^{j\omega t}$, and the coefficients are

$$B_{mn}=\frac{\int_0^{2\pi}\int_0^{\pi}p_{\rm tot}(a,\theta,\varphi)Y_n^m(\theta,\varphi)^*\sin\theta\,d\theta\,d\varphi}{j_n(ka)-\frac{j_n'(ka)}{h_n'(ka)}h_n(ka)}. \tag{4}$$

[In Ref. 5 Williams *et al.* give a different but mathematically identical expression, where n_n is a spherical Neumann function, and the identity follows from Eq. (6.66) in Ref. 6]. The pressure outside the sphere equals the sum of the incident pressure (the pressure as it would be in the absence of the sphere) and the scattered pressure. The incident pressure is[7]

$$p_{\rm inc}(r,\theta,\varphi)=\sum_{n=0}^{\infty}\sum_{m=-n}^{n}B_{mn}j_n(kr)Y_n^m(\theta,\varphi). \tag{5}$$

It is apparent that Eqs. (1) and (5) are formally identical, although the coefficients differ. Note, however, that whereas the denominator of the coefficients given by Eq. (2) can assume a value of zero, this can never happen with the coefficients given by Eq. (4); therefore, Eq. (1) gives unstable results at certain frequencies, unlike Eq. (5).

To summarize, if the sound pressure is measured on the surface of a rigid sphere, then the incident sound field can, at least in principle, be reconstructed. However, inside the sphere the problem is a forward one, but outside the sphere the problem is an ill-posed inverse one.

III. A SIMULATION STUDY

In the following simulation study there are 50 microphones flush-mounted on a sphere of radius $a=9.75$ cm. The microphones are assumed to measure the pressure at discrete positions on the sphere, and the positions and weights used in the numerical integration have been determined by numerical optimization, subject to position constraints imposed by 12 cameras. The resulting numerical integration is sufficiently accurate for spherical harmonics of degree n up to $N=5$, under the condition that $ka<N$; see the Appendix. The spherical wave expansion is therefore truncated at $n=N$, and an upper limiting frequency of 2.8 kHz must be respected to avoid aliasing in the integration and in order for the truncated wave expansion to provide a sufficiently complete representation on and inside the surface of the rigid sphere. Apart from the smoothing caused by the truncation, no further regularization is attempted in this study.

The first test case is a monopole with frequency independent volume velocity placed 20 cm from the center of the sphere. Figure 1 compares the undisturbed sound pressure at the center of the sphere with the reconstructed incident pressure with a rigid sphere calculated using Eq. (5), and the

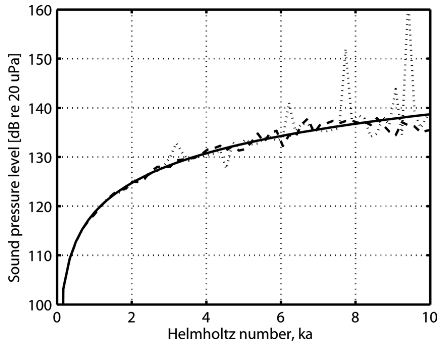

FIG. 1. Sound pressure level at the center of the sphere generated by a monopole 20 cm from the center of the sphere as a function of *ka*. Solid line, true pressure; dashed line, reconstructed incident pressure with a rigid sphere [Eq. (5)]; dotted line, reconstructed pressure with an open sphere [Eq. (1)].

reconstructed pressure with an open sphere calculated using Eqs. (1) and (2). It is apparent that the open sphere technique gives erratic results at certain discrete frequencies because of the zeros in the denominator of Eq. (2). The two lowest frequencies where this problem occurs correspond to the first zeros of j_0 ($ka=\pi$) and j_1 ($ka\simeq 4.49$). By contrast, the rigid sphere gives stable results even at values of ka larger than 5.

The remaining results presented in this Letter have been determined using the rigid sphere technique. Figure 2 shows a typical result with a monopole, which again is 20 cm from the center of the sphere. Figure 2 compares the "true" and the reconstructed incident pressures at $ka=2$ along a line through the center of the sphere and the monopole. The reconstruction is very good inside the sphere and acceptable (within 1.5 dB of the true value) at a distance of up to 5 cm outside the sphere. At higher frequencies (not shown) the region with good reconstruction outside the sphere is reduced.

As mentioned in the foregoing there is a potential problem in the use of a solid sphere in spherical NAH: The sound

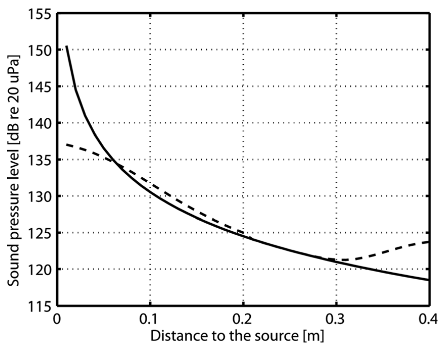

FIG. 2. Sound pressure level generated by a monopole along a line through the monopole and the center of the sphere. The source is 20 cm from the center of the sphere, and the frequency is 1.1 kHz ($ka=2$). Solid line, true pressure; dashed line, reconstructed incident pressure.

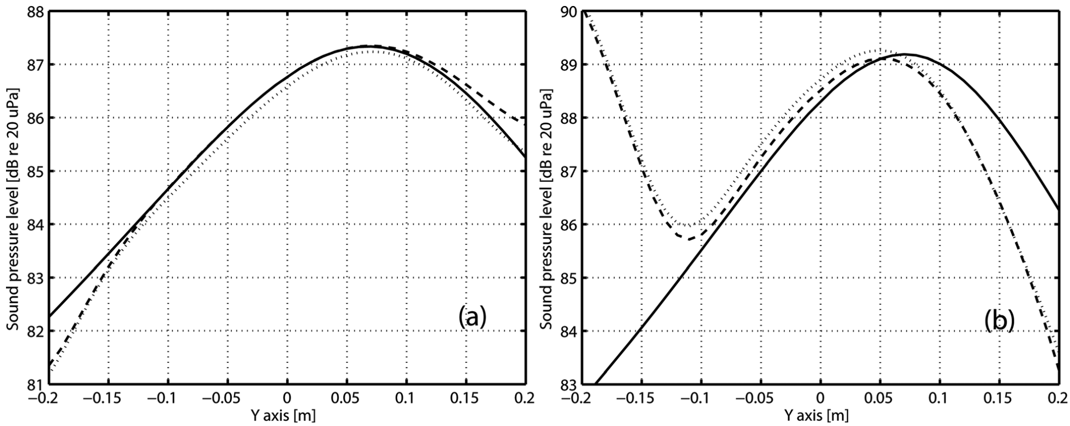

FIG. 3. Sound pressure level generated by a simulated vibrating panel in a baffle along a line parallel to the panel at $ka = 2$. The origin of the y axis is opposite the center of the panel. (a) Center of the sphere 20 cm from the panel; (b) center of the sphere is 15 cm from the panel. Solid line, true pressure; dashed line, reconstructed incident pressure without effects of back scattering from the sphere; dotted line, reconstructed incident pressure with backscattering taken into account.

field scattered back toward the source by the sphere may be reflected by the source, and thus the presence of the sphere may change the incident sound field. Obviously, the reflection depends on the shape and size of the source. A point driven simply supported panel mounted in an infinite baffle gives full reflections and might therefore be a suitable test case. Such a panel (a 5-mm-thick, simply supported steel plate with dimensions 20 × 20 cm) has been modeled with a conventional modal sum; and the sound field generated by the panel is calculated using a numerical approximation to Rayleigh's first integral,[6] i.e., the panel is replaced by a collection of monopoles with amplitudes and phase angles corresponding to the vibrational velocity. The reflections of the backscattered field have been taken into account by introducing an image sphere behind the panel. The image sphere scatters the sound emitted by the monopoles, and the measurement sphere is therefore exposed to the direct sound field and to the sound field scattered back from the image sphere.

Figure 3 shows some of the results for $ka = 2$. In Fig. 3(a) the center of the sphere is 20 cm from the panel, and in Fig. 3(b) it is 15 cm from the panel, which means that in the latter case the nearest point on the sphere is 5.25 cm from the panel. Figure 3 shows the true and reconstructed incident sound pressures along a line through the center of the sphere and parallel to the plate with and without taking the reflection of the backscattered pressure into account. As can be seen, the backscattered pressure has a very modest influence. Other results (not shown) confirm that the influence of the backscattered pressure is surprisingly small.

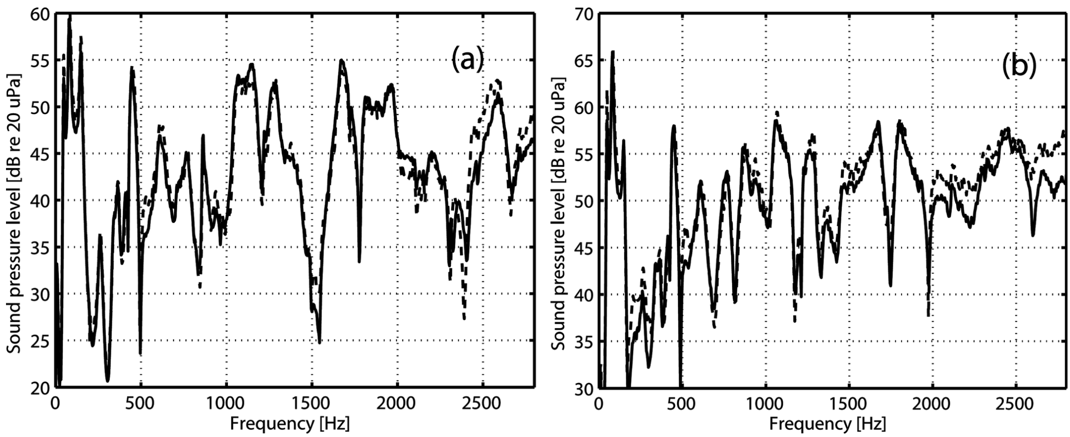

FIG. 4. Sound pressure level generated by a vibrating box. The nearest part of the sphere is 5.25 cm above the surface of the box. (a) Sound pressure at the center of the sphere; (b) sound pressure at the point on the sphere nearest the box. Solid line, true pressure (measured without the sphere); dashed line, reconstructed incident pressure.

IV. EXPERIMENTAL RESULTS

Some experiments have been carried out in a small anechoic room with a free space of about 60 m^3 and a lower limiting frequency of 100 Hz. The sphere corresponded to the one described in the foregoing simulations. The data acquisition was obtained using a multichannel "PULSE" analyzer produced by Brüel & Kjær (B&K, Nærum, Denmark). The true sound pressure was measured (without the sphere) with a B&K 4192 microphone.

Figure 4 shows the results of measuring near a complicated source, a box of dimensions 44 × 44 × 44 cm. The box was made of fiberboard, but the top surface was a 1-mm-thick aluminum plate driven by an inertial exciter. The spherical array was placed with its center 15 cm above the vibrating surface. Figure 4(a) shows the true and reconstructed pressures at the center of the sphere, and Fig. 4(b) shows a similar comparison at the point on the sphere nearest (5.25 cm above) the vibrating surface. At the center, the agreement is good in the entire frequency range up to 2.8 kHz; at the nearest point on the sphere the agreement is good up to 2 kHz and fair up to 2.8 kHz.

V. CONCLUSIONS

Spherical holography based on an array of microphones flush-mounted on a rigid sphere avoids the instability problem of spherical holography based on an open, acoustically transparent sphere. On the other hand, the sound pressure scattered back toward the source by the rigid sphere might be reflected by the source and thus change the incident sound field. However, both simulations and experimental results indicate that this is not a serious problem in practice. The results also indicate that acceptable results can be obtained inside the sphere and outside it at distances up to half the radius of the sphere at frequencies up to $ka = 2$. At frequencies between $ka = 2$ and the upper limiting frequency imposed by the truncation of the expansion in spherical harmonics, the region of acceptable reconstruction is limited to inside the sphere.

APPENDIX: POSITIONS AND WEIGHTS IN THE NUMERICAL INTEGRATION

The derivation of Eq. (4) for the spherical wave coefficients of the incident sound field has been based on application of the continuous orthogonality relation of the spherical harmonics on the measurement sphere,[6]

$$\int_0^{2\pi}\int_0^{\pi} Y_n^m(\theta,\varphi)Y_\nu^\mu(\theta,\varphi)^* \sin\theta\, d\theta\, d\varphi = \delta_{n\nu}\delta_{m\mu}. \qquad \text{(A1)}$$

A corresponding discrete orthogonality relation across the microphone locations was enforced during the design of the spherical array,

$$\sum_i \alpha_i Y_n^m(\theta_i,\varphi_i)Y_\nu^\mu(\theta_i,\varphi_i)^* = \delta_{n\nu}\delta_{m\mu} \quad \text{for} \quad \nu \le N, \quad n \le N. \qquad \text{(A2)}$$

Here, i is an index over microphone positions, (θ_i,φ_i) are the angular positions of the microphones, and α_i is a set of integration weights. The 50-element array design used throughout the present study is the result of an optimization in which the maximum weighted residual of Eq. (A2) with $N = 6$ was minimized. By application of large weights to all residuals corresponding to $N = 5$ in Eq. (A2), the equation could be fulfilled exactly with $N = 5$, and with very small residuals for n and/or ν equal to 6. In the optimization, a constraint was used to keep all microphones some minimum angular distance away from 12 camera positions. The output from the design optimization was the microphone positions and associated integration weights of Eq. (A2).

Using the discrete orthogonality, Eq. (A2), an expression for the spherical expansion coefficients of degree n up to $N = 5$ can be derived from Eq. (3) with $r = a$ by multiplication with the complex conjugate spherical harmonic function $Y_\nu^\mu(\theta_i,\varphi_i)^*$ followed by summation over all microphone positions. As a result, the following formula for spherical harmonics coefficients B_{mn} is obtained:

$$B_{mn} = \frac{\sum_i \alpha_i p_{\text{tot}}(a,\theta_i,\varphi_i)Y_n^m(\theta_i,\varphi_i)^*}{j_n(ka) - \dfrac{j_n'(ka)}{h_n'(ka)}h_n(ka)}. \qquad \text{(A3)}$$

The derivation assumes that the sound pressure on the rigid surface does not contain spherical harmonics components of degree n higher than N. This assumption will hold to a good approximation as long as ka is smaller than N.[6] As components of higher degree appear when ka increases, aliasing components will appear in coefficients obtained with Eq. (A3).

[1] J. J. Christensen and J. Hald, "Beamforming," Brüel & Kjær Tech. Rev. **1**, 1–48 (2004).

[2] M. Park and B. Rafaely, "Sound-field analysis by plane-wave decomposition using spherical microphone array," J. Acoust. Soc. Am. **118**, 3094–3103 (2005).

[3] J. Meyers and G. W. Elko, "A spherical microphone array for spatial sound recordings," J. Acoust. Soc. Am. **111**, 2346 (2002).

[4] E. G. Williams, N. Valdivia, and P. C. Herdic, "Volumetric acoustic vector intensity imager," J. Acoust. Soc. Am. **120**, 1887–1897 (2006).

[5] E. G. Williams and K. Takashima, "Vector intensity reconstructions in a volume surrounding a rigid spherical microphone array," J. Acoust. Soc. Am. **127**, 773–783 (2010). See Secs. 6.3 and 6.4.

[6] E. G. Williams, *Fourier Acoustics. Sound Radiation and Nearfield Acoustical Holography* (Academic Press, San Diego, 1999). See Secs. 2.10, 6.3, and 6.4.

[7] F. Jacobsen, G. Moreno, E. Fernandez Grande, and J. Hald, "Near field acoustic holography with microphones mounted on a rigid sphere," in *Proceedings of Inter-Noise 2008*, Shanghai, China, 2008.

Additional papers

Paper H

inter.noise 2010
noise and sustainability
13-16 June 2010 . Lisbon . Portugal
www.internoise2010.org

SEPARATION OF RADIATED SOUND FIELD COMPONENTS FROM WAVES SCATTERED BY A SOURCE UNDER NON-ANECHOIC CONDITIONS

Efren Fernandez Grande, Finn Jacobsen

Acoustic Technology. B. 352, Department of Electrical Engineering (Technical University of Denmark). 2800 Lyngby, Copenhagen, Denmark.
efg@elektro.dtu.dk , fja@elektro.dtu.dk

Abstract

A method of estimating the sound field radiated by a source under non-anechoic conditions has been examined. The method uses near field acoustic holography based on a combination of pressure and particle velocity measurements in a plane near the source for separating outgoing and ingoing wave components. The outgoing part of the sound field is composed of both radiated and scattered waves. The method compensates for the scattered components of the outgoing field on the basis of the boundary condition of the problem, exploiting the fact that the sound field is reconstructed very close to the source. Thus the radiated free-field component is estimated simultaneously with solving the inverse problem of reconstructing the sound field near the source. The method is particularly suited to cases in which the overall contribution of reflected sound in the measurement plane is significant.

Keywords: Near-field Acoustic Holography (NAH), sound field separation, sound radiation.

1 Introduction

In the original formulations of Near-field acoustic Holography (NAH) [1, 2], it is a requirement that all the sources are confined to one side of the microphone array. This requirement stems from the fact that it is not possible to determine whether the sound is coming from one or the other side of the array based on simple measurements of the sound pressure in one single plane. If the pressure in the measurement plane is contaminated by components coming from the other side, all the measured acoustic energy would be attributed to the primary source, leading to an erroneous reconstruction of the field [2–6].

Conventional NAH methods require that the measurement is performed under free-field conditions to avoid reflections from the source-free half space [3]. However, it is not always possible to perform the measurements under free-field conditions. This paper considers the case in which there is sound reflected from the source-free half space[1].

To minimize the influence of sound coming from the source-free half space separation techniques can be used. These techniques separate the outgoing sound field from the source and the incoming sound field from reflections or other sources. Some of these separation methods rely on a measurement of the field in two closely spaced parallel planes [7–11]. Other approaches are based on a combined measurement of the sound pressure and particle velocity of the field [12, 13]. The so called p-u method has been the subject of several research papers. It relies on the measurement of the pressure and particle velocity. It is a rather simple method that makes use of the fact that, unlike the pressure, the particle velocity is a vector that changes sign if the sound is coming from one or the other side of the array. Thus, by adding or subtracting the pressure and particle velocity based estimates of the sound field, the contribution of sound coming form each side of the array can be determined [13–16].

These techniques make it possible to estimate the outgoing field from the source, which is in general a good indicator of its acoustic radiation. However, the outgoing component of the sound field may be composed of both radiated and scattered waves by the source. The scattered sound propagates in the same direction as the radiated sound. It is therefore not trivial to separate the two components. Recently some techniques based on the Helmholtz integral formulation have been proposed to compensate for the scattered field and determine the free-field radiation by the source [17, 18].

This paper describes and examines a technique based on Statistically Optimized Near-field Acoustic Holography (SONAH) [3, 19, 20] and the p-u separation method for estimating the free field radiation by a source in the presence of reflections. The method compensates for the scattered component of the outgoing field based on the boundary conditions of the problem, and thus makes it possible to estimate the source's free field radiation.

2 Theoretical background

2.1 Statistically Optimized Near-field Acoustic Holography

The method examined in this paper is based on Statistically Optimized Near-field Acoustic Holography (SONAH). A detailed description of the SONAH method can be found in [20]. In SONAH, the measured sound field is expressed as a decomposition of plane elementary waves with different weightings. In matrix form it can be expressed as

$$\mathbf{p}(\mathbf{r}_h) = \mathbf{Bc}, \tag{1}$$

where $\mathbf{p}$ is a column vector with the measured pressures, $\mathbf{c}$ is a column vector with the n coefficients of the elementary functions, and $\mathbf{B}$ is a matrix with the elementary wave functions $\alpha(\mathbf{r}_{hm})$ at the measurement positions,

$$\alpha_n(\mathbf{r}) = e^{-j(k_{x,n}x + k_{y,n}y + k_{z,n}(z - z^+))}. \tag{2}$$

The regularized solution to the inversion of equation 1 is

$$\mathbf{c} = (\mathbf{B}^H\mathbf{B} + \lambda\mathbf{I})^{-1}\mathbf{B}^H\mathbf{p}(\mathbf{r}_h), \tag{3}$$

[1] For simplicity, the source-free half space will be also referred as the "wrong" side of the array

where λ is the regularization parameter. Once the coefficients are known, the sound field at each position of the reconstruction plane can be obtained as $p(\mathbf{r}_s) = \alpha(\mathbf{r}_s)\mathbf{c}$:

$$p(\mathbf{r}_s) = \alpha(\mathbf{r}_s)(\mathbf{B}^H\mathbf{B} + \lambda\mathbf{I})^{-1}\mathbf{B}^H\mathbf{p}(\mathbf{r}_h), \tag{4}$$

so that the sound pressure in the reconstruction plane can be expressed in terms of the measured pressure in the hologram plane. The reconstruction of the field can as well be done based on measurement of the particle velocity,

$$\mathbf{u}_z(\mathbf{r}_s) = \alpha(\mathbf{r}_s)(\mathbf{B}^H\mathbf{B} + \lambda\mathbf{I})^{-1}\mathbf{B}^H\mathbf{u}_z(\mathbf{r}_h). \tag{5}$$

The pressure can be estimated from the normal velocity making use of Euler's equation of motion,

$$p(\mathbf{r}_s) = \gamma(\mathbf{r}_s)(\mathbf{B}^H\mathbf{B} + \lambda\mathbf{I})^{-1}\mathbf{B}^H\mathbf{u}_z(\mathbf{r}_h), \tag{6}$$

where $\gamma(\mathbf{r}) = (-j\omega\rho)\int\alpha(\mathbf{r})dz$:

$$\gamma(\mathbf{r}) = \rho c\frac{k}{k_z}\alpha(\mathbf{r}). \tag{7}$$

In order to describe the separation method in a simple way it is convenient to introduce a simplified notation of SONAH, in which the acoustic quantities in the hologram and in the reconstruction plane are related through a transfer matrix that accounts for the propagation of the elementary waves in which the field is decomposed. This is expressed as

$$\mathbf{p}(\mathbf{r}_h) = \mathbf{C}_{pp}\mathbf{p}(\mathbf{r}_s),$$
$$\mathbf{u}_z(\mathbf{r}_h) = \mathbf{C}_{pu}\mathbf{p}(\mathbf{r}_s).$$

The matrix $\mathbf{C}_{pp}$ relates the pressure in the measurement plane to the pressure in the reconstruction plane and $\mathbf{C}_{pu}$ relates the pressure in the reconstruction plane with the particle velocity in the measurement plane. Based on this notation, the reconstruction equations can be expressed in a simple way. For instance, the pressure in the reconstruction plane is[2] $\mathbf{p}(\mathbf{r}_s) = \mathbf{C}_{pp}^{-1}\mathbf{p}(\mathbf{r}_h)$ or from the normal velocity $\mathbf{p}(\mathbf{r}_s) = \mathbf{C}_{pu}^{-1}\mathbf{u}(\mathbf{r}_h)$.

2.2 Sound field separation

In the sound field separation technique used in this investigation, it is assumed that the pressure measured in the hologram plane is due to a superposition of outgoing waves from the primary source and incoming waves corresponding to the reflected sound from the source-free half space. In the conventional formulation of SONAH, a single set of elementary wave functions is used to model the sound field radiated by the source. In this case, two sets of elementary wave functions must be used. The first set of elementary wave functions (α and γ) models the outgoing field from the primary source, and an additional set of functions models the incoming sound field. Let the new set of elementary functions be

$$\psi_n(\mathbf{r}) = e^{-j(k_{x,n}x + k_{y,n}y - k_{z,n}(z-z^-))}, \tag{8}$$

[2]Note that the inversion of the transfer matrices needs regularization

$$\vartheta(\mathbf{r}) = (-j\omega\rho) \int \psi(\mathbf{r}) dz. \tag{9}$$

The $\psi(\mathbf{r})$ wave functions are analogous to α, and they are used for pressure-to-pressure and velocity-to-velocity predictions. The $\vartheta(\mathbf{r})$ are analogous to γ, and they are used for estimating the sound pressure from the normal component of the particle velocity.

The sound filed separation presented here is only concerned with the sound pressure field, although an analogous methodology can be used to estimate the particle velocity field. The sound field measured in the hologram plane can be expressed as the contribution from the outgoing and incoming components as:

$$\mathbf{p}(\mathbf{r}_h) = \mathbf{C}_{ppo}\mathbf{p}_o(\mathbf{r}_s) + \mathbf{C}_{ppi}\mathbf{p}_i(\mathbf{r}_s), \tag{10}$$

$$\mathbf{u}_z(\mathbf{r}_h) = \mathbf{C}_{puo}\mathbf{p}_o(\mathbf{r}_s) - \mathbf{C}_{pui}\mathbf{p}_i(\mathbf{r}_s), \tag{11}$$

where the subscripts o and i of the transfer matrices indicate whether they refer to the outgoing or incoming fields, thus requiring the use of different elementary wave functions. The transfer matrices C_{ppo}, C_{puo}, use the outgoing elementary wave functions α and γ respectively, and the transfer matrices C_{ppi}, C_{pui}, use the incoming elementary wave functions ψ and ϑ , and $\mathbf{p}_o(\mathbf{r}_s)$ and $\mathbf{p}_i(\mathbf{r}_s)$ are the outgoing and incoming pressure fields at the reconstruction positions, which can be calculated from (10) and (11) as:

$$\mathbf{p}_o(\mathbf{r}_s) = \left(\mathbf{C}_{puo} + \mathbf{C}_{pui}\mathbf{C}_{ppi}^{-1}\mathbf{C}_{ppo}\right)^{-1} \left(\mathbf{u}_z(\mathbf{r}_h) + \mathbf{C}_{pui}\mathbf{C}_{ppi}^{-1}\mathbf{p}(\mathbf{r}_h)\right), \tag{12}$$

$$\mathbf{p}_i(\mathbf{r}_s) = \left(\mathbf{C}_{pui} + \mathbf{C}_{puo}\mathbf{C}_{ppo}^{-1}\mathbf{C}_{ppi}\right)^{-1} \left(\mathbf{C}_{puo}\mathbf{C}_{ppo}^{-1}\mathbf{p}(\mathbf{r}_h) - \mathbf{u}_z(\mathbf{r}_h)\right). \tag{13}$$

However, the outgoing field is composed of both radiated and scattered waves,

$$p_o(\mathbf{r}) = p_f(\mathbf{r}) + p_s(\mathbf{r}), \tag{14}$$

where $(p_f,\ u_{zf})$ is the free field sound radiated by the source, and $(p_s,\ u_{zs})$ is the scattered sound. If $\mathbf{r}_s$ is sufficiently close to the boundary of the source, and if the source can be regarded as rigid, the boundary conditions apply,

$$p_s(\mathbf{r}_s) = p_i(\mathbf{r}_s), \tag{15}$$

where p_s is the scattered sound pressure and p_i is the incident sound pressure. Making use of eqs. (14) and (15),

$$p_f(\mathbf{r}_s) = p_o(\mathbf{r}_s) - p_i(\mathbf{r}_s). \tag{16}$$

From equations (12), (13) and (16) the free field radiation by the source can be estimated as:

$$\begin{aligned}\mathbf{p}_f(\mathbf{r}_s) = &\left(\mathbf{C}_{puo} + \mathbf{C}_{pui}\mathbf{C}_{ppi}^{-1}\mathbf{C}_{ppo}\right)^{-1} \left(\mathbf{u}_z(\mathbf{r}_h) + \mathbf{C}_{pui}\mathbf{C}_{ppi}^{-1}\mathbf{p}(\mathbf{r}_h)\right) - \\ &\left(\mathbf{C}_{pui} + \mathbf{C}_{puo}\mathbf{C}_{ppo}^{-1}\mathbf{C}_{ppi}\right)^{-1} \left(\mathbf{C}_{puo}\mathbf{C}_{ppo}^{-1}\mathbf{p}(\mathbf{r}_h) - \mathbf{u}_z(\mathbf{r}_h)\right).\end{aligned} \tag{17}$$

3 Numerical results

The method has been tested by means of a numerical simulation study. The study consists of a simply supported baffled plate radiating in the presence of a disturbing monopole. The dimensions of the plate are 0.3 x 0.3 m, it is 3 mm thick, made of aluminum and driven at the center. The plate is centered at the origin of coordinates and the monopole is placed at (x=0,y=0.1,z=3) m. The sound from the monopole that is reflected by the baffle is modeled by means of a virtual source, assuming a perfect reflection ($R = 1$). The measurement aperture is 0.3 x 0.3 m, with a measurement grid of 11 x 11 positions uniformly spaced. The measurement plane is at $z_h = 4\ cm$, and the reconstruction plane at $z_s = 1\ cm$. The measurement noise corresponds to a signal-to-noise ratio (SNR) of 25 dB. Using the method described in the previous section, the free field radiation by the primary source (the baffled plate) can be estimated.

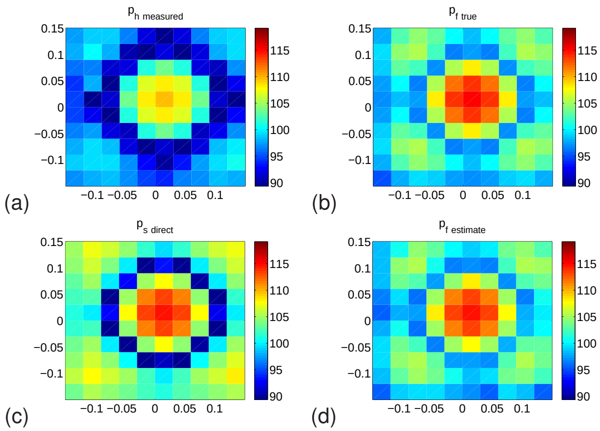

Figure 1 – Pressure field of a baffled plate driven at 850 Hz in the presence of a disturbing monopole radiating from the opposite side of the array. (a) Pressure in the hologram plane. (b) True free field pressure in the reconstruction plane. (c) Reconstruction with the direct formulation of SONAH. (d) Estimation of the free field with equation (17)

Figure 1 shows the pressure in the hologram plane, the true pressure in the reconstruction plane, the reconstruction with eq. (4) where no separation of the sound field is used, and finally the estimation of the free field pressure produced by the primary source using eq. (17).

Figure 2 shows a comparison between the direct reconstruction of the pressure field based in the direct SONAH formulation, and the estimated free field radiation based on eq. (17). It shows the reconstruction for two cases: one in which the influence of the disturbing monopole is strong (3 dB higher than the source), and another in which the pressure produced by the monopole in the measurement aperture is about 7 dB less than the one produced by the plate. It is apparent that the method can estimate the sound pressure successfully even if the the disturbance is not very strong. It should however be noted that this result is based in simulated measurements, in which the agreement between the reconstructions based on pressure and particle velocity is almost perfect.

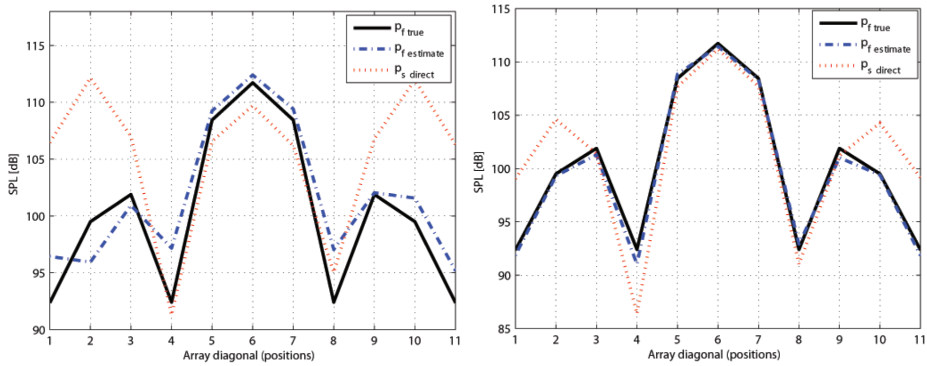

Figure 2 – Sound pressure level across the diagonal of a baffled plate driven at 850 Hz, radiating in the presence of a disturbing monopole at the opposite side of the array. True pressure, reconstructed pressure with eq. (17), and direct reconstruction with eq. (4) without separating the sound field. Left: the monopole radiation is 3 dB higher than the plate. Right: the monopole radiation is about 6 dB less than the plate.

4 Experimental results

An experimental study has been conducted to investigate the applicability of technique described in this paper. The experimental setup consists of a primary source radiating in the presence of a large reflecting panel. The primary source is a vibrating plate mounted on a rigid wooden box. The dimensions of the plate are $45 \times 45\ cm^2$, it is 3 mm thick, made of aluminum and driven acoustically by a loudspeaker inside the box. The origin of the coordinate system is at the bottom left corner of the plate. A large reflecting panel is positioned parallel to the plate, at $0.6\ m$ distance $(x, y, 0.6)\ m$, of dimensions $1.2 \times 1.5\ m$. The pressure and the normal component of the particle velocity were measured in 10×10 positions uniformly spaced $5\ cm$ from each other. The measurement aperture is thus $50 \times 50\ cm^2$, at $z_h = 6\ cm$, and the reconstruction plane at $z_s = 2\ cm$. The set-up of the experiment is sketched in Figure 3.

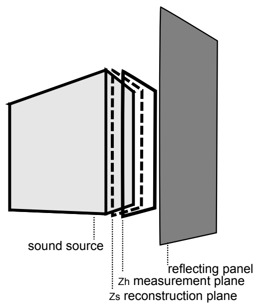

Figure 3 – Set-up of the measurement. The plate (primary source) is at $z = 0$, the hologram plane is at $z_h = 6$ cm, the reconstruction plane at $z_s = 2$ cm, and the reflecting panel at $z = 60$ cm

The pressure and the normal component of the particle velocity fields were measured in the hologram plane, both in the presence of the reflecting panel and without it. Also the true acoustic field radiated by the source was measured in the reconstruction plane under free field conditions, without the influence of the reflecting panel.

Figure 4 shows the measured pressure field in the hologram plane, the true pressure in the reconstruction plane, the reconstructed pressure without separating the sound field using eq. (4), and the estimation of the free field pressure produced by the primary source using eq. (17).

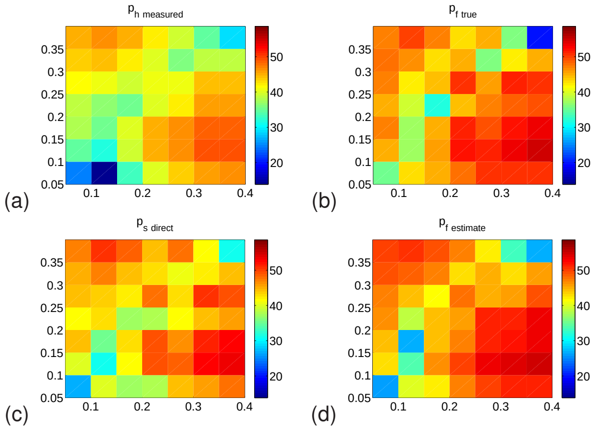

Figure 4 – SPL at 500 Hz of the primary source radiating in the presence of a reflecting panel. (a) Measured pressure in the hologram plane. (b) Measured free field pressure in the reconstruction plane. (c) Reconstruction with the direct formulation, equation (4) . (d) Estimation of the free field pressure with equation (17)

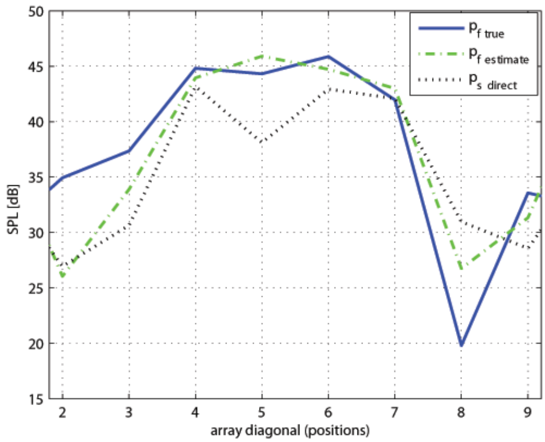

Figure 5 – SPL across the diagonal of the aperture at 500 Hz. The primary source is radiating in the presence of a reflecting panel at the opposite side of the array. True pressure, reconstructed pressure with eq. (17), and direct reconstruction with eq. (4) without separating the sound field.

Figure 5 shows the true pressure and the reconstructed pressures across the diagonal of the aperture at 500 Hz. It seems that it is somewhat more accurate to reconstruct the field using the free field estimation (eq. (17)), where the outgoing field is estimated and the scattered components compensated for, than the direct formulation (eq. (4)).

However, it should be remarked that there is a significant error associated with the estimation of the free field sound radiation using eq. (17). This mis-estimation is illustrated in Figure 6. The figure shows the reconstruction of the sound field in the case where there is no reflected sound from the opposite side of the primary source. Thus, the field measured in the hologram plane is only the one radiated by the source. The figure illustrates the error implicit in the method due to the fact that the pressure and particle velocity based estimates of the sound field are in practice not identical. Therefore, if there is just a small disturbance, or no disturbance at all from the side of the array opposite the primary source, it is consistently more accurate and straight forward to reconstruct the acoustic field based on the direct formulation.

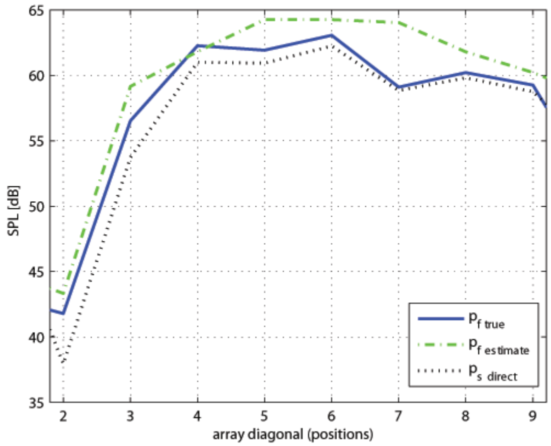

Figure 6 – True and reconstructed pressure with eq.(17) and eq.(4) when the primary source is radiating without the disturbance from any source or reflection from the opposite side of the array. SPL across the aperture diagonal at 400 Hz

5 Discussion

The study indicates that based on eq. (17), the sound pressure field radiated by the primary source can be estimated satisfactorily, particularly in the presence of extraneous noise from the opposite side of the array. However, there are limitations to the accuracy of the technique.

The method relies on the assumption that the sound pressure and particle velocity based estimates of the sound field are identical. This assumption is not completely true in practice, and there is an important source of error associated to it. Therefore, eq. (17) gives a more accurate reconstruction than eq. (4) provided that the disturbing sound is sufficiently strong. Otherwise, if the disturbance is not very significant, the latter yields a more accurate and straightforward reconstruction of the sound field. This result is in agreement with previous studies [14, 15]. This observation explains as well the accurate results obtained in the numerical study, since simulated measurements do obviously not suffer from the errors and uncertainty encountered in actual measurements.

It should also be noted that the set of elementary wave functions ψ used to model the incoming sound field (see eq. (8)) are scaled in the virtual plane z^-. This investigation revealed that the correct modeling of the incoming field depends strongly on the position of this virtual plane. Throughout the study, the best results were consistently found when the virtual plane was set at $z^- = 2z_h + z^+$.

6 Conclusion

A method of estimating the sound field radiated by a source under non-anechoic conditions has been described in this paper. A numerical and experimental study of the technique reveal that the technique can reconstruct the sound pressure field radiated by the primary source satisfactorily, particularly when there is a strong disturbance by sound coming from the wrong side of the array. If the disturbance is not very significant it is more accurate to reconstruct the sound field based on the conventional direct formulation.

References

[1] E. G. Williams. *Fourier Acoustics - Sound Radiation and Nearfield Acoustic Holography*. Academic Press, 1999.

[2] J. D. Maynard, E. G. Williams, and Y. Lee. Nearfield acoustic Holography I: Theory of generalized holography and the development of NAH. *J. Acoust. Soc. Am*, 78:1395–1413, 1985.

[3] J. Hald. Patch near-field acoustical holography using a new statistically optimal method. *Proceedings of Inter-Noise, Prague*, 2003.

[4] A. Sarkissian. Method of superposition applied to patch near-field acoustical holography. *J. Acoust. Soc. Am.*, 118:671ï£¡678, 2005.

[5] Z. Wang and Wu S. F. Helmholtz equation-least-squares method for reconstructing the acoustic pressure field. *J. Acoust. Soc. Am.*, 102:2020ï£¡2032, 1997.

[6] N. Valdivia and E. G. Williams. Approximations of inverse boundary element methods with partial measurements of the pressure field. *J. Acoust. Soc. Am.*, 123:109ï£¡120, 2008.

[7] G. V. Frisk, A. V. Oppenheim, and D. R. Martinez. A technique for measuring the plane-wave reflection coefficient of the ocean bottom. *J. Acoust. Soc. Am.*, 68:602–612, 1980.

[8] M. Tamura. Spatial Fourier transform method of measuring reflection coefficients at oblique incidence. I: Theory and numerical examples. *J. Acoust. Soc. Am.*, 88:2259–2264, 1990.

[9] Z. Hu and J. S. Bolton. The measurement of plane-wave reflection coefficients by using two-dimensional spatial transforms. *J. Acoust. Soc. Am.*, 88:S173, 1990.

[10] J. Hald. Patch holography in cabin environments using a two-layer hand held array with an extended SONAH algorithm. In *Proceedings of Euronoise*, Tampere, Finland, 2006.

[11] C. X. Bi, X. Z. Chen, and J. Chen. Sound field separation technique based on equivalent source method and its application in near field acoustic holography. *Sound And Vibration*, 123:1472–1478, 2008. doi: 10.1121/1.2837489.

[12] C.X. Bi and X.Z. Chen. Sound field separation technique based on equivalent source method using pressure-velocity measurements and its application in Nearfield Acoustic Holography. In *Proceedings of Internoise, Shanghai, China,*, Shangai, China, 2008.

[13] Y. B. Zhang, F. Jacobsen, C. X. Bi, and X. Z. Chen. Near field acoustic holography based on the equivalent source method and pressure-velocity transducers. *J. Acoust. Soc. Am.*, 126:1257–1263, 2009. doi: 10.1121/1.3179665.

[14] F. Jacobsen and V. Jaud. Statistically optimized near field acoustic holography using an array of pressure-velocity probes. *J. Acoust. Soc. Am.*, 121:1550–1558, 2007. doi: 10.1121/1.2434245.

[15] F. Jacobsen, X. Chen, and V. Jaud. A comparison of statistically optimized near field acoustic holography using single layer pressure-velocity measurements and using double layer pressure measurements (L). *J. Acoust. Soc. Am.*, 123:1842–1845, 2008. doi: 10.1121/1.2875308.

[16] Y. B. Zhang, X. Z. Chen, and F. Jacobsen. A sound field separation technique based on measurements with pressure-velocity probes (L). *J. Acoust. Soc. Am.*, 125:3518–3521, 2009. doi: 10.1121/1.3127128.

[17] C. Langrenne, M. Melon, and A. Garcia. Boundary element method for the acoustic characterization of a machine in bounded noisy environment. *J. Acoust. Soc. Am*, 121:2750–2757, 2007. doi: 10.1121/1.2713670.

[18] C. Langrenne, M. Melon, and A. Garcia. Measurement of confined acoustic sources using near-field acoustic holography. *J. Acoust. Soc. Am.*, 126:1250–1256, 2009. doi: 10.1121/1.3183594.

[19] R. Steiner and J. Hald. Near-field acoustical holography without the errors and limitations caused by the use of spatial dft. *Int. J. Acoust. Vib.*, 6:83–89, 2001.

[20] J. Hald. Basic theory and properties of statistically optimized near-field acoustical holography. *J. Acoust. Soc. Am*, 125:2105–2120, 2009. doi: 10.1121/1.3079773.

Paper I

inter•noise 2009
innovations in practical noise control
2009 August 23-26
Ottawa, Canada

Patch near-field acoustic holography: The influence of acoustic contributions from outside the source patch

Efren Fernandez Grande[a]
Finn Jacobsen[b]
Yong-Bin Zhang[c]
Acoustic Technology
Building 352, Elektro DTU (Technical University of Demark)
2800 Lyngby, Copenhagen, Denmark

ABSTRACT

It is a requirement of conventional Near-field Acoustic Holography that the measurement area covers the entire surface of the source. In the case of Patch Near-field Acoustic Holography (patch NAH), the measurement area can be reduced to cover only a specific area of the source which is of particular interest (known as the "patch" or "source patch"). The area of the source beyond this patch is not of interest in the analysis. However, its acoustic output may nevertheless contribute to the total sound field in the measurement plane, and influence the reconstruction of the field close to the patch. The purpose of this paper is to investigate how the acoustic radiation from outside the patch area influences the reconstruction of the sound field close to the source. The reconstruction is based on simulated measurements of sound pressure and particle velocity.

The methods used in this paper are the Statistically Optimized NAH (SONAH) and the Equivalent source Method (ESM), also known as the Wave Superposition Method. Particular attention is drawn to how the equivalent sources in the ESM could be distributed in order to achieve an acceptable reconstruction of the sound field. It has been shown that an acceptable reconstruction of the normal velocity can be achieved if the contributions from beyond the patch area are accounted for.

1. INTRODUCTION

Near-field acoustical holography (NAH) provides a reconstruction of the sound field in the space close to the source, based on the measurement of the radiated field on a two dimensional surface.[1,2] The measurements are typically performed with an array of transducers (microphones or

[a] Email address: efg@elektro.dtu.dk
[b] Email address: fja@elektro.dtu.dk
[c] Email address: zybmy1997@163.com

particle velocity transducers) covering an area that should extend well beyond the source, so that the sound field has decayed sufficiently.[3-7] Patch Near-field Acoustical Holography (Patch NAH) deals with the case where the reconstruction area (the source or reconstruction patch) covers only a part of the source.[8-11] However, if the area of the source is greater than the patch, it may happen that the source outside of the patch contributes to the sound field on the measurement area, and therefore influences the reconstruction of the field inside the source patch. In other words, there might be a contribution from the area of the source which is outside of the patch.

It is well known that the normal component of the particle velocity decays faster than the pressure with the distance to a region with local radiation of sound. Previous studies have shown that, due to this phenomenon, NAH based on particle velocity measurements has the advantage of minimizing the error introduced by the finite measurement window (and other advantages related to the ill-posed nature of the problem).[6-7] Similar advantages can be expected for Patch NAH, since the normal velocity of the region outside of the patch is expected to decay faster towards the patch region than the pressure and therefore have a smaller influence on the reconstruction near the source patch. Therefore, in this specific study, it could be advantageous to base the reconstruction of the sound field on particle velocity measurements.

There are different methods than can be used for Patch NAH, such as the Statistically Optimized Near-field Acoustic Holography (SONAH),[12-14] the Equivalent Source Method (ESM), also known as the Superposition Method,[15-16] and the Fourier based NAH[1-5] (which would require an extrapolation of the measured field).[8,17] This paper focuses mainly on the ESM. The SONAH method will also be used as a reference for comparison, due to its applicability to the specific case.

2. BRIEF THEORETICAL BACKGROUND

The SONAH method is based on an elementary wave expansion in separable coordinates (in this case Cartesian coordinates). Once the acoustic field is known at the measurement positions, it can be expressed as an expansion of plane waves with different weights. Based on this expansion, the sound field can be calculated at the reconstruction plane z_S. The detailed formulation can be found in references 12-13.

The fundamental idea behind the equivalent source method (ESM) is to model the radiated sound field as if it were produced by a combination j of monopoles placed at set of positions $\boldsymbol{r}_j$ with strengths q_j:

$$p(\mathbf{r}) = \sum_j q_j G(\mathbf{r}, \mathbf{r_j}) \tag{1}$$

where $G(\boldsymbol{r},\boldsymbol{r}_j)$ is the Green's function from each source $\mathbf{r_j}$ to the field point $\mathbf{r}$. The strength of each equivalent source can be determined based on the measurement data at $\mathbf{r_h}$, since the pressure $p(\mathbf{r_h})$ at the measurement positions is known. Once the strengths (q_j) of the equivalent sources are known, it is trivial to calculate the pressure or particle velocity at any other arbitrary position. In a similar fashion, the strengths of the equivalent sources can as well be calculated based on the measurement of the particle velocity, and then calculate as well the pressure and particle velocity at any other arbitrary position. The detailed formulation can be found in references 15 and 16.

3. METHODOLOGY

The investigation presented in this paper is based on computer simulations. A simply supported plate is used as a source. A monopole source is used to simulate the effect of sound coming from outside of the source patch (but still in the source region). The setup of the test case is sketched in figure 1.

The plate used is 0.6 x 0.6 m, aluminium, driven at the centre, at a frequency of 800 Hz, simply supported and centred at the origin of coordinates. The measurement area is also 0.6 x 0.6 m placed 10 cm away from the source (z_h = 0.1 m). The array consists of 16 x 16 transducers with a spacing 4 cm between each. The reconstruction area is a concentric area to the measurement at 3 cm distance from the source (z_s = 0.03 m). The disturbing monopole source is placed at coordinates (x = 0, y = -0.6, z = 0).

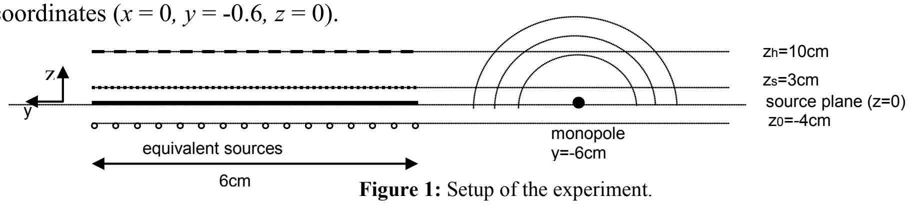

Figure 1: Setup of the experiment.

The effect of the monopole can be described by the signal-to-"noise" ratio of the pressure produced by the plate relative to the pressure produced by the monopole:

$$SNR_m = 10\log_{10}\frac{|p_{plate}|^2}{|p_{monopole}|^2} \tag{2}$$

In the present study, this signal-to-noise ratio varies from 50 dB, where the influence of the monopole is neglible, to -2 dB, where the overall pressure generated by the monopole is greater than the one generated by the plate. In addition to the noise introduced by the monopole, random noise of SNR = 40 dB is included in the simulations.

The error in the reconstructions is defined as:

$$Error(\%) = \frac{||p_s - p_{true}||_2^2}{||p_{true}||_2^2} \times 100 \tag{3}$$

4. THE POSITIONS OF THE EQUIVALENT SOURCES

In the ESM, the positions of the equivalent sources are essential, and they can influence to a great extent the accuracy of the reconstruction. The equivalent sources should be placed behind the actual source, and distributed over a space so that they can represent the radiated sound field properly.

If the radiated sound is coming only from the source patch, it is a good solution to place the sources just behind the patch. However, if there are significant acoustic contributions from outside the patch (as in this case), such a distribution of sources is not a good choice, because the equivalent sources may fail to model the contribution from outside the patch. In the present investigation, the equivalent sources should be placed in such a way that they can describe the contribution of the monopole placed outside of the patch (see Figure 1).

Four different equivalent source distributions have been investigated. In the first one, the equivalent sources are only placed behind the patch. In the second distribution, the equivalent sources surround the source patch, so that any sound from the source region but coming from outside the patch can be modelled to some extent. There are as many sources as measurement positions. The third distribution is similar to the second, but there are more equivalent sources than measurement positions (the system is underdetermined). In the last distribution, the equivalent sources are extended well beyond the patch area, so that they can model a greater region and include radiation from sources outside of the patch. The meshes are sketched in Figure 2.

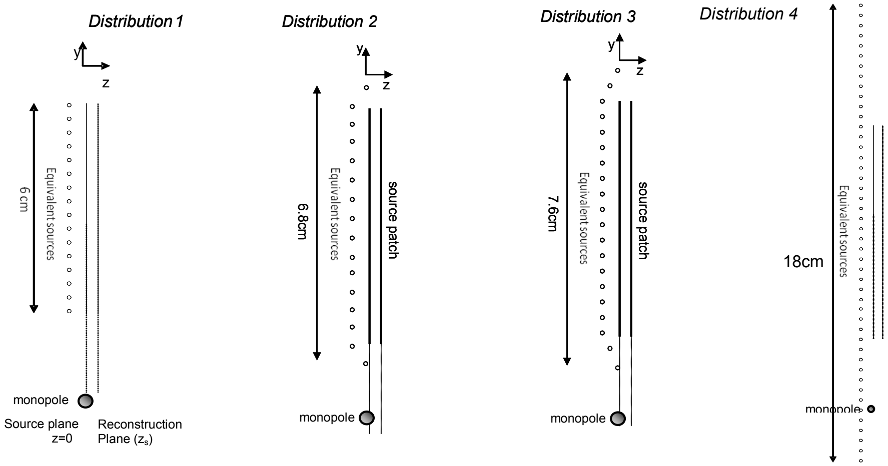

Figure 2: Four different distributions of equivalent sources: Just behind the patch (distr. 1); surrounding the patch (distr. 2 and 3) ; extended beyond the area of the source patch (distr. 4). Note that distribution 4 has been scaled down

5. RESULTS

Using the setup described in section 3, different cases have been studied. First, sound pressure and velocity are reconstructed for the case where the plate is radiating without contributions from outside of the patch. Then, the influence of noise coming from outside of the patch is studied, and the performance of the different equivalent source distributions is evaluated. The reconstruction is done at 800 Hz frequency.

A. Vibrating plate

The reconstruction based on the pressure and on the normal velocity of a point driven plate using the ESM is shown in Figure 3. The patch area covers the source, and there are no additional contributions from outside of the patch (all the radiation is from the plate). The SONAH and the ESM methods yield very similar results.

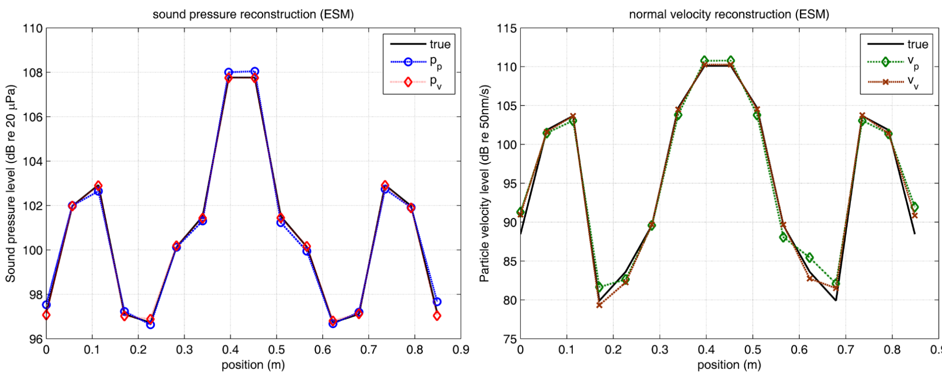

Figure 3: ESM reconstruction of the sound pressure level (left) and normal particle velocity (right) of a vibrating simply supported plate. The quantities are plotted across a diagonal of the array. The quantities are reconstructed based on measurements of both the sound pressure (p_p;v_p) and the particle velocity (p_v;v_v).

The reconstruction is very good in any case, and both the normal particle velocity and the sound pressure can be reconstructed quite accurately. The greater deviation happens when the normal velocity is reconstructed based on sound pressure measurements.

In this case, the noise level is SNR = 40 dB. If the noise is increased to SNR = 30 dB, the reconstruction becomes slightly worse, especially for the pressure based reconstruction of the normal velocity. These results are in agreement with refs. 6 and 7.

B. Error in the presence of a disturbing monopole source

If there is a contribution to the sound field from a source area external to the patch (in this case a monopole), the reconstruction conditions become much more demanding and the reconstruction error increases. Figure 4 shows the reconstruction error in the presence of a disturbing monopole placed outside of the patch. The radiation of the monopole is increased so that the signal-to-noise ratio (SNR_{mon}) ranges from 50 to -2 dB (see sect. 3).

Both the SONAH and the ESM methods have been used. It is important to note that for the ESM, the equivalent sources have been placed only behind the patch – distribution 1 (figure 2).

The setup of the experiment is particularly favourable for the SONAH method, due to the fact that the source is of planar geometry and the monopole source is on the same plane as the plate. Thus, the elementary waves can account more easily for the influence of the monopole.

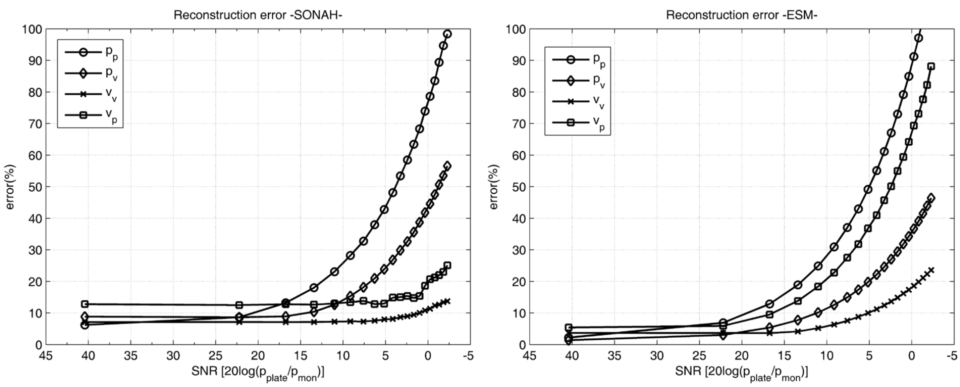

Figure 4: Reconstruction error (%) for SONAH (left) and ESM (right) under the influence of a disturbing monopole outside of the patch. The quantities are pressure and normal velocity based on pressure measurements (p_p and v_p) and based on particle velocity measurements (p_v and v_v).

In any case, the error for the sound pressure reconstruction is very high, regardless of whether it is based on sound pressure or particle velocity measurements. This is because the actual sound pressure field in both the measurement and the reconstruction plane is severely disturbed by the monopole contribution, thus yields a significant reconstruction error. On the other hand, the normal velocity field in the patch is less disturbed, because the normal component of the particle velocity of the monopole has decayed significantly in the patch region.

From Figure 4b, it is apparent that the equivalent source distribution used for the ESM fails to model the sound produced by the monopole. This yields a high reconstruction error, especially for reconstruction based on sound pressure measurements (not so bad for the reconstruction based on the normal velocity, since the field is anyway local).

It is apparent from this results that it is essential to investigate the performance of alternative equivalent source distributions to achieve a more accurate reconstruction using ESM.

C. Alternative equivalent source distributions for ESM

In this section, the performance of the equivalent source distributions proposed in section 4 is investigated. These distributions attempt to model the contribution from the disturbing monopole outside of the patch, by: a) surrounding the patch with sources that can more or less describe the sound field external to it (distributions 2 and 3), and b) extending the equivalent sources throughout an area well beyond the source patch (distribution 4). The reconstruction error for the four different distributions is shown in Figure 5.

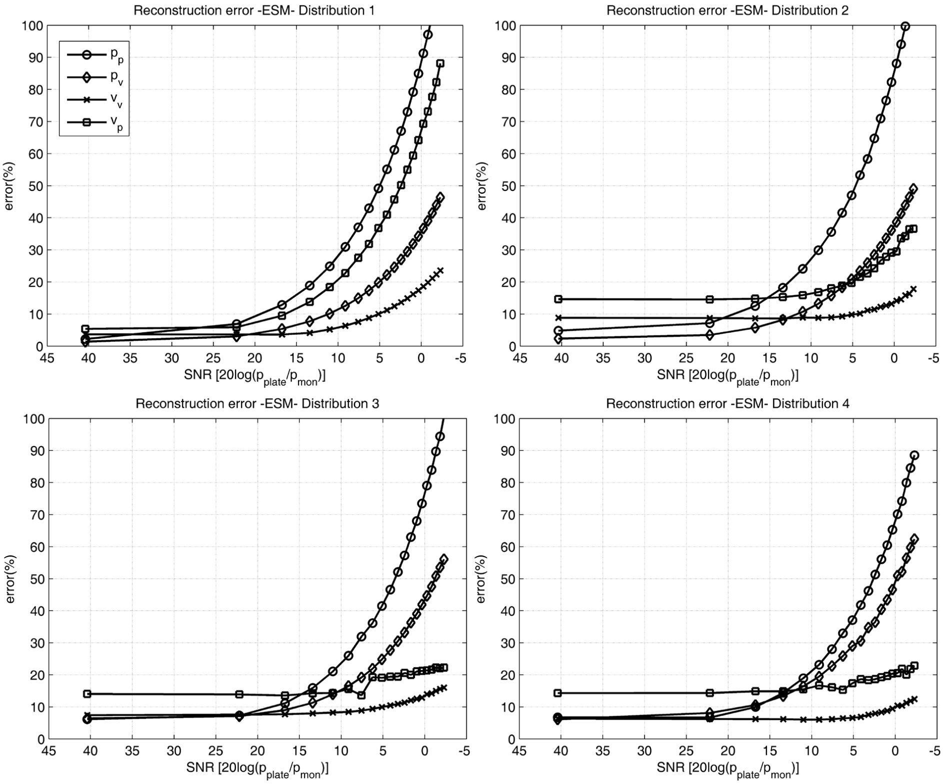

Figure 5: Reconstruction error using the ESM for different distribution of equivalent sources, under the influence of a disturbing monopole outside of the patch. Distribution 1 (top left); Distribution 2 (top right); Distribution 3 (bottom left); Distribution 4 (bottom right)

It is clear from Figure 5 that as soon as the contribution of the monopole is modelled, the error decreases considerably, especially for the reconstruction of the normal velocity based on the sound pressure. This is because the disturbance from the monopole is now accounted for by the additional equivalent sources and the plate's radiation can be better described without the influence of the monopole contribution.

It seems that when the influence of the monopole is severe, extending the equivalent sources beyond the patch (distribution 4) is very favourable. However, the results achieved by surrounding the source with equivalent sources are also good (distributions 2 and 3), with the additional advantage that they are more economical (less equivalent sources, and less knowledge about the position of the disturbing sources is required).

On the other hand, when the influence of the monopole is small (SNR_{mon} < 30 dB), the least error in the reconstruction is achieved by placing the equivalent sources just behind the source patch (distribution 1). Thus, if there is no significant contribution from outside of the patch, it is unnecessary to extend the equivalent sources beyond the patch area (furthermore, it has a negative influence on the reconstruction of the sound field in the source patch).

Figure 6 illustrates how the extended mesh models the monopole source when SNR_{mon} = 0 dB. It shows the strength of the equivalent sources for the reconstruction based on sound pressure and normal velocity measurements. It is apparent how in the case of the normal velocity the influence of the monopole is underestimated. This illustrates how in normal velocity based reconstruction there is not a significant advantage in extending the distribution of equivalent sources.

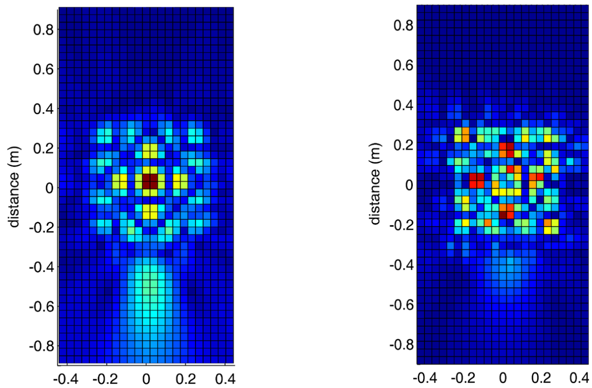

Figure 6: Strength of the equivalent sources in the presence of a disturbing monopole ($SNR_{monopole}$ = 0) for distribution 4. Pressure based reconstruction (left) normal velocity based reconstruction (right)

Figure 7 shows the reconstruction of the sound pressure and normal particle velocity when SNR_{mon} = 0 dB (the pressure produced by the monopole at the measurement positions is as high as the pressure produced by the plate).

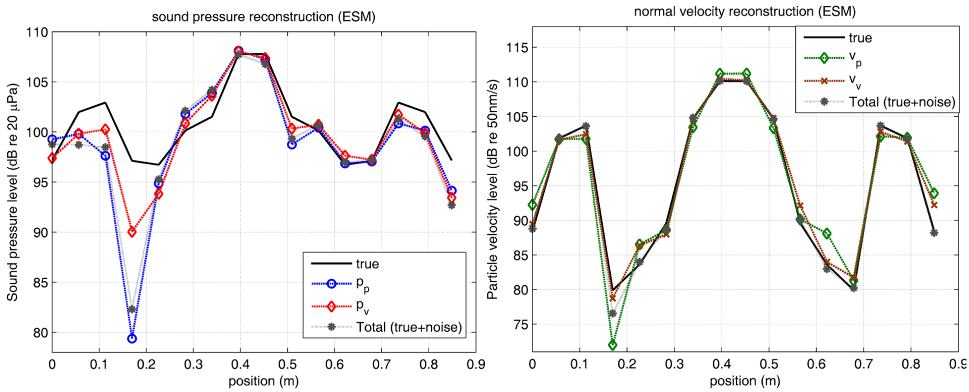

Figure 7: ESM reconstruction of the sound pressure level (left) and normal particle velocity (right) of a vibrating simply supported plate in the presence of a disturbing monopole (SNR = 0 dB). The quantities are plotted across the diagonal of the array. The quantities are both based in measurements of both the sound pressure (p_p;v_p) and in measurements of the particle velocity (p_v;v_v). The total sound field in the reconstruction plane is also shown

In Figure 7(a) it is apparent how the true pressure (produced by the plate) differs very much from the total pressure (from the plate and the monopole). It is also apparent how the reconstruction based on pressure measurements tends to reconstruct the total pressure field. On the other hand, the normal velocity field (Figure 7(b)) is much less influenced by the disturbing source, and the total normal velocity field is almost produced only by the plate. Thus, it becomes clear how the reconstruction based on the normal velocity (p_v) is less influenced by the disturbing source.

6. DISCUSSION

In the presence of disturbing sound from the source region beyond the patch, it is possible to achieve an acceptable reconstruction of the normal component of the particle velocity on the source patch. The reconstruction has been found to be better if it is based on the measurement of the particle velocity rather than on the sound pressure. These results agree with previous investigations of NAH based on particle velocity measurements.[6,7] On the other hand, the reconstruction of the sound pressure yields a high error when there are strong contributions from beyond the patch (above 15 dB SNR), no matter whether it is based on the sound pressure or the particle velocity. The reason for this is that the pressure field is significantly influenced by the disturbing field by the monopole, and there is a strong bias in the reconstruction. However, the error for the velocity based reconstruction was slightly lower than for the pressure based reconstruction. These results are not surprising if we consider that the influence of the normal velocity from the disturbing sources in the measurement and reconstruction areas is much smaller than the disturbance of the sound pressure.

Particular attention should be given to finding a good equivalent source distribution for the ESM that performs satisfactorily under the given conditions. For that purpose, it is essential to model the contributions coming from beyond the patch area. It has been found that a good way to model these contributions is to surround the patch with equivalent sources or to extend the equivalent source distribution beyond the patch (without increasing the measurement points). These distributions provide a satisfactory reconstruction of the particle velocity. The improvement is very significant for the pressure based reconstruction of the normal velocity. The reconstruction based on the particle velocity is not so much affected.

On the other hand, the distribution of equivalent sources should be adjusted depending on the specific sound field. If there is not a significant contribution from beyond the patch area, extending the equivalent sources beyond the patch does not improve the reconstruction of the sound field. In this case the additional equivalent sources do not contain relevant information about the sound field, and they have a negative influence on the reconstruction. It is thus preferable to distribute the sound sources just behind the patch.

7. CONCLUSIONS

In Patch NAH, the normal velocity can be reconstructed satisfactorily even if there is a strong disturbance from the source area beyond the patch. However, to achieve a proper reconstruction it is essential to account for the acoustic contribution from beyond the patch area. This requirement is particularly important for the pressure based reconstruction of the normal velocity. If this requirement is not fulfilled, the reconstruction error is very severe. On the other hand, if the reconstruction is based on the measurement of the particle velocity the error is low, even if the contributions from beyond the patch are not modelled. On the whole, in the presence of disturbing sound from the source area beyond the patch, velocity based reconstructions were found to be more accurate than sound pressure based reconstructions.

REFERENCES

[1] E. G. Williams, "Fourier Acoustics – Sound Radiation and Nearfield Acoustical Holograpgy" (Academic Press, London, 1999).

[2] E. G. Williams, J. D. Maynard, & E. Skudrzyk. "Sound source reconstructions using a microphone array," J. Acoust. Soc. Am. 68, 340-344 (1980).

[3] J. D. Maynard, E. G. Williams, and Y. Lee, "Nearfield acoustic holography: I. Theory of generalized holography and development of NAH," J. Acoust. Soc. Am. 78, 1395-1413 (1985).

[4] W. A. Veronesi and J. D. Maynard, "Nearfield acoustic holography (NAH): II. Holographic reconstruction algorithms and computer implementation," J. Acoust. Soc. Am. 81, 1307-1322 (1987).

[5] E. G. Williams, H. D. Dardy, and K. B. Washburn, "Generalized nearfield acoustical holography for cylindrical geometry: Theory and experiment," J. Acoust. Soc. Am. 81, 389-407 (1987).

[6] F. Jacobsen and Y. Liu, "Near field acoustic holography with particle velocity transducers," J. Acoust. Soc. Am. 118, 3139–3144 (2005).

[7] F. Jacobsen and V. Jaud, "Statistically optimized near field acoustic holography using an array of pressure-velocity probe," J. Acoust. Soc. Am. 121, 1550–1558 (2007).

[8] E. G. Williams, B. H. Houston, & P. C. Herdic. "Fast Fourier transform and singular value decomposition formulations for patch nearfield acoustical holography," J. Acoust. Soc. Am. 114, 1322-1333 (2003)

[9] A. Sarkissian, "Method of superposition applied to patch near-field acoustic holography," J. Acoust. Soc. Am. 118, 671-678 (2005).

[10] J. Hald, ''Planar near-field acoustical holography with arrays smaller than the sound source,'' Proceedings of the 17th International Congress on Acoustics, Rome, Italy, Vol. I, part A (2001)

[11] K. Saijyou and S. Yoshikawa, ''Reduction methods of the reconstruction error for large-scale implementation of near-field acoustical holography,'' J. Acoust. Soc. Am. 110, 2007–2023 (2001).

[12] J. Hald, "Basic theory and properties of statistically optimized near-field acoustical holography," J. Acoust. Soc. Am. 125, 2105-2120 (2009)

[13] R. Steiner and J. Hald, "Near-field acoustical holography without the errors and limitations caused by the use of spatial DFT," Int. J. Acoust. Vib. 6, 83-89 (2001).

[14] Y. T. Cho, J. S. Bolton, and J. Hald, "Source visualization by using statistically optimized nearfield acoustical holography in cylindrical coordinates," J. Acoust. Soc. Am. 118, 2355-2364 (2005).

[15] A. Sarkissian, "Method of superposition applied to patch near-field holography," J.Acoust. Soc. Am. 118 671-678 (2005).

[16] N. Valdivia and E. G. Williams, "Study of the comparison of the methods of equivalent sources and boundary element methods for near-field acoustic holography," J. Acoust. Soc. Am. 120 3694-3705 (2006).

[17] E. G. Williams, "Continuation of acoustic near-fields," J. Acoust. Soc. Am. 113, 1273-1281 (2003).

Three-dimensional supersonic intensity

1 Introduction

This note proposes a generalization of the supersonic intensity to a free-field three-dimensional space. The supersonic acoustic intensity has been formulated so far for two-dimensional surfaces in planar and cylindrical coordinates, which are indeed suitable for application to many acoustic sources. This preliminary study proposes a formulation of the supersonic intensity in a general 3-D free-field. In general lines, a form of the radiation filter-mask, or radiation kernel, is determined that would make it possible to calculate the supersonic intensity over the 3-D space.

2 Theory

Given a sound field over a three-dimensional space, it can be expressed as a (inverse) Fourier transform,

$$p(x,y,z) = \frac{1}{8\pi^3} \iiint_{-\infty}^{\infty} P(k_x,k_y,k_z) e^{-j(k_x x + k_y y + k_z z)} dk_x dk_y dk_z, \qquad \text{(A.1)}$$

where $P(k_x, k_y, k_z)$ is the angular spectrum in Cartesian coordinates. Typically in acoustic holography, only two of the three wavenumber components need to be explicitly determined, since the third is naturally related through the wavelength in the medium ($k^2 = k_x^2 + k_y^2 + k_z^2$).

In three dimensions, the sound pressure (or particle velocity) that is radiated into the far field can be expressed as:

$$p^{(s)}(x, y, z) = p(x, y, z) *** h^{(s)}(x, y, z), \tag{A.2}$$

where the operator $***$ denotes a three-dimensional convolution. Given a three-dimensional Fourier transform, the convolution theorem between a function $p(x, y, z)$ and another $h^{(s)}(x, y, z)$ applies, and equation (A.2) can be expressed as,

$$p^{(s)}(x, y, z) = \frac{1}{8\pi^3} \iiint_{-\infty}^{\infty} P(k_x, k_y, k_z) H^{(s)}(k_x, k_y, k_z) e^{-j(k_x x + k_y y + k_z z)} dk_x dk_y dk_z, \tag{A.3}$$

where $H^{(s)}(k_x, k_y, k_z)$ is a frequency domain filter, that corresponds to the 'radiation circle' in three dimensions. This wavenumber domain filter $H^{(s)}(\mathbf{k}_r)$ is a sphere in the wavenumber domain that satisfies

$$H^{(s)}(k_x, k_y, k_z) = \begin{cases} 1 & \text{if } (k_x \leq k) \cup (k_y \leq k) \cup (k_z \leq k) \\ 0 & \text{if } (k_x > k) \cap (k_y > k) \cap (k_z > k). \end{cases} \tag{A.4}$$

This definition might appear redundant, because it is just a projection of the radiation circle into the third dimension k_z with radius k. Essentially, all acoustic waves satisfy the condition $k^2 = k_x^2 + k_y^2 + k_z^2$, and any pair of coordinates of propagating waves satisfies $(k_\alpha^2 + k_\beta^2) < k^2$. Thus all the propagating waves "lie" on the surface of the sphere of radius k in the wavenumber domain. This step is however, necessary for the derivation that follows.

Equation (A.3) is a three-dimensional filtering process where the evanescent waves are discarded, and only the propagating waves remain. In order to calculate the three-dimensional radiation kernel $h^{(s)}(\mathbf{r})$, it is necessary to inverse Fourier transform the three-dimensional radiation filter $H^{(s)}(k_x, k_y, k_z)$ back into space domain,

$$h^{(s)}(x, y, z) = \frac{1}{8\pi^3} \iiint_{-\infty}^{\infty} H^{(s)}(k_x, k_y, k_z) e^{-j(k_x x + k_y y + k_z z)} dk_x dk_y dk_z. \tag{A.5}$$

Given the spherical symmetry of the problem, it is convenient to transform into spherical coordinates, and expand the terms into the corresponding set of radial and angular orthogonal functions, namely spherical Bessel and spherical harmonics.

The three-dimensional radiation filter can be expanded into spherical harmonics as,

$$H^{(s)}(k_r, k_\phi, k_\theta) = \sum_{m=0}^{\infty} \sum_{n=-m}^{m} H_m^n(k_r) Y_m^n(k_\phi, k_\theta). \tag{A.6}$$

Multiplying by $Y_m^n(k_\phi, k_\theta)^*$ and integrating over k_θ and k_ϕ, making use of the orthogonality of the functions, the radial coefficients of the expansion are

$$H_m^n(k_r) = \int_0^{2\pi} \int_0^{\pi} H(k_r, k_\phi, k_\theta) Y_m^n(k_\phi, k_\theta)^* \sin(k_\theta) dk_\theta dk_\phi. \tag{A.7}$$

On the other hand, the Fourier kernel is expressed in a spherical harmonic expansion as

$$e^{-j(k_x x + k_y y + k_z z)} = 4\pi \sum_{m=0}^{\infty} \sum_{n=-m}^{m} (-j)^m j_m(k_r r) Y_m^n(\phi, \theta)^* Y_m^n(k_\phi, k_\theta). \tag{A.8}$$

Inserting these last equations into Eq. (A.5), yields

$$\begin{aligned} h^{(s)}(\vec{r}) = \frac{1}{2\pi^2} \iiint & \sum_{k=0}^{\infty} \sum_{l=-k}^{k} H_k^l(k_r) Y_k^l(k_\phi, k_\theta)^* \\ & \times \sum_{m=0}^{\infty} \sum_{n=-m}^{m} (-j)^m j_m(k_r r) Y_m^n(\phi, \theta)^* Y_m^n(k_\phi, k_\theta) d\Omega, \end{aligned} \tag{A.9}$$

where $d\Omega = k_r^2 \sin k_\theta dk_r dk_\theta dk_\phi$. Making use again of the orthogonality of the spherical harmonics yields,

$$h^{(s)}(\vec{r}) = \frac{1}{2\pi^2} \int_0^{\infty} \sum_{m=0}^{\infty} \sum_{n=-m}^{m} H_m^n(k_r) (-j)^m j_m(k_r r) Y_m^n(\phi, \theta)^* k_r^2 dk_r. \tag{A.10}$$

Because the wavenumber filter $H^{(s)}(k_r, k_\phi, k_\theta)$ is rotationally symmetric, its expansion is only a function of the zeroth order term. Additionally, the radial function of the wavenumber filter is unity if $k_r \leq k$, and it is zero otherwise. This results in

$$h^{(s)}(r) = \frac{1}{2\pi^2} \int_0^{k} j_0(k_r r) k_r^2 dk_r. \tag{A.11}$$

To evaluate the integral, the relation $\int z^2 j_0(z) dz = z^2 j_1(z)$ is used (see chap. 10 of ref. [145]), or alternatively one can integrate over the sinusoidal functions that define the spherical Bessel functions, to arrive to

$$h^{(s)}(r) = \frac{k^2}{2\pi^2 r} j_1(kr), \tag{A.12}$$

which is the three-dimensional filter mask in space domain that we wanted to determine. Based on this filter mask, the propagating terms of any given sound field can be calculated via a three-dimensional convolution.

This study is nevertheless preliminary and requires further examination and validation.

Supersonic intensity and irrotational active intensity

This appendix considers briefly a possible relation between the supersonic intensity and the zero-curl component of the acoustic intensity vector, the so-called irrotational acoustic intensity.

1 Irrotational active intensity

The irrotational intensity is the component of the active sound intensity vector that has zero curl. Based on the Helmholtz decomposition, the sound intensity vector can be decomposed into a rotational and a solenoidal component. The rotational component corresponds to the active sound intensity, and the solenoidal part to the reactive sound intensity [135]. Additionally, the active sound intensity can be decomposed further into a zero-curl (irrotational) component, and a nonzero-curl (rotational) component:

$$\mathbf{I} = \nabla \times \mathbf{A} = \nabla\beta + \nabla \times \phi, \tag{A.13}$$

where the 'irrotational' zero-curl component is $\nabla\beta$ and the 'rotational' non-zero curl component is $\nabla \times \phi$.

It has been discussed throughout the dissertation that the active component of the sound intensity describes the flow of acoustic energy. However, the active intensity does not discriminate between near-field flows that are circulatory, and far-field flows that propagate effectively out to the far field.

Some years ago, it was suggested that the zero-curl component of the active intensity may be associated with far-field radiation, whereas the nonzero-curl may be associated with near-field circulatory intensity paths [132].

The validity of the irrotational component of the active sound intensity as a descriptor of the far-field energy was examined for the interaction of propagating waves where it seems to hold. However, as pointed out by Mann [135], this quantity seems to neglect the interaction between several closely spaced point sources.

Given N point sources, the irrotational or zero-curl component of the active intensity is (see [135])

$$\nabla\beta = k\sum_{i=1}^{N} A_i^2 \frac{\mathbf{r}_i}{\mathbf{r}_i^3}, \tag{A.14}$$

whereas the rotational (curled) component is

$$\nabla\times\phi = k\sum_{n=1}^{N}\sum_{m=1}^{N} A_m A_n \frac{\mathbf{r}_m}{\mathbf{r}_n\mathbf{r}_m^2}(kr_m cos\theta_{nm} + sin\theta_{nm}) \text{ with } m \neq n. \tag{A.15}$$

These two expressions show, as pointed out by Mann, that the irrotational component of the acoustic intensity neglects the interaction between the point sources in the total power output.

Nontheless, the zero-curl component of the active intensity aims at describing a similar phenomenon as the supersonic intensity does, trying to identify the far field output of a sound source.

2 Conservation of power of the supersonic intensity

Regarding the supersonic intensity, it has been shown analytically and experimentally that it fulfills the conservation of power. As explained in the foregoing, the supersonic acoustic intensity is the field composed by the waves that propagate to the far field. The supersonic intensity of a point source can be calculated by integrating the wavenumber spectrum over the radiation circle instead of over the whole spectrum (see sect. 2.15.1 of ref. [1], or ref. [113]). Based on this analytical description, it is possible to express a combination of point sources and describe them in an integral form. Note that in this case the integrands are not rotationally symmetric, thus there is a dependency of the polar angle in the plane, as well as the radial component.

Let there be two monopoles in the same plane, at positions (ρ_1, ϕ_1) and (ρ_2, ϕ_2).

The supersonic intensity can be expressed as (due to the lack of rotationally symmetry, the integration is done over the radial and polar angles),

$$p^{(s)}(\rho,\phi,z) = \frac{\rho_0 ck}{4\pi^2}\int_0^{2\pi}\int_0^{k}(Q_1 e^{-jk_\rho \rho\cos(\theta-\phi)}e^{jk_\rho\rho_1\cos(\theta-\phi_1)} + Q_2 e^{jk_\rho\rho\cos(\theta-\phi)}e^{jk_\rho\rho_2\cos(\theta-\phi_2)})\cdot\frac{e^{jz\sqrt{k^2-k_\rho^2}}}{\sqrt{k^2-k_\rho^2}}k_\rho dk_\rho d\theta, \tag{A.16}$$

$$u_z^{(s)}(\rho,\phi,z) = \frac{1}{4\pi^2}\int_0^{2\pi}\int_0^{k}(Q_1 e^{jk_\rho \rho\cos(\theta-\phi)}e^{jk_\rho\rho_1\cos(\theta-\phi_1)} + Q_2 e^{jk_\rho\rho\cos(\theta-\phi)}e^{jk_\rho\rho_2\cos(\theta-\phi_2)})\cdot e^{jz\sqrt{k^2-k_\rho^2}}k_\rho dk_\rho d\theta. \tag{A.17}$$

These integrals can be evaluated numerically, and the supersonic intensity calculated as

$$I_z^{(s)}(\mathbf{r}) = \frac{1}{2}\mathrm{Re}\{p(\mathbf{r})\cdot u(\mathbf{r})^*\}. \tag{A.18}$$

The example of two monopoles with a quadrature phase shift, where $Q_2 = Q_1 e^{j\pi/2}$ was considered, as well as the case of a dipole $Q_1 = -Q_2$. The phase shift gives rise to a near field in which part of the energy flows from one source into the other, thus there is a clear interaction of the sources. Figure 1 shows the calculated sound power for a dipole, calculated from the active, supersonic and irrotational sound intensity. The underestimation from the supersonic intensity is due to the finite aperture error.

The experiment confirmed that the interaction between the sources is accounted for with the supersonic intensity, and that it amounts to the total net power output. In other words, the total power output of the two sources is not the result of adding their power separately, as seems to be the case from the irrotational intensity.

This is however a preliminary examination, but it demonstrates that the two quantities do not seem to be directly related.

Fuerthermore regarding the conservation of power of the supersonic intensity, the power of the vibrating plate of the experimental results of Paper E is shown in Fig. 2. The figure demonstrates the experimental validity of the supersonic intensity regarding the conservation of power.

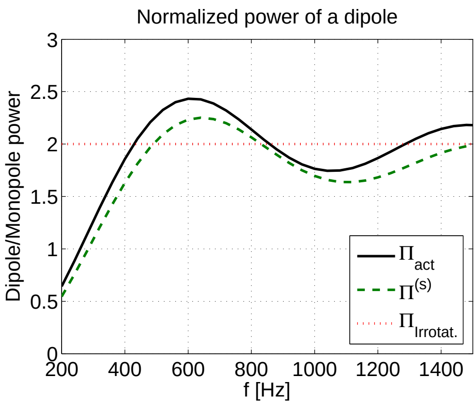

Figure 1: Power radiated by a dipole normalized to the power by a single monopole. The figure shows the power calculated from the active, the supersonic and the irrotational acoustic intensity.

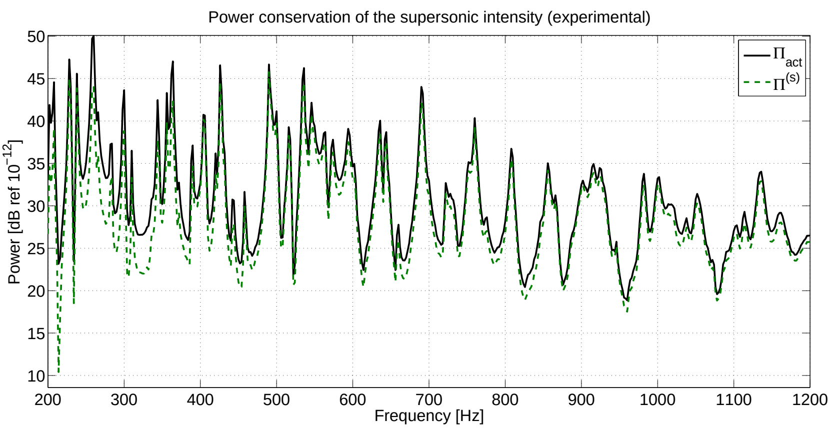

Figure 2: Acoustic power of the baffled plate used in the physical experiment of Paper E, calculated from the active intensity and the supersonic intensity. The figure demonstrates the conservation of power of the supersonic intensity.

23 February 2012

www.elektro.dtu.dk
Department of Electrical Engineering
Acoustic Technology
Technical University of Denmark
Ørsteds Plads
Building 348
DK-2800 Kgs. Lyngby
Denmark
Tel: (+45) 45 25 38 00
Fax: (+45) 45 93 16 34
Email: info@elektro.dtu.dk

ISBN 978-87-92465-82-5